NATIONAL TECHNICAL UNIVERSITY OF ATHENS

Postgraduate Studies Program “Computational Mechanics”

Development of computational algorithms and thermodynamic models for multiphase, multicomponent CO_2 mixtures

MSc Thesis

of

Ilias K. Nikolaidis

Supervisors:

Prof. Andreas G. Boudouvis

School of Chemical Engineering, NTUA, Greece

Prof. Ioannis G. Economou

Texas A&M University at Qatar, Chemical Engineering Program

Athens, October 2015

Abstract

Carbon Capture and Sequestration (CCS) is a technology designed to reduce carbon dioxide (CO_2) emissions from large point sources of production. CCS has grown in recent years from lab and pilot scale activity to a full blown industrial process. Preliminary conceptual design, detailed design, simulation and optimization of a CCS process require, among others, accurate knowledge of the physical properties of the chemical system involved. CO_2 is typically captured from fossil fuel power plants and is transported through pipelines to the appropriate storage location. This fluid stream contains different chemical impurities in various concentrations, that depend on the initial process and the type of pre-treatment imposed to the stream prior to transportation. Accurate knowledge of the physical properties of the chemical system as a function of temperature, pressure and composition is required. Quite often, the system exists in more than one phase (i.e., liquid, vapor and/or solid) and as a result process design calculations have to take into account the phase equilibrium conditions and also the composition of the relevant phases and the respective physical property values.

The calculation of the physical properties of the stream and the phase equilibria are calculated traditionally with Equations of State (EoS). The two challenges that arise are the accurate prediction or correlation of the physical properties of the system and the conditions of instability, where the system is going to split into two or more coexisting phases. Moreover, calculation of phase equilibria itself generates various computational challenges and the need of robust algorithms has driven a wealth of mathematical formulations of the phase equilibrium problem.

In this work, a robust numerical scheme for the calculation of constant composition (isoplethic) phase diagrams of complex multicomponent mixtures has been developed. The scheme refers to the sequential calculation of the phase envelope of a mixture by guiding the estimation for the equilibrium curve via the introduction of a “spring” that sets the slope value of the modified tangent plane distance with respect to either temperature or pressure. A simple variation of the proposed method allows direct estimation of the Cricondentherm (maximum temperature) and/or Cricondenbar (maximum pressure) points, thus avoiding the calculation of the entire phase diagram. Extensive tests of the proposed scheme for different types of phase diagrams, using both cubic and higher order EoS have been performed. Moreover, several EoS have been used to model the vapor - liquid phase behavior of binary, ternary and multicomponent mixtures of CO_2 with other gases. Extensive comparisons with experimental data available in the literature have been performed to validate the predictive and the correlative capabilities of each fluid equation of state. Calculations have been also

extended to modeling the two and multiphase solid – fluid equilibria of binary CO_2 mixtures, so that the effect of impurities on the solidification phenomena could be assessed. A new algorithm for the calculation of the solid – liquid – gas (SLG) equilibrium has been developed and different solid modeling approaches have been coupled with various fluid EoS. The resulting models have been validated against experimental SLG data available in the literature.

Abstract in Greek

Η δέσμευση και γεωλογική αποθήκευση του άνθρακα (Carbon Capture and Sequestration) είναι μία τεχνολογία σχεδιαμένη για τη μείωση των εκπομπών διοξειδίου του άνθρακα (CO_2) από μεγάλες σημειακές πηγές παραγωγής. Η διεργασία έχει εξελιχθεί τα τελευταία χρόνια από εργαστηριακή και πιλοτική κλίμακα σε πλήρη βιομηχανική διεργασία, ενώ ο προκαταρκτικός και αναλυτικός σχεδιασμός, η προσομοίωση και βελτιστοποίηση της διεργασίας απαιτούν, μεταξύ άλλων, ακριβή γνώση των φυσικοχημικών ιδιοτήτων του εμπλεκόμενου χημικού συστήματος. Το CO_2 δεσμεύεται συνήθως από ηλεκτροπαραγωγικές μονάδες καύσης ορυκτών καυσίμων και μεταφέρεται μέσω δικτύου αγωγών σε κατάλληλους χώρους αποθήκευσης. Το ρεύμα που μεταφέρεται περιέχει διάφορες χημικές προσμίξεις σε διαφορετικά επίπεδα συγκεντρώσεων, τα οποία εξαρτώνται από την αρχική διεργασία και το είδος της προεπεξεργασίας η οποία εφαρμόζεται στο ρεύμα πριν τη μεταφορά. Η ακριβής γνώση των φυσικοχημικών ιδιοτήτων του χημικού συστήματος ως συνάρτηση της θερμοκρασίας, της πίεσης και της σύστασης είναι απαραίτητη. Επιπλέον, συχνά το σύστημα συνυπάρχει σε παραπάνω από μία φάσεις (υγρή, ατμώδης και/ή στερεή) και συνεπώς ο σχεδιασμός της διεργασίας πρέπει να λάβει υπόψη τις συνθήκες ύπαρξης ισορροπίας φάσεων, όπως επίσης και τη σύσταση και τις ιδιότητες των φάσεων.

Ο υπολογισμός των φυσικοχημικών ιδιοτήτων του ρεύματος και η ισορροπία φάσεων, υπολογίζονται παραδοσιακά με καταστατικές εξισώσεις (ΚΕ). Οι δύο προκλήσεις οι οποίες προκύπτουν είναι η ακριβής πρόβλεψη ή συσχέτιση των φυσικοχημικών ιδιοτήτων και ο προσδιορισμός των συνθηκών αστάθειας, όπου το σύστημα θα διαχωριστεί σε δύο ή περισσότερες συνυπάρχουσες φάσεις. Επιπλέον, ο ίδιος ο υπολογισμός της ισορροπίας φάσεων παρουσιάζει διάφορες προκλήσεις και η ανάγκη για εύρωστους αλγορίθμους έχει οδηγήσει σε μια πληθώρα μαθηματικών διατυπώσεων.

Στην παρούσα εργασία αναπτύχθηκε ένα εύρωστο αριθμητικό σχήμα για τον υπολογισμό του διαγράμματος ισορροπίας φάσεων υπό σταθερή σύσταση για πολύπλοκα, πολυσυστατικά μείγματα. Το σχήμα αναφέρεται στον διαδοχικό υπολογισμό του διαγράμματος φάσης ενός μείγματος με το να οδηγείται η εκτίμηση για την καμπύλη ισορροπίας μέσω της εισαγωγής ενός «ελατηρίου» το οποίο θέτει την τιμή της κλίσης της τροποποιημένης εφαπτομενικής απόστασης από επίπεδο ως προς την θερμοκρασία ή την πίεση. Με μια απλή τροποποίηση, η προτεινόμενη μέθοδος επιτρέπει τον απευθείας προσδιορισμό των σημείων Cricondentherm (σημείο μέγιστης θερμοκρασίας) και/ή Cricondenbar (σημείο μέγιστης πίεσης), αποφεύγοντας με αυτόν τον τρόπο τον υπολογισμό ολόκληρου του φασικού διαγράμματος. Στο πλαίσιο εφαρμογής της μεθόδου, πραγματοποιήθηκαν εκτενείς δοκιμές του προτεινόμενου σχήματος σε διαφορετικούς τύπους διαγραμμάτων φάσης, χρησιμοποιώντας κυβικές και ανώτερης τάξης καταστατικές

εξισώσεις. Επιπλέον, διαφορετικές ΚΕ χρησιμοποιήθηκαν για τη μοντελοποίηση της ισορροπίας φάσεων υγρού – ατμού δυαδικών, τριαδικών και πολυσυστατικών μειγμάτων CO_2 με άλλα αέρια. Εκτενής σύγκριση με πειραματικά δεδομένα διαθέσιμα στη βιβλιογραφία πραγματοποιήθηκε, για να αξιολογηθούν οι ικανότητες πρόβλεψης και συσχέτισης της κάθε ΚΕ. Οι υπολογισμοί επιπλέον επεκτάθηκαν στη μοντελοποίηση της διφασικής και πολυφασικής ισορροπίας στερεού – ρευστού δυαδικών μειγμάτων CO_2, έτσι ώστε να αξιολογηθεί η επίδραση προσμίξεων στα φαινόμενα στερεοποίησης. Ένας νέος αλγόριθμος για τον υπολογισμό της ισορροπίας στερεού – υγρού – αερίου αναπτύχθηκε και διαφορετικές προσεγγίσεις μοντελοποίησης της στερεής φάσης συζεύκτηκαν με διάφορες ΚΕ ρευστής φάσης. Οι προβλέψεις των μοντέλων που προέκυψαν αξιολογήθηκαν με βάση πειραματικά δεδομένα διαθέσιμα στη βιβλιογραφία.

Acknowledgements

I want to dedicate this part of my thesis to thank certain people that have guided and helped me to complete this thesis, had a positive impact on my work or spent with me constructive time and helped me through the postgraduate studies program "Computational Mechanics".

I am sincerely grateful to my supervisors, Professor Andreas Boudouvis and Professor Ioannis Economou for their guidance and help from the beginning of the postgraduate course till the end. I want to especially thank Professor Economou for giving me the opportunity to spend 5 months in Qatar as a visiting student in Texas A&M University and the close supervision and collaboration we had. Moreover, I would also like to thank the third member of my supervising committee, Professor Doros Theodorou. Although, we did not collaborate closely, he has given me constructive advice during his lectures and also he was more than willing to discuss my questions.

Furthermore, I am deeply indebted to my senior colleagues Assistant Professor Georgios Boulougouris, Dr. Loukas Peristeras and Dr. Dimitrios Tsangaris, with whom we have worked closely to carry out the CO_2QUEST project. Their experience and help have been invaluable to me. I would like to thank especially Georgios Boulougouris and Loukas Peristeras for the time they have dedicated to help, teach and answer my questions. Moreover, I would also like to express my gratitude to my colleagues and friends in Texas A&M University at Qatar who made my stay in Doha a nice experience and also helped me in scientific topics, but also in everyday life; Dr. Vasileios Michalis, Dr. Othon Moultos, Dr. Panagiotis Krokidas.

I would like to express my gratitude for the financial support from the 7th European Commission Framework Program for Research and Technological Development "Impact of the Quality of CO_2 on Storage and Transport" (Project No.: 309102). I am also thankful to Texas A&M University at Qatar for a visiting student assistantship.

At this point I wish to thank my classmates in the postgraduate studies program "Computational Mechanics" with whom we have worked together to complete all the different tasks. Specifically I would like to thank Panagiotis Giannatselis for the countless hours we have spent to help each other.

Finally, I want to thank my family, Kostas, Lemonia and Marina, for their everyday support and encouragement, who continuously strive to help and give me all the prerequisites to continue on.

Table of Contents

List of Tables

List of Figures

List of Abbreviations

AAD	Average Absolute Deviation
BIPs	Binary Interaction Parameters
CCS	Carbon Capture and Sequestration
CFD	Computational Fluid Dynamics
DIPPR	Design Institute for Physical Properties
DRV	Double Retrograde Vaporization
EoS	Equation of State
GERG	Groupe Européen de Recherches Gazières
PC-SAFT	Perturbed Chain – SAFT
PR	Peng - Robinson
REFPROP	Reference Fluid Thermodynamic and Transport Properties
RK	Redlich - Kwong
SAFT	Statistical Associating Fluid Theory
SLE	Solid – Liquid Equilibrium
SLG	Solid – Liquid – Gas
SLLE	Solid – Liquid – Liquid Equilibrium
SLVE	Solid – Liquid – Vapor Equilibrium
SRK	Soave – Redlich - Kwong
SVE	Solid – Vapor Equilibrium
TPD	Tangent Plane Distance
vdW	Van der Waals

vdW1f	van der Waals one-fluid
VLE	Vapor – Liquid Equilibrium
VLLE	Vapor – Liquid – Liquid Equilibrium

List of Symbols

Latin Letters

A^{res}	Residual Helmholtz energy
b	Co-volume parameter for the cubic equations of state
C	Number of components in a mixture
c_P	Isobaric heat capacity per mole
d	Packing fraction
D_{ij}	Global constants of the Alder equation
$\frac{e}{k}$	SAFT dispersion energy parameter by Chen and Kreglewski
$\hat{f}_i^F$	Fugacity of component i in phase F.
g_{ij}^{seg}	Radial distribution function of hard spheres at contact
g	Gibbs free energy per mole
G	Gibbs free energy
h	Enthalpy per mole
J_{ij}	Element of a Jacobian matrix
K_i	Equilibrium ratio of vapor over liquid composition of component i
k	Boltzmann's constant
k_{ij}	Binary interaction parameter
l_{ij}	Binary interaction parameter
M_i	Number of association sites per molecule of species i
$\bar{m}$	Number of spherical segments in a chain in SAFT and PC-

	SAFT EoS
n_i	Number of moles of component i
P	Pressure
P^+	Reference pressure
P_c	Critical pressure
P_{tr}	Triple point pressure
$P_{0i}^{sat}(T)$	Saturation pressure of the pure solid former i at solid-fluid equilibrium conditions and temperature T
Q	Modified tangent plane distance function
q	Under relaxation parameter
R	Universal gas constant
s	Entropy per mole
S	Specification variable
T	Temperature
T_c	Critical temperature
T_{tr}	Triple point temperature
T_{0i}^{SL}	Melting temperature of pure solid former i
T_{0i}^{SV}	Sublimation temperature of pure solid former i
u^0	Segment dispersion energy in SAFT EoS
V_i	Vapor phase mole flow if component i
v	Molar volume
v_{0i}^{S}	Pressure, temperature independent pure solid i molar volume

$v_{0i}^{L^*}$	Molar liquid volume at the solid-liquid transition
v^{00}	Characteristic volume of the segment in SAFT EoS
W_i	Incipient phase mole numbers of component i
w_i	Incipient phase mole fraction of component i
X^{A_i}	Fraction of molecules of species i that are not hydrogen bonded at site A
x_i	Liquid phase mole fraction of component i
y_i	Vapor phase mole fraction of component i
z_i	Feed phase mole fraction of component i
Z	Compressibility factor

Greek Letters

$\alpha(T)$	Temperature dependent function for the attractive term of cubic EoS
α^{res}	Residual Helmholtz energy per mole
β	Vapor fraction
δ_{ij}	Kronecker delta
ε	Dispersion energy parameter used by PC-SAFT EoS
$\varepsilon^{A_iB_i}$	Association energy
ζ_k	Zeta function
η	Packing fraction
θ	Theta parameter used by the bead spring method
ϑ	Reduced temperature

$\kappa^{A_i B_i}$	Association volume
μ	Chemical potential
π	Reduced pressure
ρ	Molar density
σ	Segment diameter parameter used by PC-SAFT
$\hat{\varphi}_i^F$	Fugacity coefficient of a component i in phase F
Ψ	Helmholtz energy per volume
ω	Acentric factor

1. Introduction

1.1. Motivation

Fossil fuels are currently the most widely used sources for power and heat generation and they are also used by heavy industrial manufacturing operations. The result of this extended consumption of fossil fuels contributes significantly to the increased levels of greenhouse gases in the atmosphere, which subsequently leads to environmental problems such as global warming. The most important greenhouse gas, in terms of quantity and impact, is CO_2.

Worldwide, there are more than 8000 large stationary CO_2 emission sources and their cumulative emissions in 2005 were reported[1] as being 13,466 megatons of CO_2 per year (Mt/yr). Furthermore, in 2007 global energy use accounted for over 85% of the 37,000,000,000 tons (37 Gt) of CO_2 released to the atmosphere. In the United States, nearly 40% of atmospheric CO_2 can be attributed to combustion of fossil fuels to produce electricity, with another 30% resulting from industrial processes and 30% from transportation. As demands for energy have increased globally, CO_2 levels have risen sharply, from preindustrial levels of 280 ppm a century ago to over 380 ppm in 2009. These levels are projected to increase even more dramatically over the next 50 years as global demands for energy are anticipated to double.[2] Moreover, fossil fuels will continue to play an important role in power and heat production and also be used by large industrial application in the foreseeable future.[3,4]

As a result, significant amount of research has been conducted for the development of new technologies that try to reduce the levels of CO_2 in the atmosphere. The most mature technology at the moment is the Carbon Capture and Sequestration (CCS), which is the process of capturing carbon dioxide from the flue gas of a large point source (typically a power plant), transporting it to a sequestration site and then depositing it to a geological formation, which can be a saline aquifer or a depleted oil well.

The CCS process can be divided into three main parts: CO_2 capture, transport and storage. There are in general three main methodologies for the capture process: the oxyfuel combustion capture, the pre-combustion capture, the post-combustion capture and each one of these techniques results into different stream compositions and level of impurities.[4-6]

Transport of the CO_2 stream is usually done with the use of pipelines, ships, rail or road. The choice of transport depends on the quantity of CO_2 that needs to be transported, the distance and terrain to be travelled, and the specifications of the CO_2 stream produced at the

capture facility. In most cases, transporting CO_2 via pipeline will be the most cost effective mode of transport. The instances where transport by ship may prove more economical would be if CO_2 needs to be moved over very large distances (>1000 km) or over large bodies of water. Transport via rail or road is only expected to be feasible for moving CO_2 on a small scale for specialist applications.[5]

Pipeline transport is a technology where extensive research has been conducted because of the transport of natural gas streams and also high pressure releases of natural gas substances are relatively well understood. But, CO_2 possesses some unusual physical properties which make its release behavior more challenging to predict. CO_2 has a triple point pressure and temperature of 5.18 bar and 216.55 K respectively, and at atmospheric pressure it exists in either a solid or gaseous state, with a sublimation temperature of 194.25 K. This means that there is likely to be complex phase-transition when CO_2 decompresses from an initial dense-phase state in the pipeline (i.e. as a supercritical or liquid fluid) into a solid and gaseous state at atmospheric pressure.[7] Moreover, CO_2 pipelines may be crossing in the close proximity of populated areas. CO_2 is a colorless and odorless gas under ambient conditions and is toxic if inhaled in air at concentrations around 5%, and likely to be fatal at concentrations of around 10%. As a result, a more thorough investigation, regarding the hazards of CO_2 pipeline construction should be performed.

Finally, the most economical way of transporting carbon dioxide is in the supercritical state, as it has both the high density of a liquid and the favorable flow characteristics of a gas. However, it is not possible to maintain pipeline temperatures above the critical temperature in all situations. It is, therefore, important to ensure pressure drops are managed and pipeline pressures are kept above vapor - liquid equilibrium conditions to maintain a single dense phase flow and avoid liquid slugs and other operational problems that may eventuate if conditions fall within the region where a two phase flow may occur. Operating pressures of existing CO_2 pipelines are in the range of 85 to 210 bar where CO_2 is a dense phase fluid over a wide range of temperatures. To maintain sufficiently high pressures over long distances, intermediate pumping stations are required at certain intervals along the pipeline.[5] Moreover, in the supercritical state, CO_2 is a powerful solvent, which can cause sealing and corrosion problems to the pipelines.

Taking into account the aforementioned facts, it is understood that the thermodynamic modeling of pure CO_2 and CO_2 mixtures relevant to CCS applications is of key significance. Most importantly, calculation of the phase equilibria of these mixtures at different conditions of temperature and pressure is a key step to the design and assessment of the whole process.

1.2. Objectives

The main objectives of this thesis have been the following:

- Development of a new robust numerical scheme for the calculation of the constant composition vapor – liquid phase envelopes of multicomponent mixtures.
- Validation against experimental data available in the literature, of the predictive and correlative capabilities of different Equations of State (EoS) for the vapor liquid phase equilibrium (VLE) modeling of binary CO_2 mixtures with other components, relevant to CCS processes.
- Extension of calculations of the constant composition vapor – liquid phase envelopes to ternary and quaternary mixtures of CO_2 and validation against available experimental data. Calculations conducted, as pure predictions and with the use of interaction parameters fitted to the binary VLE experimental data.
- Development of solid models by coupling different solid modeling approaches with various fluid EoS and assessment of the accuracy of the resulting models in predicting the pure CO_2 solid – fluid saturation lines.
- Investigation of the effect of adding impurities on the pure CO_2 solid – fluid saturation line.
- Development of an efficient algorithm for the calculation of the three phase solid – liquid – vapor/gas (SLV/SLG) equilibrium line for binary mixtures.
- Evaluation and validation against experimental binary SLG data of CO_2 mixtures of the various solid models.

2. Thermodynamic Models

2.1. Equations of State for Fluids

2.1.1. Cubic Equations of State

An Equation of State (EoS) is the mathematical relation that correlates the pressure (P), the temperature (T) and the molar volume (v) of a pure compound at thermodynamic equilibrium state and is expressed mathematically with the functional form:

$$\mathrm{f}(\mathrm{P}, \mathrm{T}, v) = 0 \tag{2.1}$$

From the three properties that are present in Eq. (2.1), one can be considered as dependent variable and the other two as independent, for a single phase component based on the Gibbs phase rule. In this way, the EoS can be solved for one of these variables, while the other two are set. In practical problems, the common case is the equation to be solved for volume (or for density), at constant pressure and temperature and then, all the other properties can be determined using specific thermodynamic relations. However, volumetric data are most commonly expressed by an EoS that uses temperature and volume as independent variables, and therefore it is a matter of practical importance to have available equations for the thermodynamic properties also in terms of T and v.[8]

The two- and especially the three-parameter cubic EoS represent a family of classical but still very useful and widely applied engineering models. The most well-known EoS are the van der Waals (vdW), Redlich – Kwong (RK) (now mostly of historical value) and especially the Soave – Redlich – Kwong (SRK)[9] and Peng – Robinson (PR)[10] equations. The last two are typically employed in the petroleum and chemical industries.[11]

A general expression for a cubic EoS is[12]:

$$\mathrm{P} = \frac{\mathrm{RT}}{v - \mathrm{b}} - \frac{\alpha(\mathrm{T})}{(v + \delta_1 \mathrm{b})(v + \delta_2 \mathrm{b})} \tag{2.2}$$

where R is the gas constant and $\alpha(\mathrm{T})$ and b are component-specific parameters that account for the attractive intermolecular interactions and the excluded volume of the component respectively. To calculate these parameters, the critical temperature ($\mathrm{T_c}$), the critical pressure ($\mathrm{P_c}$) and the acentric factor (ω) of a pure compound have to be known. For $\delta_1 = 1$ and $\delta_2 = 0$, Eq. (2.2) takes the form of SRK EoS and for $\delta_1 = 1 + \sqrt{2}$ and $\delta_2 = 1 - \sqrt{2}$, Eq. (2.2) takes the form of PR EoS. In Table 2-1, the expressions for the two cubic equations of state and their parameters used in this work are presented.

Table 2-1: Expressions for the energy ($\boldsymbol{\alpha(T)}$) and co-volume (**b**) parameters for the cubic equations of state used in this work.

EoS	Equation	$\boldsymbol{\alpha(T)}$	$\boldsymbol{\alpha_c}$	**b**
SRK	$P = \frac{RT}{v-b} - \frac{\alpha(T)}{v(v+b)}$	$\alpha_c[1+m(1-\sqrt{T_r})]^2$ $m = 0.48 + 1.574\omega - 0.176\omega^2$	$0.42748\frac{(RT_c)^2}{P_c}$	$0.08664\frac{RT_c}{P_c}$
PR	$P = \frac{RT}{v-b} - \frac{\alpha(T)}{v(v+b)+b(v-b)}$	$\alpha_c[1+m(1-\sqrt{T_r})]^2$ $m = 0.37464 + 1.542\omega - 0.26992\omega^2$	$0.45724\frac{(RT_c)^2}{P_c}$	$0.07780\frac{RT_c}{P_c}$

Extension of the two EoS to mixtures requires suitable mixing rules for the two parameters, the energy parameter and the co-volume one. One widely used way to extend the cubic EoS to mixtures is via the so-called van der Waals one-fluid (vdW1f) mixing rules (quadratic composition dependency for both parameters) and the classical combining rules (Lorentz – Berthelot), i.e. the geometric mean rule for the cross-energy and the arithmetic mean rule for the cross co-volume parameter.[11]

$$\alpha = \sum_{i=1}^{n}\sum_{j=1}^{n} x_i x_j \alpha_{ij} \qquad \alpha_{ij} = \sqrt{\alpha_i \alpha_j}(1-k_{ij}) \tag{2.3}$$

$$b = \sum_{i=1}^{n}\sum_{j=1}^{n} x_i x_j b_{ij} \qquad b_{ij} = \frac{b_i + b_j}{2}(1-l_{ij}) \tag{2.4}$$

The k_{ij} and l_{ij} parameters are called binary interaction parameters (BIPs) and are used to optimize the EoS performance by fitting the models to phase equilibrium data. Of the two interaction parameters, k_{ij} is by far the most important one and usually l_{ij} is set to zero.[11] As a result, the mixing rule for the co-volume parameter is simplified to:

$$b = \sum_{i=1}^{n} x_i b_i \tag{2.5}$$

Eqs. (2.3) and (2.5) are the ones that have been used in this work to extend the calculations with SRK and PR equations of state to mixtures.

2.1.2. SAFT and PC-SAFT Equations of State

The SAFT[13-15] and PC-SAFT[16] EoS are theoretically derived models, based on rigorous perturbation theory. The basis of this theory has been developed by Wertheim,[17-20] who proposed a model for systems with a repulsive core and multiple attractive sites capable of forming chains and closed rings. Wertheim derived his theory by expanding the Helmholtz energy in a series of integrals of molecular distribution functions and the association

potential. He showed that many integrals in this series must be zero and, hence, a simplified expression for the Helmholtz energy can be obtained.[14] This way, the Helmholtz energy of a fluid can be described as the sum of the Helmholtz energy of a simple reference fluid which is known accurately and a perturbation term, the development of which is the challenging part.

In this framework, SAFT and PC-SAFT equations of state are written as summations of residual Helmholtz energy (A^{res}) terms that are the result of different molecular interactions. In SAFT, the fluid is first assumed to consist of equal-sized hard spheres and then, attraction between the spheres is introduced via the use of a potential that accounts for the dispersion forces. Next, the spheres are allowed to form chains (covalent bonds) and finally, specific interaction sites are introduced which enable the chains to associate. Most commonly, the association interaction accounts for the hydrogen bonds that appear between the molecules. Each one of these contributions to the molecular interactions results in a residual Helmholtz energy term that has to be added to the summation. Figure 2-1 shows a schematic representation of the steps that are followed to form a pure fluid in SAFT.

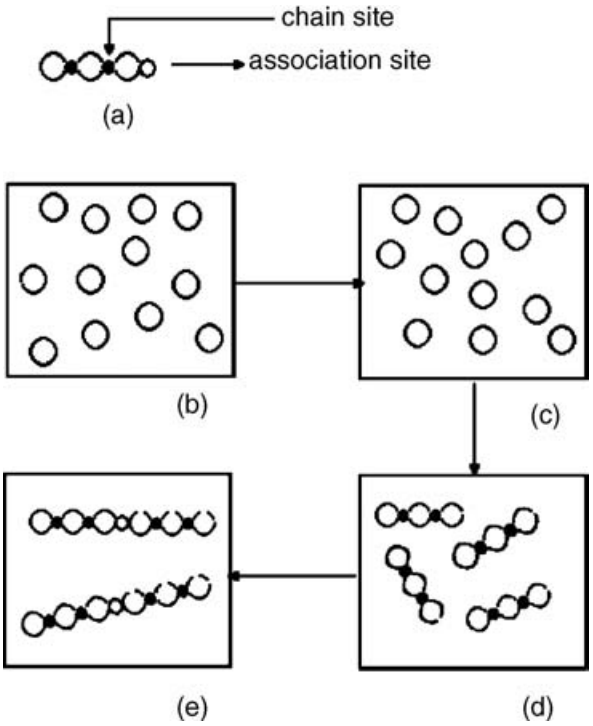

Figure 2-1: (a) Molecule in SAFT; (b) Hard spheres fluid; (c) Introduction of dispersion forces; (d) Chain formation; (e) Association complexes are formed; Figure taken from[11].

The residual Helmholtz energy of the fluid can now be written as:

$$\frac{A^{res}(T,\rho)}{NRT} = \frac{\alpha^{hs}(T,\rho)}{RT} + \frac{\alpha^{disp}(T,\rho)}{RT} + \frac{\alpha^{chain}(T,\rho)}{RT} + \frac{\alpha^{assoc}(T,\rho)}{RT} \qquad (2.6)$$

where α is the molar Helmholtz energy and the superscripts *res*, *hs*, *disp*, *chain* and *assoc* refer to residual, hard sphere, dispersion, chain and asscociation respectively.

The difference between SAFT and PC-SAFT is that PC-SAFT uses as reference fluid, the hard chain fluid instead of the hard spheres fluid that is used by SAFT. This means that, instead of adding the dispersion forces to hard spheres and then the chain formation to occur, hard sphere chains are formed and then dispersion forces between chains are added. This has as a result, that PC-SAFT uses the same hard sphere, chain and association terms as SAFT but the dispersion term is different due to the perturbation being added to hard chains and not to hard spheres. Figure 2-2 shows a schematic representation of the steps that are followed to form a pure fluid in PC-SAFT.

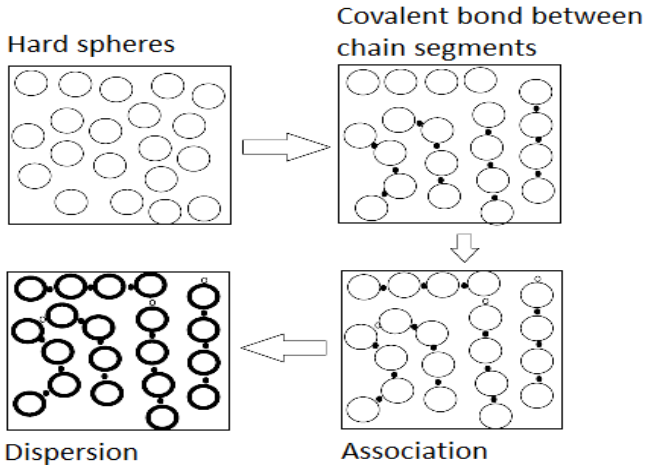

Figure 2-2: Schematic representation of the formation of a pure fluid within the PC-SAFT framework.

Table 2-2 summarizes the individual terms that are mentioned in Eq. (2.6) for the SAFT equation of state.

Table 2-2: Expressions for the individual Helmholtz energy terms used by SAFT EoS for mixtures.

SAFT		
Hard Sphere term	$\frac{\alpha^{hs}}{RT} = \frac{1}{\zeta_0}\left[\frac{3\zeta_1\zeta_0}{1-\zeta_3} + \frac{\zeta_2^3}{\zeta_3(1-\zeta_3)^2} + \left(\frac{\zeta_2^3}{\zeta_3^2} - \zeta_0\right)\ln(1-\zeta_3)\right]$	Carnahan-Starling EoS for hard spheres
Dispersion term	$\frac{\alpha^{disp}}{RT} = \sum_{i=1}^{4}\sum_{j=1}^{9} D_{ij}\left(\frac{u}{kT}\right)^i\left(\frac{\eta}{\tau}\right)^j$	Alder equation from molecular dynamics simulations
Chain term	$\frac{\alpha^{chain}}{RT} = (1-m)\ln\frac{1-0.5\eta}{(1-\eta)^3}$	Based on Wertheim's first-order perturbation theory (TPT1)
Association term	$\frac{\alpha^{assoc}}{RT} = \sum_i x_i\left[\sum_{A_i}\left(\ln X^{A_i} - \frac{X^{A_i}}{2}\right) + \frac{1}{2}M_i\right]$	Based on Wertheim's first-order perturbation theory (TPT1)

Table 2-3: Necessary relations and parameters for the calculation of the Helmholtz energy terms in SAFT EoS.

$d = \tau\rho m v^0 = \tau\rho m v^{00}\left(1 - C\cdot\exp\left(-\frac{3u^0}{kT}\right)\right)^3$	Packing fraction
$\frac{u}{k} = \frac{u^0}{k}\left(1 + \frac{e}{kT}\right)$	Temperature dependent energy parameter
$X^{A_i} = \left[1 + \sum_j \sum_{B_j} \rho_j X^{B_j} \Delta^{A_i B_j}\right]^{-1}$	Fraction of molecules of species i that are not hydrogen bonded at site A
$\Delta^{A_i B_j} = d_{ij}^3 g_{ij}^{seg}(d_{ij}) \kappa^{A_i B_j}\left[\exp\left(\frac{\varepsilon^{A_i B_j}}{kT} - 1\right)\right]$	Hydrogen bond strength between position A of a molecule and position B of another molecule
$g_{ij}^{seg}(d_{ij}) \approx g_{ij}^{hs}(d_{ij}^+) = \frac{1}{1-\zeta_3} + \left(\frac{d_i d_j}{d_i + d_j}\right)\frac{3\zeta_2}{(1-\zeta_3)^2} + \left(\frac{d_i d_j}{d_i + d_j}\right)^2 \frac{2\zeta_2^2}{(1-\zeta_3)^2}$	Radial distribution function of hard spheres at contact
$\zeta_k = \frac{\pi N_{Av}}{6}\rho \sum_i X_i m_i d_{ii}^k$	Zeta function
m	Number of spherical segments in a chain
v^{00}	Characteristic volume of the segment
u^0	Segment dispersion energy
M_i	Number of association sites per molecule of species i
$\varepsilon^{A_i B_i}$	Association energy
$\kappa^{A_i B_i}$	Association volume
D_{ij}	Global constants of the Alder equation
$\tau = 0.74048$	
$C = 0.12$	

As it has been already mentioned, the result of the perturbation being added to a hard chain fluid rather than a hard spheres fluid is that PC-SAFT EoS uses a different dispersion term from SAFT. Table 2-4 summarizes the Helmholtz energy term due to dispersion used by PC-SAFT.

Table 2-4: Dispersion term expression used by PC-SAFT EoS

	PC-SAFT
Dispersion term	$\frac{\alpha^{disp}}{RT} = -2\pi\rho I_1(\eta,\bar{m})\overline{m^2\varepsilon\sigma^3} - \pi\rho m C_1 I_2(\eta,\bar{m})\overline{m^2\varepsilon^2\sigma^3}$

, where:

Table 2-5: Necessary relations and parameters for the calculation of the Helmholtz energy terms in PC-SAFT EoS

$C_1 = \left(1 + Z^{hc} + \rho\frac{\partial Z^{hc}}{\partial\rho}\right)^{-1}$	
$I_1(\eta,\bar{m}) = \sum_{i=0}^{6}\alpha_i(\bar{m})\eta^i$	
$I_2(\eta,\bar{m}) = \sum_{i=0}^{6} b_i(\bar{m})\eta^i$	
$\alpha_i(\bar{m}) = \alpha_{0i} + \frac{\bar{m}-1}{\bar{m}}\alpha_{1i} + \frac{\bar{m}-1}{\bar{m}}\frac{\bar{m}-2}{\bar{m}}\alpha_{2i}$	
$b_i(\bar{m}) = b_{0i} + \frac{\bar{m}-1}{\bar{m}}b_{1i} + \frac{\bar{m}-1}{\bar{m}}\frac{\bar{m}-2}{\bar{m}}b_{2i}$	
Z^{hc}	Hard chain contribution to compressibility factor
σ	Segment diameter
ε	Dispersion energy

One of the especially attractive features of SAFT and PC-SAFT, which stems from their theoretical origin, is that no mixing rules are needed in the chain and association terms. These terms are thus rigorously extended to mixtures. Mixing rules are needed, however, in the dispersion term of the equations. Moreover, combining rules are needed for the segment energy and volume (or diameter) parameters and the Lorentz–Berthelot rules are typically used. As with cubic EoS, a binary interaction parameter is often used in the combining rule for the cross-energy parameter. Typically, the van der Waals one-fluid mixing rules are used.[11] In Table 2-6 the mixing and combining rules used in SAFT and PC-SAFT are shown.

Table 2-6: Mixing and combing rules used in SAFT and PC-SAFT

$\bar{m} = \sum_i x_i m_i$	SAFT , PC-SAFT
$u_{ij} = \sqrt{u_i u_j}\left(1 - k_{ij}\right)$	SAFT
$(v^0)_{ij} = \left\{\frac{1}{2}\left[(v^0)_i^{1/3} + (v^0)_j^{1/3}\right]\right\}^3$	SAFT
$\frac{u}{kT} = \frac{\sum_i \sum_j x_i x_j m_i m_j \left[\frac{u_{ij}}{kT}\right](v^0)_{ij}}{\sum_i \sum_j x_i x_j m_i m_j (v^0)_{ij}}$	SAFT
$\varepsilon_{ij} = \sqrt{\varepsilon_i \varepsilon_j}\left(1 - k_{ij}\right)$	PC-SAFT
$\sigma_{ij} = \frac{\sigma_i + \sigma_j}{2}$	PC-SAFT
$\overline{m^2 \varepsilon \sigma^3} = \sum_i \sum_j x_i x_j m_i m_j \left[\frac{\varepsilon_{ij}}{kT}\right] \sigma_{ij}^3$	PC-SAFT
$\overline{m^2 \varepsilon^2 \sigma^3} = \sum_i \sum_j x_i x_j m_i m_j \left[\frac{\varepsilon_{ij}}{kT}\right]^2 \sigma_{ij}^3$	PC-SAFT
$\varepsilon^{A_i B_j} = \frac{1}{2}\left(\varepsilon^{A_i B_i} + \varepsilon^{A_j B_j}\right)$	SAFT , PC-SAFT
$\kappa^{A_i B_j} = \sqrt{\kappa^{A_i B_i} \kappa^{A_j B_j}} \left(\frac{\sqrt{\sigma_i \sigma_j}}{\frac{1}{2}\left(\sigma_i + \sigma_j\right)}\right)^3$	SAFT , PC-SAFT

2.2. Solid Models

2.2.1. Correlation Model

The calculation of the two phase solid-fluid, i.e solid-liquid (SLE) and solid-vapor (SVE), equilibria requires the equilibration of the chemical potentials of a solid forming compound in the two coexisting phases at the same temperature and pressure:

$$\mu_i^S(T,P) = \mu_i^F\left(T,P,\mathbf{x}^F\right) \tag{2.7}$$

where μ_i^S stands for the chemical potential of the solid former in a pure solid phase and μ_i^F is the chemical potential of the same compound in the coexisting fluid phase mixture of molar composition characterized by the vector $\mathbf{x}^F$. If the ideal gas reference state is used to measure the chemical potential for both phases, Eq. (2.7) can be substituted by the equation of fugacities[8]:

$$\hat{f}_i^S(T,P) = \hat{f}_i^F\left(T,P,\mathbf{x}^F\right) \tag{2.8}$$

This leads subsequently to satisfaction of:

$$P_{0i}^{sat}(T)\hat{\varphi}_{0i}^{sat}\left(T,P_{0i}^{sat}\right)\exp\left[\frac{v_{0i}^S}{RT}\left(P-P_{0i}^{sat}(T)\right)\right] = x_i^F\hat{\varphi}_i^F\left(T,P,\mathbf{x}^F\right)P \tag{2.9}$$

, where

Table 2-7: Individual terms present in Eq. (2.9)

$P_{0i}^{sat}(T)$	Saturation pressure of the pure solid former at solid-fluid equilibrium conditions and temperature T
$\hat{\varphi}_{0i}^{sat}\left(T,P_{0i}^{sat}\right)$	Fugacity coefficient of the pure solid former at temperature T and pressure P_i^{sat}
$\hat{\varphi}_i^F\left(T,P,\mathbf{x}^F\right)$	Fugacity coefficient of the solid former in the fluid mixture of molar composition $\mathbf{x}^F$, at temperature T and pressure P
v_{0i}^S	Pressure, temperature independent pure solid molar volume

To use Eq. (2.9) for the modeling of two phase solid-fluid equilibrium, it is necessary to couple a fluid equation of state with a model that provides the saturation pressure of the solid former at solid-fluid equilibrium. This solid model can be a correlation fitted to experimental data at solid-liquid or solid-vapor equilibrium conditions.

2.2.2. Thermodynamic Integration Model

An alternative way to model solid – fluid (either vapor or liquid) equilibria is to use an EoS for the entire region of conditions with proper selection of reference states.[21] In this derivation, the reference state selected is the *pure, subcooled melt* for the case of solid – liquid equilibrium and the *pure, superheated vapor* for the case of solid – vapor equilibrium, at system temperature and standard pressure (P^+). The standard pressure is chosen by taking into account the existence of measured (or calculated) caloric data at this reference state.

Based on these reference states, the chemical potential of component (i) in each phase (S: solid phase, F: fluid phase) is given by[21]:

$$\mu_i^S(T,P) = \mu_{0i}^S(T,P) + RT\ln\frac{x_i^S\varphi_i^S(T,P,\mathbf{x}^S)P}{\varphi_{0i}^S(T,P)P} \tag{2.10}$$

$$\mu_i^F(T,P,\mathbf{x}^F) = \mu_{0i}^{F^*}(T,P) + RT\ln\frac{x_i^F\varphi_i^F(T,P,\mathbf{x}^F)P}{\varphi_{0i}^{F^*}(T,P)P} \tag{2.11}$$

At equilibrium, the chemical potential of each component must satisfy Eq. (2.7). Thus, the equation that describes the solubility of a solid component in the fluid phase is:

$$x_i^F = \frac{x_i^S\varphi_i^S}{\varphi_{0i}^S}\cdot\frac{\varphi_{0i}^{F^*}}{\varphi_i^F}\cdot\exp\left[-\frac{1}{RT}\left(\mu_{0i}^{F^*}(T,P)-\mu_{0i}^S(T,P)\right)\right] \tag{2.12}$$

The difference of the chemical standard state potentials of the pure substance in Eq. (2.12) equals to the Gibbs free energy change Δg^{SF^*}:

$$\mu_{0i}^{F^*}(T,P) - \mu_{0i}^S(T,P) = g_{0i}^{F^*}(T,P) - g_{0i}^S(T,P) = \Delta g^{SF^*} \tag{2.13}$$

The Gibbs energy change Δg^{SF^*} can be determined by means of a thermodynamic cycle which takes the pressure dependence of solid/fluid equilibria adequately into account. This cycle can be divided into three steps:

The starting point is represented by state A at system temperature and (high) system pressure. In the first step, this state has to be converted isothermally to the introduced standard pressure P^+. The second step from point B (P^+, T) to point E (P^+, T) is an isobaric thermodynamic cycle, similar to the one described by Prausnitz et al.[8] Between points B and E, steps "heating up the solid to its melting curve", "melting" and "cooling down the liquid to the hypothetical state of the subcooled melt" can be calculated. Subsequently, the third and final step follows, in which the isothermal change from point E at standard pressure P^+ to point F at system pressure P is considered. This cycle is the same for both solid – liquid and

solid – vapor equilibrium, but in the latter case instead of subcooled melt, superheated vapor exists.

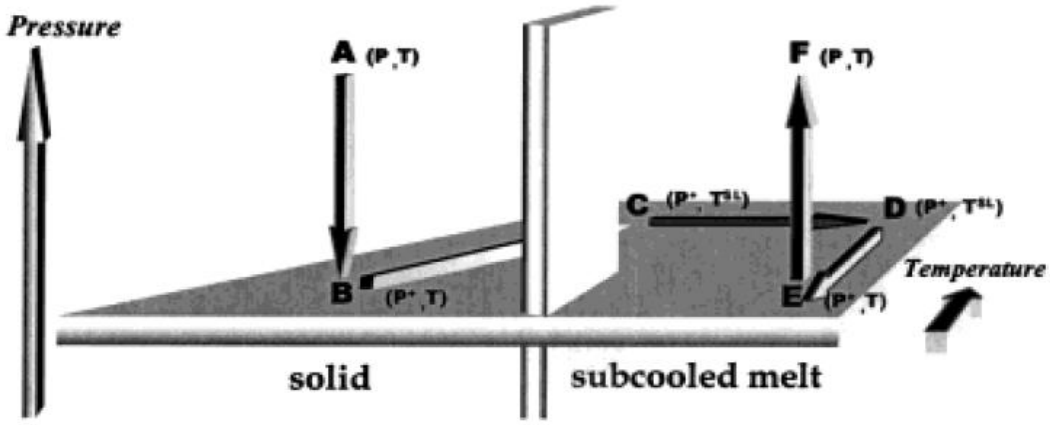

Figure 2-3: Thermodynamic cycle for the calculation of solid – fluid phase equilibria. Figure taken from Seiler et al.[21]

The calculation of the Gibbs energy change is done by thermodynamic integration and is expressed as three steps[21]:

Step 1 (from point A to point B)

By means of Gibbs – Duhem equation:

$$\mathrm{dg} = -\mathrm{sdT} + v\mathrm{dP} \tag{2.14}$$

$$\Delta g_{step1} = g_{0i}^{S}(T, P^{+}) - g_{0i}^{S}(T, P) = \int_{P}^{P+} v_{0i}^{S}\,\mathrm{dP} \tag{2.15}$$

Step 2 (from point B to point E)

$$\Delta g_{step2} = g_{0i}^{F^*}(T, P^{+}) - g_{0i}^{S}(T, P^{+}) = \Delta h^{SF^*} - T\Delta s^{SF^*} \tag{2.16}$$

$$\Delta g_{step2} = \Delta h^{SF^*}\left(1 - \frac{T}{T_{0i}^{SF}}\right) - \int_{T}^{T_{0i}^{SF}} \Delta c_{P,0i}^{SF^*}\,\mathrm{dT} + T\int_{T}^{T_{0i}^{SF}} \frac{\Delta c_{P,0i}^{SF^*}}{T}\,\mathrm{dT} \tag{2.17}$$

Step 3 (from point E to point F)

$$\Delta g_{step3} = g_{0i}^{F^*}(T, P) - g_{0i}^{F^*}(T, P^{+}) = \int_{P+}^{P} v_{0i}^{F^*}\,\mathrm{dP} \tag{2.18}$$

Applying the aforementioned thermodynamic integration process, the equation that applies to the solid – liquid equilibrium case is:

$$x_i^L = \frac{x_i^S \varphi_i^S}{\varphi_{0i}^S} \frac{\varphi_{0i}^{L^*}}{\varphi_i^L} \cdot \exp[-\frac{\left(v_{0i}^S - v_{0i}^{L^*}\right)(P^+ - P)}{RT} - \frac{\Delta h_{0i}^{SL}}{RT}\left(1 - \frac{T}{T_{0i}^{SL}}\right) + \frac{\Delta c_{P,0i}^{SL^*}}{RT}\left(T_{0i}^{SL} - T\right) - \frac{\Delta c_{P,0i}^{SL^*}}{R} \ln \frac{T_{0i}^{SL}}{T}] \quad (2.19)$$

Furthermore, assuming that the solid phase contains only one component, the equation becomes:

$$x_i^L = \frac{\varphi_{0i}^{L^*}}{\varphi_i^L} \cdot \exp[-\frac{\left(v_{0i}^S - v_{0i}^{L^*}\right)(P^+ - P)}{RT} - \frac{\Delta h_{0i}^{SL}}{RT}\left(1 - \frac{T}{T_{0i}^{SL}}\right) + \frac{\Delta c_{P,0i}^{SL^*}}{RT}\left(T_{0i}^{SL} - T\right) - \frac{\Delta c_{P,0i}^{SL^*}}{R} \ln \frac{T_{0i}^{SL}}{T}] \quad (2.20)$$

In Eq. (2.20) the fugacity coefficients are calculated by a fluid equation of state.

In order to use Eq. (2.20) the following physical properties of the solid forming compound are needed at the standard pressure P^+:

Table 2-8: Physical properties needed for the application of the thermodynamic integration model at solid-liquid equilibrium conditions

Δh_{0i}^{SL}	Enthalpy of melting at melting temperature T_{0i}^{SL}
T_{0i}^{SL}	Melting temperature
$v_{0i}^{L^*}$	Molar liquid volume at the solid-liquid transition
v_{0i}^{S}	Pure solid molar volume
$\Delta c_{P,0i}^{SL^*}$	Difference of the molar, isobaric heat capacities between the hypothetical subcooled melt and the solid.

Inherent to the model described by Eq. (2.20) are the following assumptions which must be emphasized:

- The solid phase consists of only one component.
- The solid volume is pressure independent.
- The liquid volume is pressure independent.
- The isobaric heat capacities are temperature independent.

In the case of solid-vapor equilibrium, the assumption of pressure independent vapor volume is not a good one and can lead to high errors. Thus, the term of the equation that occurs from integral at ***step 3*** is calculated from the of Gibbs energy change using a fluid equation of state. The equation now is formulated as:

$$x_i^V = \frac{\varphi_{0i}^{V^*}}{\varphi_i^V} \cdot \exp[-\frac{\left(v_{0i}^S\right)(P^+ - P)}{RT} - \ln\left[\frac{\varphi_{0i}^{V^*}(T,P)P}{\varphi_{0i}^{V^*}(T,P^+)P^+}\right] - \frac{\Delta h_{0i}^{SV}}{RT}\left(1 - \frac{T}{T_{0i}^{SV}}\right) + \frac{\Delta c_{P,0i}^{SV^*}}{RT}\left(T_{0i}^{SV} - T\right) - \frac{\Delta c_{P,0i}^{SV^*}}{R}\ln\frac{T_{0i}^{SV}}{T}] \quad (2.21)$$

In order to use Eq. (2.21) the following physical properties of the solid forming compound are needed at the standard pressure P^+:

Table 2-9: Physical properties needed for the application of the thermodynamic integration model at solid-vapor equilibrium conditions

Δh_{0i}^{SV}	Enthalpy of melting at sublimation temperature T_{0i}^{SV}
T_{0i}^{SV}	Sublimation temperature
v_{0i}^S	Pure solid molar volume
$\Delta c_{P,0i}^{SV^*}$	Difference of the molar, isobaric heat capacities between the hypothetical superheated vapor and the solid.

Inherent to the model described by Eq. (2.21) are the following assumptions which must be also emphasized:

- The solid phase consists of only one component.
- The solid volume is pressure independent.
- The isobaric heat capacities are temperature independent.

2.2.3. Gibbs Free Energy Equation of State for Solid CO_2

Simple correlation equations for sublimation and melting pressures as a function of temperature can be very accurate but do not allow for flash calculations. For this reason Jager and Span[22] established a new EoS, that describes the thermodynamic behavior of solid CO_2, based on the Gibbs free energy. It is an empirical model which is explicit in the Gibbs free energy by using a fundamental expression for it and is fitted to experimental data (heat capacity, molar volume, expansion coefficient and compressibility) of solid CO_2.

The Gibbs free energy can be written as:

$$g(P,T) = h_0 - Ts_0 + \int_{T0}^{T} c_P(T,P_0)\,dT - T\int_{T0}^{T} \frac{c_P(T,P_0)}{T}dT + \int_{P0}^{P} v(P,T)\,dP \qquad (2.22)$$

Jager and Span used appropriate functional forms for the heat capacity, the expansion coefficient and the partial derivative of the molar volume with respect to pressure, so that these quantities could be accurately fitted to experimental data. The equation that was derived and provides the Gibbs free energy is:

$$\begin{aligned}
\frac{g}{RT_0} &= g_0 + g_1\Delta\vartheta + g_2\Delta\vartheta^2 \\
&+ g_3\left\{\ln\left(\frac{\vartheta^2+g_4^2}{1+g_4^2}\right) - \frac{2\vartheta}{g_4}\left[\arctan\left(\frac{\vartheta}{g_4}\right) - \arctan\left(\frac{1}{g_4}\right)\right]\right\} \\
&+ g_5\left\{\ln\left(\frac{\vartheta^2+g_6^2}{1+g_6^2}\right) - \frac{2\vartheta}{g_6}\left[\arctan\left(\frac{\vartheta}{g_6}\right) - \arctan\left(\frac{1}{g_6}\right)\right]\right\} \\
&+ g_7\Delta\pi\left[e^{f_\alpha(\vartheta)} + K(\vartheta)g_8\right] \\
&+ g_9K(\vartheta)\left[(\pi+g_{10})^{(n-1)/n} - (1+g_{10})^{(n-1)/n}\right]
\end{aligned} \qquad (2.23)$$

In Table 2-10, the various terms of Eq. (2.23) are provided. The result of fitting to the aforementioned experimental data is that the solid model uses 23 adjustable parameters. The values of these parameters are summarized in Table 2-11. All parameters are kept in the original values proposed by Jager and Span,[22] except for two, namely the g_0 and g_1 parameters, which have to be retuned for every fluid EoS the solid model is going to be coupled with (i.e. SRK, PR, SAFT, PC-SAFT). The purpose of tuning these two parameters for every different fluid EoS is to ensure that the corresponding solid-fluid model is going to be thermodynamically consistent.

Table 2-10: Individual terms and expressions used in Eq. (2.23)

$T_0 = 150\ (K)$
$\vartheta = T/T_0$
$\Delta\vartheta = \vartheta - 1$
$\pi = \frac{P}{101325}\ (Pa)$
$\Delta\pi = \pi - 1$
$K(\vartheta) = g_0^{\kappa}\vartheta^2 + g_1^{\kappa}\vartheta + g_2^{\kappa}$
$f_{\alpha}(\vartheta) = g_0^{\alpha}(\vartheta^2 - 1) + g_1^{\alpha}\ln\left(\frac{\vartheta^2 - g_2^{\alpha}\vartheta + g_3^{\alpha}}{1 - g_2^{\alpha} + g_3^{\alpha}}\right) + g_4^{\alpha}\ln\left(\frac{\vartheta^2 + g_2^{\alpha}\vartheta + g_3^{\alpha}}{1 + g_2^{\alpha} + g_3^{\alpha}}\right) + g_5^{\alpha}\left[\arctan\left(\frac{\vartheta - g_6^{\alpha}}{g_7^{\alpha}}\right) - \arctan\left(\frac{1 - g_6^{\alpha}}{g_7^{\alpha}}\right)\right] + g_8^{\alpha}\left[\arctan\left(\frac{\vartheta + g_6^{\alpha}}{g_7^{\alpha}}\right) - \arctan\left(\frac{1 - g_6^{\alpha}}{g_7^{\alpha}}\right)\right]$

Table 2-11: Eq. (2.23) parameters

g_0		Adjusted for each EoS
g_1		Adjusted for each EoS
g_2	-0.0020109135	Ref. [22] (in kJ/mol)
g_3	-0.0027976237	Ref. [22](in kJ/mol)
g_4	0.26427834	Ref. [22]
g_5	0.0038259935	Ref. [22] (in kJ/mol)
g_6	0.00031711996	Ref. [22] (in kJ/mol)
g_7	0.0022087195	Ref. [22]
g_8	-1.1289668	Ref. [22]
g_9	0.0092923982	Ref. [22]
g_{10}	3391.4617	Ref. [22]
g_0^{α}	0.039993365	Ref. [22]
g_1^{α}	0.0023945101	Ref. [22]
g_2^{α}	0.32839467	Ref. [22]
g_3^{α}	0.057918471	Ref. [22]
g_4^{α}	0.0023945101	Ref. [22]
g_5^{α}	-0.0026531689	Ref. [22]
g_6^{α}	0.16419734	Ref. [22]
g_7^{α}	0.17594802	Ref. [22]
g_8^{α}	0.0026531689	Ref. [22]
g_0^{κ}	0.22690751	Ref. [22]
g_1^{κ}	-0.075019750	Ref. [22]
g_2^{κ}	0.26442913	Ref. [22]

When different thermodynamic models are used to describe the fluid and the solid properties of a system, special consideration must be given to the so-called thermodynamic consistency. Models are thermodynamically consistent if they predict the same value for all thermodynamic properties at the points where regions of different phase behavior overlap (i.e. points where coexisting curves are connected). As a result, the solid-fluid models which are going to be the result of coupling the solid and fluid EoS have to be adjusted in a way, so that all properties are consistent at the specific points where this overlap occurs.

A "triple point" is the point where three phases are in equilibrium simultaneously. For a system with only one compound, only one triple point exists whereas when more compounds are present, the degrees of freedom are greater and as result there can be "triple lines" for binary systems etc. The triple point location and its properties are of great importance to the procedure of tuning the solid-fluid model to be thermodynamically consistent. That's because it is the point where the vapor-liquid (VL) equilibrium line is connected with the solid-vapor (SV) and the solid-liquid (SL) lines of a pure compound. This point of overlapping phase behavior is used to "anchor" the solid and fluid models.

In order to make the solid and fluid models thermodynamically consistent, parameters g_0 and g_1 are adjusted in a way that the Gibbs free energy of all phases (vapor, liquid and solid) is the same at the triple point. This is done by solving the system of Eqs. (2.24) and (2.25) with respect to g_0 and g_1.

$$\Delta h^{melt} = h^{sol}(T_{tr}, P_{tr}) - h^{liq}(T_{tr}, P_{tr}) \tag{2.24}$$

$$s^{sol}(T_{tr}, P_{tr}) = s^{liq}(T_{tr}, P_{tr}) - \frac{\Delta h^{melt}}{T_{tr}} \tag{2.25}$$

The solution of the above equations requires certain derivatives of the Gibbs free energy which are not presented but the reader can refer to the original publication of Jager and Span[22] for more details. The melting enthalpy at the triple point of CO_2 is set equal to 8875 J/mol as suggested by Jager and Span who treated it as an adjustable parameter. The triple temperature is set equal to the experimental value of 216.592 K. The triple pressure is predicted by every model as the "intersection" of the solid-vapor and the vapor-liquid saturation curves.

The calculation of the equilibrium pressure of pure CO_2 at a specified temperature at SL or SV equilibrium conditions is performed by numerically integrating the Clausius-Clapeyron equation. This equation provides the means to evaluate the change of the phase equilibrium conditions from one equilibrium point to another. The basis behind the Clausius-Clapeyron equation is that at each equilibrium point the Gibbs free energy of each phase in equilibrium is the same and therefore, the differential along the equilibrium phase boundary is

zero. Based on this, it can be shown that the derivative of the pressure as a function of temperature along the phase equilibrium curve is given by Eq. (2.26) and it is a function of the enthalpy and volume difference between the phases in equilibrium.

$$\left.\frac{dP}{dT}\right|_{equil} = \frac{\Delta H}{T\Delta V} \tag{2.26}$$

Properties needed for model implementation:

- Parameters for a fluid EoS and the Jäger and Span pure CO_2 solid model.
- The value of the triple point temperature (T_{tr}) for pure CO_2.
- The value of the enthalpy of melting (Δh^{melt}) at the triple point for pure CO_2.

The basic assumption of the model is:

- The pressure effect on the solid fugacity is negligible due to the high solid density.

To extend the solid-fluid equilibrium calculations to multicomponent mixtures being at equilibrium with a pure CO_2 solid phase, Eq. (2.9) has to be applied. The difference with the correlation model is that in this case the pure CO_2 solid-fluid equilibrium pressure at a specified temperature is going to be provided by the Jager and Span EoS connected with the appropriate fluid EoS and not a fitted correlation to experimental saturation pressures.

3. Phase Equilibria Computation and Algorithms

3.1. Vapor – Liquid Equilibrium

3.1.1. Equilibrium and Phase Stability

The basis for the mathematical description of the multi-phase equilibrium problem has been given by the seminal work of Gibbs who originally formulated the laws of equilibrium thermodynamics for open systems. Gibbs defined the list of variables along with the set of relations between them. These variables are the extensive and the intensive properties of each phase. Depending on the particular conditions, it is convenient to choose a different set of independent variables and use the corresponding relations to evaluate the remaining. Although there is a relative freedom to choose which variables to consider as independent, their number is strictly set by the Gibbs phase rule, according to which, the thermodynamic equilibrium state of a (non-reactive) system consisting of P phases and C components, is uniquely specified, if C – P + 2 independent variables are set.

The origin of the thermodynamic relations that govern phase equilibrium can be traced back to the first and the second law of thermodynamics for a closed system, where entropy, as an extensive and convex function of volume and energy, takes a maximum value for any given value of these variables. The vast majority of the solution schemes reformulates the problem of entropy maximization to an equivalent optimization problem of another thermodynamic potential and solves it by means of local optimization methods or nonlinear equations system solving techniques. The local properties of the thermodynamic potential in use produce the set of independent equations for the solution of the phase equilibrium problem and provide the local stability criteria.

Solving a two phase multi-component equilibrium problem requires equilibration of the chemical potential (μ) (or equivalently the fugacities) for all C components, for the same temperature (T) and pressure (P):

$$T^v = T^l \tag{3.1}$$

$$P^v = P^l \tag{3.2}$$

$$\mu_i^v = \mu_i^l, \qquad i = 1,2 \dots C \tag{3.3}$$

Given that μ can be expressed as a function of pressure, temperature and composition for each phase, the equality of the chemical potentials results in a relation between the mole

fractions and the fugacity coefficients of every component in the vapor (v) and liquid (l) phase, respectively[8]:

$$\mu_i^v = y_i^v \hat{\varphi}_i^v P^v = x_i^l \hat{\varphi}_i^l P^l = \mu_i^l, \qquad i = 1,2 \dots C \tag{3.4}$$

The condition of equal fugacities is only a necessary condition for phase equilibrium to exist though. Except for the satisfaction of Eq. (3.4), the corresponding phases have to be stable at the current conditions of temperature and pressure. This happens, if and only if, the total Gibbs free energy of the system is at its global minimum.

The requirement for phase stability i.e. location of the global minimum of the Gibbs free energy is formally addressed by the introduction of the tangent plane distance criterion as demonstrated by Michelsen.[23]

The Gibbs free energy change when δn_i moles of a component i are transferred from a liquid to a vapor phase is given by:

$$\delta G = \left(\mu_i^v - \mu_i^l\right) \delta n_i \tag{3.5}$$

At the global minimum, the Gibbs free energy change must be zero for any transfer of material, if δn_i is infinitesimally small. If a phase of molar composition $\mathbf{z}$ and chemical potentials $\boldsymbol{\mu}(\mathbf{z})$ is considered and an infinitesimal amount δe of a new phase with composition $\mathbf{w}$ is formed, the change in Gibbs free energy is:

$$\delta G = \delta e \sum_{i=1}^{C} w_i(\mu_i(\mathbf{w}) - \mu_i(\mathbf{z})) \tag{3.6}$$

The original phase with composition $\mathbf{z}$ is stable when δG is non-negative for any positive δe and this necessary condition for stability is expressed mathematically as:

$$\sum_{i=1}^{C} w_i(\mu_i(\mathbf{w}) - \mu_i(\mathbf{z})) \geq 0 \tag{3.7}$$

for any composition $\mathbf{w}$. Eq. (3.7) is the tangent plane condition of Gibbs. It can be also shown that this condition is also a sufficient condition for stability.[12]

To verify the stability of a phase, it has to be ensured that the tangent plane distance is non-negative for all valid compositions. A computational approach can be based on the fact that if all its minima or at least the global minimum is non-negative, the tangent plane distance is non-negative everywhere. Upon minimizing the tangent plane distance from the Gibbs free energy surface in the composition space, we are looking for a set of compositions, that when in equilibrium, the tangent plane forms a convex hull with the surface.[24] A

representative example is shown in Figure 3-1 for the methane – n-butane mixture at 290 K and 5.5 MPa using the PC-SAFT equation of state.

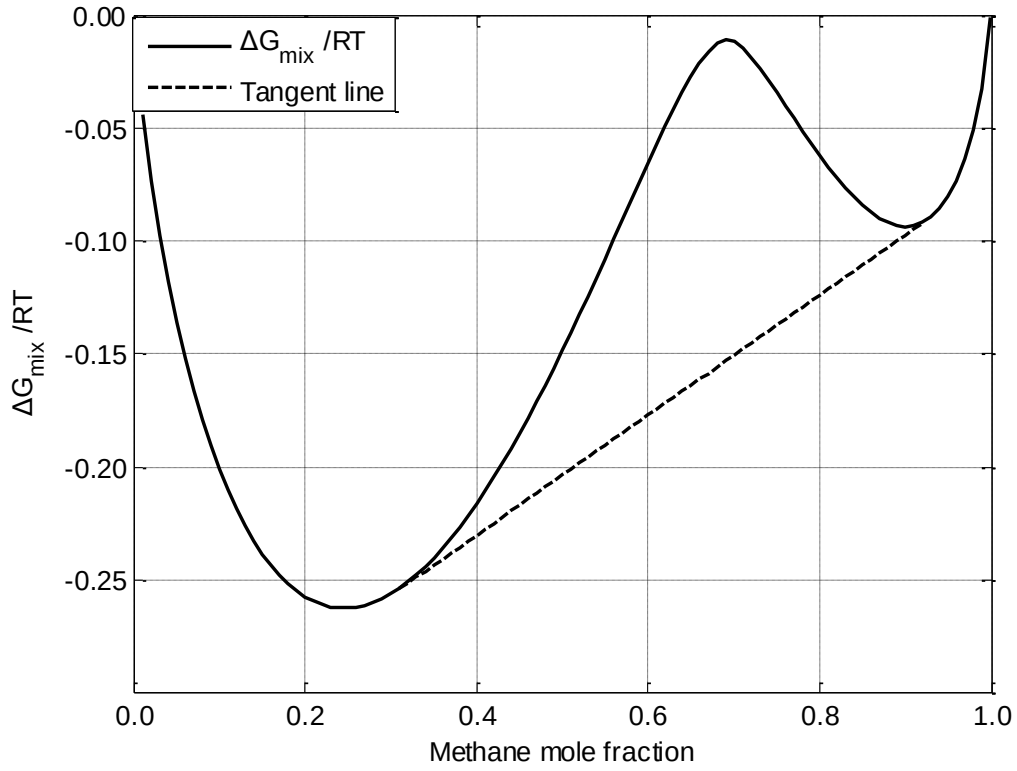

Figure 3-1: Tangent plane distance, ΔG_{mix}, calculated with the PC-SAFT EoS for the binary methane – n-butane mixture at 290 K and 5.5 MPa.

Locating a global minimum is far from trivial and has attracted the attention of many researchers. To this end, Floudas and co-workers have shown[25-29] that it is possible to recast the phase equilibrium problem in the form of the difference of two convex functions and by applying the "Branch and Bound" algorithm[30] to obtain global solutions for both the minimization of the Gibbs free energy and the tangent plane distance function. The topological analysis of the Gibbs free energy and global optimization methods for the phase stability problem has been the subject of extensive research and application to phase equilibrium calculations by various authors.[31-37]

The application of the tangent plane distance (TPD) criterion is not limited to testing the stability of a phase. A trial phase composition that yields a negative TPD can be also utilized to provide initial estimates for a flash calculation[12] (the flash calculation is discussed in the next section).

In this work, the TPD criterion has been applied to test the stability of a phase prior to a flash calculation, so that wasted calculations are avoided for single phase specifications and also to provide initial estimates for the flash when a phase is verified to be unstable. The

resulting phases are also tested for stability to ensure that cases of more than two phases being at equilibrium are not encountered.

The procedure followed to minimize the TPD is the one proposed by Michelsen[12], where the reduced tangent plane distance is modified accordingly, so that an unconstrained minimization formulation is possible:

$$Q(\mathbf{W}) = 1 + \sum_i W_i(\ln W_i + \ln\hat{\varphi}_i(\mathbf{W}) - d_i - 1) \tag{3.8}$$

where:

$$d_i = \ln z_i + \ln\hat{\varphi}_i(\mathbf{z}) \tag{3.9}$$

W_i are composition variables that are treated as mole numbers. The stationary points of Q satisfy:

$$\frac{\partial Q}{\partial W_i} = \ln W_i + \ln\hat{\varphi}_i(\mathbf{W}) - d_i = 0 \tag{3.10}$$

The solution of the set of equations defined by (3.10) can be performed by applying Newton's method for minimization or a simpler successive substitution method where the phase composition at iteration $k+1$ is determined from properties calculated at the composition of previous iteration:

$$\ln W_i^{(k+1)} = d_i - \ln\hat{\varphi}_i\left(\mathbf{W}^{(k)}\right) \tag{3.11}$$

The successive substitution method is the one used in this work to minimize the TPD and verify stability.

3.1.2. Isothermal Two-Phase Flash

Phase equilibrium calculations can be separated in two main categories: a) Flash calculations[23,38-40]: i.e. computations of the composition of the coexisting phases and the amount of each one of them given the temperature, the pressure and the overall composition of a non-stable mixture, b) Phase envelope calculations where the phase equilibrium boundaries are determined for a mixture with specified composition and phase fraction.

The isothermal flash is probably the most important equilibrium calculation, while the fixation of both temperature and pressure makes the flash a calculation for which a robust and reliable algorithm is easily written.[12] Also, a very important feature of this calculation is that the correct solution corresponds to the global minimum of the Gibbs free energy.

The most well-known methods for performing the flash calculation are a successive substitution method called the Rachford-Rice method and the direct Gibbs free energy minimization technique which utilizes composition derivatives of the fugacity coefficients.

The Rachford-Rice method is based on the iterative solution of Eq. (3.12) for the vapor fraction (β).

$$g(\beta) = \sum_{i=1}^{C} (y_i - x_i) = \sum_{i=1}^{C} z_i \frac{K_i - 1}{1 - \beta + \beta K_i} = 0 \tag{3.12}$$

The equation is usually solved by means of Newton's method, using:

$$g'(\beta) = -\sum_{i=1}^{C} z_i \frac{(K_i - 1)^2}{(1 - \beta + \beta K_i)^2} < 0 \tag{3.13}$$

where $K_i = \frac{y_i}{x_i}$ and from the equifugacity relation $K_i = \frac{\hat{\varphi}_i^l}{\hat{\varphi}_i^v}$.The function $g(\beta)$ is monotonically decreasing and a solution in the interval $(0,1)$ exists if:

$$g(0) = \sum_{i=1}^{C} z_i K_i - 1 > 0 \tag{3.14}$$

$$g(1) = 1 - \sum_{i=1}^{C} \frac{z_i}{K_i} < 0 \tag{3.15}$$

The liquid mole fractions (x_i) and the vapor mole fractions (y_i) are calculated at the solution using:

$$x_i = \frac{z_i}{1 - \beta + \beta K_i}, \qquad y_i = \frac{K_i z_i}{1 - \beta + \beta K_i} \tag{3.16}$$

The iterative procedure is initiated using initial estimates for the equilibrium compositions of the coexisting liquid and vapor phases, so that the K_i values can be calculated. In this work, the initial estimates for the K_i values are the result of a preceding stability analysis calculation which verifies the stability of the initial phase. If the feed phase is deemed to be unstable, the resulting K_i values are given as initial estimates to the flash calculation. This way, the Newton iterative procedure is initiated and after convergence the change in the K_i values is tested. If the difference between the K_i factors of the previous and the current iteration is higher than a preset tolerance, the calculation is repeated using the new values for K_i.

Michelsen[38] has shown that the convergence properties of the successive substitution method are identical to solving the complete set of equilibrium equations, using as independent variables the vapor phase amounts of every component, but neglecting specific terms of the Jacobian of the system. The set of equilibrium equations can be written as:

$$g_i(\mathbf{V}) = \ln\hat{f}_i^v - \ln\hat{f}_i^l = 0, \qquad i = 1,2 \dots C \tag{3.17}$$

The Jacobian for the set of the C coupled equations is given by:

$$J_{ij} = \frac{\partial g_i}{\partial V_j} = \frac{\partial \ln\hat{f}_i^v}{\partial V_j} - \frac{\partial \ln\hat{f}_i^l}{\partial V_j} \tag{3.18}$$

and after expansion of the derivatives:

$$J_{ij} = \frac{1}{\beta(1-\beta)}\left(\frac{z_i}{x_i y_i}\delta_{ij} - 1 + (1-\beta)\bar{\Phi}_{ij}^v + \beta\bar{\Phi}_{ij}^l\right) \tag{3.19}$$

$$\bar{\Phi}_{ij} = n_T \left.\frac{\partial \ln\hat{\varphi}_i}{\partial n_j}\right|_{T,P}, \qquad n_T = \sum_{k=1}^{C} n_k \tag{3.20}$$

Solving the set of equations defined in (3.17) and using the Jacobian of (3.19) is equivalent to solving the total Gibbs free energy minimization problem with the Hessian being identical to the Jacobian.

If the approximation of the successive substitution method is done, i.e. the fugacity coefficients are composition independent, the Jacobian can be replaced by the approximate expression[12]:

$$J_{ij}^A = \frac{1}{\beta(1-\beta)}\left(\frac{z_i}{x_i y_i}\delta_{ij} - 1\right) \tag{3.21}$$

The correction formula in Newton's method is given by:

$$\mathbf{V}^{(k+1)} = \mathbf{V}^{(k)} + \Delta\mathbf{V} \tag{3.22}$$

$$\mathbf{J}^A \cdot \Delta\mathbf{V} = -\mathbf{g}\left(\mathbf{V}^{(k)}\right) \tag{3.23}$$

Defining the error vector in the k^{th} iteration by $\mathbf{e}^{(k)} = \mathbf{V}^{(k)} - \mathbf{V}^{\infty}$, where $\mathbf{V}^{\infty}$ is the solution and subtracting $\mathbf{V}^{\infty}$ from Eq. (3.22), we get for the successive substitution method:

$$\mathbf{e}^{(k+1)} = \mathbf{e}^{(k)} - \left(\mathbf{J}^{A}\right)^{-1}\mathbf{g}^{(k)} \tag{3.24}$$

Using a Taylor series expansion of $\mathbf{g}$ from $\mathbf{V}^{\infty}$:

$$\mathbf{g}^{(k)} \cong \mathbf{g}^{\infty} + \mathbf{J}^{E}\left(\mathbf{V}^{(k)} - \mathbf{V}^{\infty}\right) = \mathbf{J}^{E}\mathbf{e}^{(k)} \tag{3.25}$$

where $\mathbf{J}^{E}$ is the exact Jacobian. Combining Eqs. (3.24) and (3.25) we get:

$$\mathbf{e}^{(k+1)} = \mathbf{e}^{(k)} - \left(\mathbf{J}^{A}\right)^{-1}\mathbf{J}^{E}\mathbf{e}^{(k)} = \left(\mathbf{I} - \left(\mathbf{J}^{A}\right)^{-1}\mathbf{J}^{E}\right)\mathbf{e}^{(k)} \tag{3.26}$$

$$\mathbf{M} = \mathbf{I} - \left(\mathbf{J}^{A}\right)^{-1}\mathbf{J}^{E} \tag{3.27}$$

Eq. (3.26) essentially implies that the error vector of the $(k + 1)^{th}$ iteration is the result of the effect of the $\mathbf{M}$ tensor on the error vector of the k^{th} iteration. The result of the effect of a tensor on a vector is the expansion of the vector on the tensor's normalized eigenvectors and the scaling of the occurring vector projections with the corresponding eigenvalue of every eigenvector. Mathematically this can be expressed as:

$$\mathbf{e}^{(k+1)} = \sum_{j} \lambda_j\left(\mathbf{u_j}\otimes\mathbf{u_j}\right)\mathbf{e}^{(k)} = \sum_{j} \lambda_j \mathbf{u_j}\cdot\left(\mathbf{u_j}\cdot\mathbf{e}^{(k)}\right) \tag{3.28}$$

As a result, a necessary condition for convergence of the successive substitution method is that the dominant eigenvalue of the $\mathbf{M}$ matrix must be smaller than unity. The error vector at the $(k + m)$ iteration will be:

$$\mathbf{e}^{(k+m)} = \sum_{j} \lambda_j \mathbf{u_j}\cdot\left(\mathbf{u_j}\cdot\mathbf{e}^{(k+m-1)}\right) \tag{3.29}$$

When m becomes sufficiently large, the error vector will be aligned with the eigenvector that corresponds to the largest eigenvalue (λ_{max}) and it will be given by:

$$\mathbf{e}^{(k+m)} \cong \lambda_{max}^{m}\mathbf{u}_{max}\cdot\left(\mathbf{u}_{max}\cdot\mathbf{e}^{(k+m-1)}\right) \tag{3.30}$$

Eq. (3.30) implies that the convergence of the iterative procedure is linear with a convergence factor being equal to λ_{max}. For non-ideal mixtures the dominant eigenvalue is almost invariably located in the interval $0 < \lambda_{max} < 1$ and this has as an important effect that the successive substitution method can only converge to stationary points that represent minima of the Gibbs free energy.[12]

3.1.3. Saturation Point Calculations

As it has already been mentioned, the phase envelope determination is a calculation where the phase equilibrium boundaries for a mixture with specified composition and phase fraction are determined at different temperatures and pressures and the traditional way of performing the task is as a series of isolated saturation point calculations. The most important cases are when the vapor fraction β is set equal to 0 (bubble point calculation) and when the vapor fraction β is set equal to 1 (dew point calculation).

The saturation point calculations can be categorized according to the different possible specifications:

- Bubble pressure: $(T^{spec}, \mathbf{x}^{spec}) \rightarrow (P, \mathbf{y})$
- Bubble temperature: $(P^{spec}, \mathbf{x}^{spec}) \rightarrow (T, \mathbf{y})$
- Dew pressure: $(T^{spec}, \mathbf{y}^{spec}) \rightarrow (P, \mathbf{x})$
- Dew temperature: : $(P^{spec}, \mathbf{y}^{spec}) \rightarrow (T, \mathbf{x})$

If the fugacity coefficients are composition independent, all types of calculations mentioned above reduce to solving only a single equation for T or P. At the bubble point ($\beta = 0$), the liquid phase composition $\mathbf{x}$ (which is equal to the feed phase composition $\mathbf{z}$) is set to a value $\mathbf{x}^{spec}$ and the vapor phase is calculated using the formula, $y_i = K_i x_i = K_i z_i$. The equation that has to be solved iteratively is:

$$f = \sum_{i=1}^{C} z_i K_i - 1 = 0 \tag{3.31}$$

Eq. (3.31) can be solved for T (bubble temperature calculation) or P (bubble pressure calculation). According to the calculation that is going to be performed, initial estimates for the vapor phase composition and for temperature or pressure are necessary to initiate the iterative procedure. Initial estimates can be obtained using the Wilson approximation[12]:

$$\ln K_i = \ln\left(\frac{P_{ci}}{P}\right) + 5.373(1 + \omega_i)\left(1 - \frac{T_{ci}}{T}\right) \tag{3.32}$$

If temperature is specified, Eq. (3.32) enables explicit solution of Eq. (3.31), so that an initial estimate for pressure can be obtained. Then, using Eq. (3.32) again, initial estimates for the K factors can be produced and as a result for the incipient phase composition. After the initial estimates have been produced, subsequent approximations are generated using Newton's method, assuming composition independent K factors. If pressure is specified, the iteration scheme has the following form:

$$\ln K_i^{(k)} = \ln \hat{\varphi}_i^{l}\left(\mathbf{z}, T^{(k)}\right) - \ln \hat{\varphi}_i^{v}\left(\mathbf{y}^{(k)}, T^{(k)}\right) \tag{3.33}$$

$$f^{(k)} = \sum_{i=1}^{C} z_i K_i^{(k)} - 1 \tag{3.34}$$

$$\frac{df^{(k)}}{dT} = \sum_{i=1}^{C} z_i K_i^{(k)} \left(\frac{\partial \ln \hat{\varphi}_i^{l}}{\partial T} - \frac{\partial \ln \hat{\varphi}_i^{v}}{\partial T} \right) \tag{3.35}$$

$$T^{(k+1)} = T^{(k)} - f^{(k)} / \frac{df^{(k)}}{dT} \tag{3.36}$$

$$y_i^{(k+1)} = z_i K_i^{(k)} \tag{3.37}$$

A similar approach is applicable for dew point calculations.

The aforementioned method for calculating saturation points is used traditionally for calculating phase diagrams at constant temperatures (P-xy diagrams) or pressures (T-xy diagrams) and different compositions of the feed phase. The rate of convergence is determined by the non-ideality of the incipient phase and when it is increased, convergence is slow. Moreover, at the critical point convergence becomes very slow and depending on the initial estimates, divergence of the iterative procedure is very common.

Finally, another diagram which has engineering interest is the isopleth phase diagram, where the phase boundary has to be determined at constant composition of the feed phase and different pressures and temperatures. The methods that have been discussed in this section can only determine specific parts of the complete isopleth because very accurate initial estimates are needed at certain points and also retrograde behavior is present. To overcome these difficulties, specific methods that have been proposed in the literature and also the newly developed “Bead Spring” method are going to be discussed in section 4.

3.2. Solid – Fluid Equilibrium

3.2.1. Two Phase Solid – Fluid Equilibrium

3.2.1.1. Thermodynamic Integration Model

Equations (2.20) for the solid – liquid and (2.21) for the solid – vapor equilibrium correlate the equilibrium pressure (P), temperature (T) and the solid former composition (x_i^F) at the fluid phase (liquid or vapor) in equilibrium with the pure solid. In principle, specifying the value of any two of these variables determines the value of the third. In this work, two types of algorithms have been developed. One that treats (P, T) as independent variables and calculates the composition (x_i^F) and another that treats (T, x_i^F) as independent variables and calculates the equilibrium pressure (P). In both cases however, the equations are highly non-linear and specialized methods must be used in order to obtain solutions in an efficient and robust fashion.

Input variables: (T, P) → output variable: (x^F)

When pressure and temperature are selected as independent variables then the fluid phase composition at equilibrium is calculated using a successive substitution method. For example, for the solid-liquid equilibria, the solubility is calculated using equation (2.20).

Initially, a guess value for the liquid phase composition is provided which is improved by an iterative scheme of the type:

$$x^{(k+1)} = g\left(x^{(k)}\right) \tag{3.38}$$

The liquid phase mole fraction of the solid former is updated successively using Eq. (2.20). The initial estimate for the composition of the liquid phase is necessary, so that the fugacity coefficients can be calculated with the use of the fluid EoS. Because of the assumption that the solid phase is comprised of only one component, for the case of a multicomponent liquid mixture, the mole fractions of the other components are updated by keeping fixed the ratio between them. The update of the mole fraction fractions for all the other components except for the solid forming compound is given by:

$$x_i^L\big|_{i\neq s}^{(k+1)} = x_i^L\big|_{i\neq s}^{(k)} + p_{i\neq s}\cdot \Delta x_s^{(k+1)} \tag{3.39}$$

$$p_{i\neq s} = \frac{x_i^L\big|_{i\neq s}^{(0)}}{\sum_{j=1,j\neq s}^{C} x_j^{L(0)}} \tag{3.40}$$

$$\Delta x_s^{(k+1)} = x_i^L\big|_{i=s}^{(k+1)} - x_i^L\big|_{i=s}^{(k)} \tag{3.41}$$

The same principle is applied for the solid – vapor equilibrium calculations. The equation however, is slightly different. The Newton method has also been applied in but it appears that for these specific calculations the successive substitution method converges faster.

Figure 3-2 represents a flow diagram depicting the sequence of calculations, when the successive substitution method is applied to calculate solid – liquid equilibria.

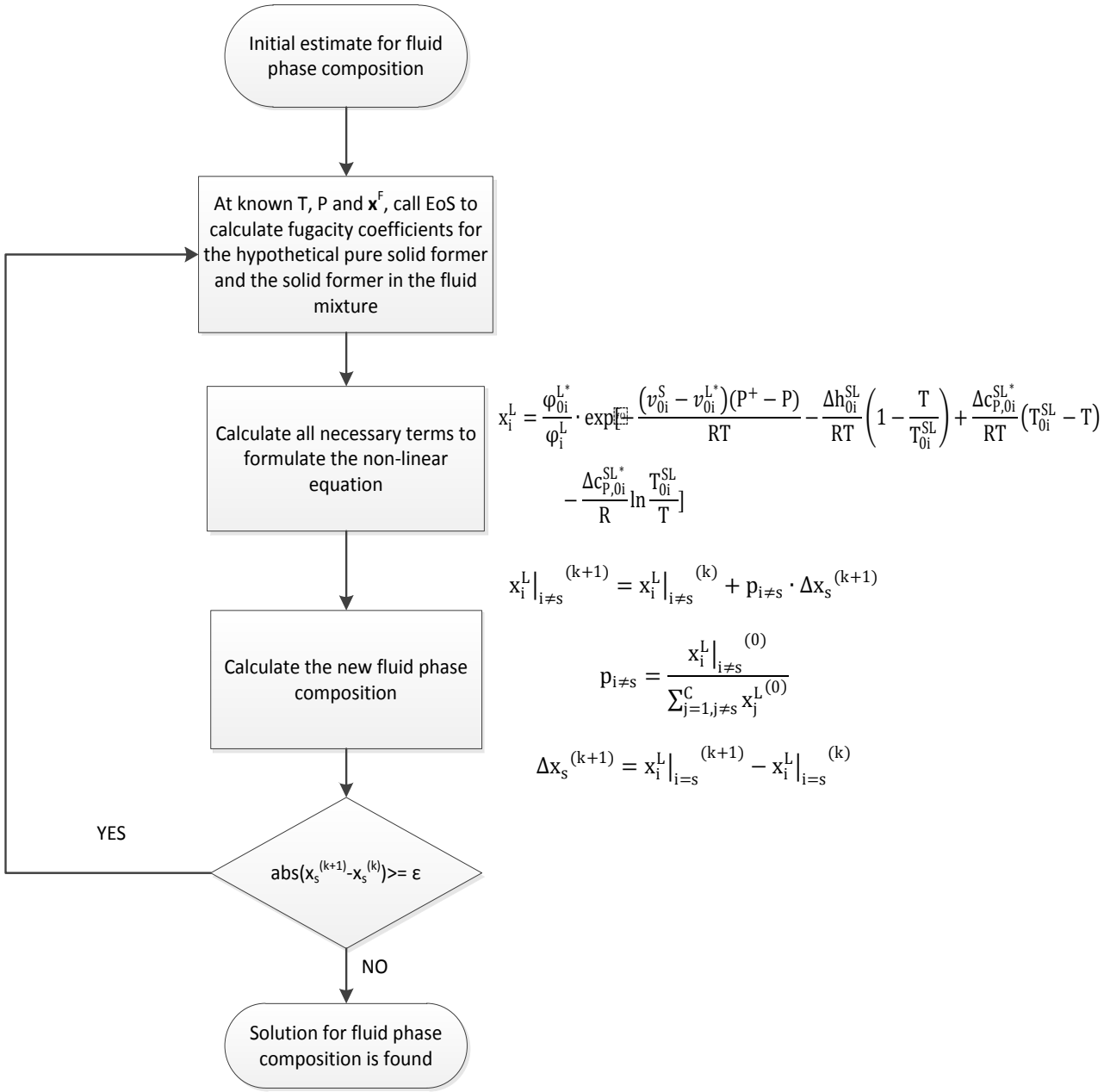

Figure 3-2: Flow diagram when the successive substitution method is used for solid – liquid equilibrium calculations.

Input variables: (T, x^F) → output variable: (P)

When temperature and fluid phase composition are used as input variables and the calculated quantity is the equilibrium pressure, the successive substitution method does not converge efficiently. The reason is that when the iterative scheme $P^{(k+1)} = g(P^{(k)})$ is applied, then:

$$\left|\frac{dg(P)}{dP}\right| > 1 \tag{3.42}$$

And, as result, the successive substitution method diverges. For this case, the Newton method has been applied and the derivative is calculated with the use of a forward difference scheme:

$$\frac{df(P)}{dP} = \frac{f(P+\varepsilon) - f(P)}{\varepsilon} \tag{3.43}$$

For the case of solid – liquid equilibrium, the equation $f(P) = 0$ that we wish to solve has the following form:

$$f(P) = \frac{\varphi_{0i}^{L^*}}{\varphi_i^L} \cdot \exp\left[-\frac{\left(v_{0i}^S - v_{0i}^{L^*}\right)(P^+ - P)}{RT} - \frac{\Delta h_{0i}^{SL}}{RT}\left(1 - \frac{T}{T_{0i}^{SL}}\right) + \frac{\Delta c_{P,0i}^{SL^*}}{RT}\left(T_{0i}^{SL} - T\right) - \frac{\Delta c_{P,0i}^{SL^*}}{R}\ln\frac{T_{0i}^{SL}}{T}\right] - x_i^L \tag{3.44}$$

For the case of solid – vapor equilibrium we have:

$$f(P) = \frac{\varphi_{0i}^{V^*}}{\varphi_i^V} \cdot \exp\left[-\frac{\left(v_{0i}^S\right)(P^+ - P)}{RT} - \ln\left[\frac{\varphi_{0i}^{V^*}(T,P)P}{\varphi_{0i}^{V^*}(T,P^+)P^+}\right] - \frac{\Delta h_{0i}^{SV}}{RT}\left(1 - \frac{T}{T_{0i}^{SV}}\right) + \frac{\Delta c_{P,0i}^{SV^*}}{RT}\left(T_{0i}^{SV} - T\right) - \frac{\Delta c_{P,0i}^{SV^*}}{R}\ln\frac{T_{0i}^{SV}}{T}\right] - x_i^V \tag{3.45}$$

In order to solve either Eq. (3.44) or Eq. (3.45), an initial estimate for the equilibrium pressure is needed. A good initial guess can be provided by using the ideal solution approximation, where the equilibrium pressure is given by:

$$P^{(0)} = \frac{P_{0i}^{sat}}{x_i^F} \tag{3.46}$$

Figure 3-3 represents a flow diagram depicting the sequence of calculations, when Newton's method is applied to calculate solid – fluid equilibria.

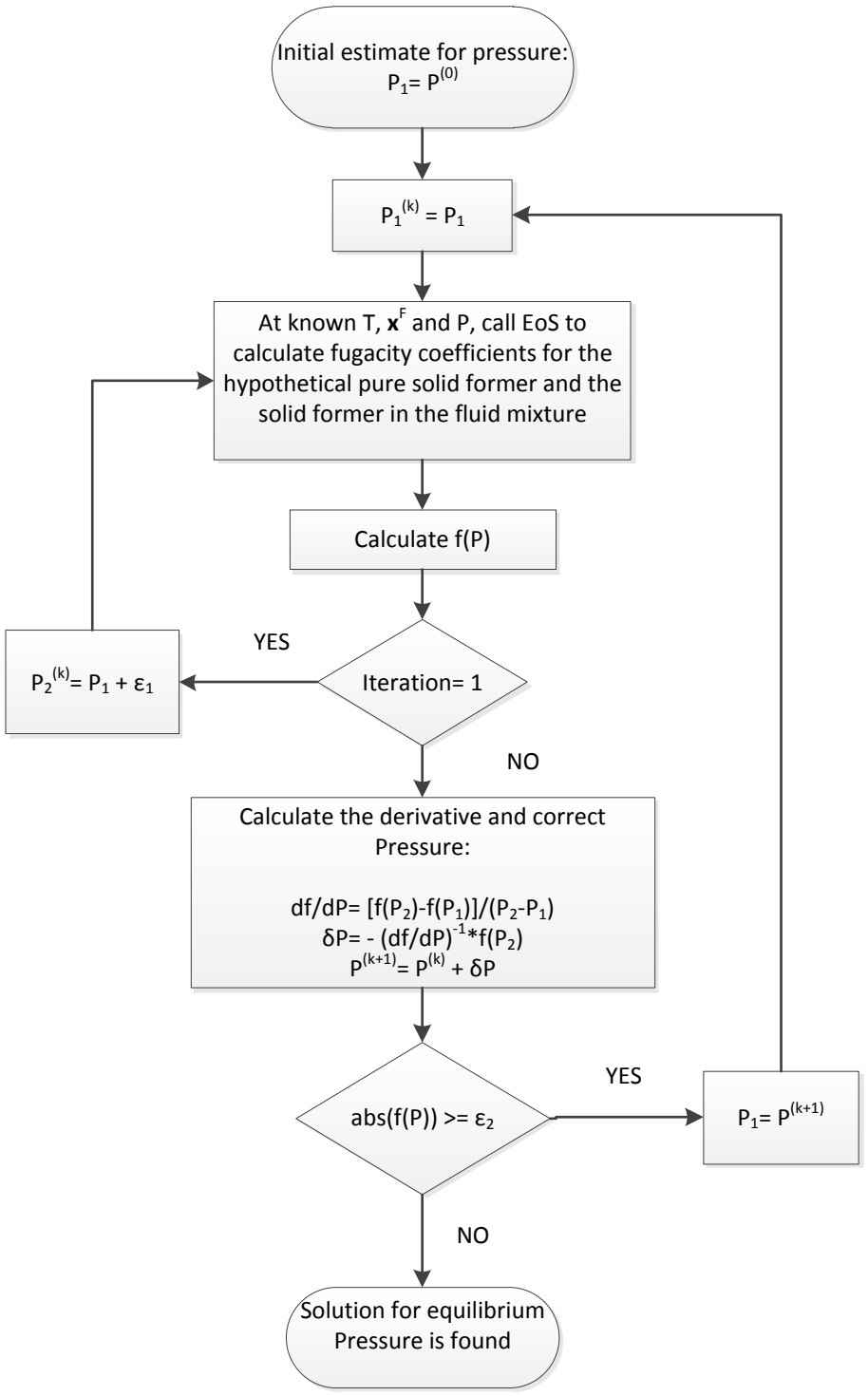

Figure 3-3: Flow diagram when Newton's method is used for solid – fluid equilibrium calculations.

3.2.1.2. Correlation, Jager and Span EoS Models

To calculate solid – fluid equilibria using the Correlation model discussed in section 2.2.1 and the Jager and Span solid EoS for CO_2 discussed in section 2.2.3, an iterative solution of Eq. (2.9) has to be applied. Similarly to the Thermodynamic Integration model, the corresponding equation can be solved with either temperature and pressure being set, or with specified temperature and composition of the fluid phase.

Input variables: (T, P) → output variable: ($\mathbf{x}^F$)

When temperature and pressure are set, Eq. (2.9) is rearranged accordingly and a successive substitution scheme is constructed:

$$x_i^{F(k+1)} = \frac{\widehat{\varphi}_{i0}^{sat}\left(T, P_{0i}^{sat}\right)P_{0i}^{sat}(T)}{P\widehat{\varphi}_i^F\left(T, P, \mathbf{x}^{F(k)}\right)} \exp\left[\frac{v_{0i}^S}{RT}\left(P - P_{0i}^{sat}(T)\right)\right] \tag{3.47}$$

Again an initial estimate for the composition of the fluid phase is necessary, so that the fugacity coefficients can be calculated with the use of the fluid EoS. The mole fractions of the other components are updated by implementing equations (3.39) - (3.41). The sequence of calculations in this case is the same with Figure 3-2 with the only difference being the terms that form the non-linear equation.

Input variables: (T, $\mathbf{x}^F$) → output variable: (P)

Contrary to the divergence of the successive substitution method when implemented at constant temperature and fluid phase composition for the Thermodynamic Integration model, it has been successfully applied to converge the Correlation and the Jager and Span models. The iterative scheme in this case takes the form:

$$P^{(k+1)} = \frac{\widehat{\varphi}_{i0}^{sat}\left(T, P_{0i}^{sat}\right)P_{0i}^{sat}(T)}{x_i^F\widehat{\varphi}_i^F(T, P^{(k)}, \mathbf{x}^F)} \exp\left[\frac{v_{0i}^S}{RT}\left(P^{(k)} - P_{0i}^{sat}(T)\right)\right] \tag{3.48}$$

Again in this case the initial estimate, provided by Eq. (3.46) is used to initiate the iterative procedure and convergence is achieved when $\text{abs}\left(P^{(k+1)} - P^{(k)}\right) \leq \varepsilon$.

3.2.2. Multiphase Solid – Fluid Equilibrium

Multiphase equilibrium refers to the simultaneous coexistence of three or more phases. There are different types of multiphase behavior which are characterized by the nature and the number of phases that coexist. Two are the most common types of multiphase equilibrium encountered in practice. The first one is characterized by a vapor phase, a liquid phase and one or more phases that consist of a pure component (e.g. solid phases, hydrate phases etc.) The second is characterized by the potential presence of two or more liquid phases at equilibrium with a vapor phase and more than one component is present at every phase in substantial amounts.

According to the type of calculation one wishes to perform, each multiphase equilibrium case requires special numerical treatment. Depending on the specified variables, a multiphase equilibrium problem can be a flash calculation, where at given T and P one seeks the compositions of the coexisting phases and the ratio between them, or the problem can take the form of tracing a phase boundary.

In this work, an algorithm for the calculation of the three phase solid – liquid – vapor (SLV) equilibrium boundary has been developed for binary mixtures. The basic equation that describes the three phase SLV equilibrium at constant temperature and pressure is:

$$\mu_i^S(T,P) = \mu_i^l\left(T,P,\mathbf{x}^l\right) = \mu_i^v(T,P,\mathbf{y}^v) \tag{3.49}$$

Eq. (3.49) leads to satisfaction of two independent equations, namely:

$$\begin{aligned} \mu_i^S(T,P) &= \mu_i^l\left(T,P,\mathbf{x}^l\right) \\ \mu_i^l\left(T,P,\mathbf{x}^l\right) &= \mu_i^v(T,P,\mathbf{y}^v) \end{aligned} \tag{3.50}$$

or:

$$\begin{aligned} \mu_i^S(T,P) &= \mu_i^v(T,P,\mathbf{y}^v) \\ \mu_i^l\left(T,P,\mathbf{x}^l\right) &= \mu_i^v(T,P,\mathbf{y}^v) \end{aligned} \tag{3.51}$$

The Gibbs phase rule for a binary system, where three phases are at equilibrium, dictates that there is only one degree of freedom to be set, so that the thermodynamic state is uniquely specified. In this work, an algorithm that calculates the three phase coexistence curve has been developed when pressure is set to a specific value ($P = P^{spec}$). The remaining unknown variables (i.e. $T, \mathbf{x}^l, \mathbf{y}^v$) are determined by combing an isothermal two phase flash calculation and the solution of a solid model for the fluid phase composition.

In this algorithm, the function of which the root we seek is given by the following equation:

$$f = \left| w_{s,Solid} - w_{s,Flash} \right| \tag{3.52}$$

where $w_{s,Solid}$ is the resulting mole fraction of the solid former in the fluid phase given by the iterative solution of a solid - fluid model at constant temperature and pressure and $w_{s,Flash}$ is the mole fraction of the solid former in the vapor or the liquid phase given by the solution of the isothermal flash. If one chooses to solve Eqs. (3.50), $w_{s,Solid}$ and $w_{s,Flash}$ are going to be the mole fractions of the solid former in the liquid phase given by the two different calculations, whereas they are going to be the vapor phase mole fractions if one chooses to solve Eqs. (3.51).

The root of Eq. (3.52) is determined by setting an initial estimate for the equilibrium temperature and this value is corrected by applying Newton's method. When the temperature corrections are applied, the flash calculation and the solid – fluid equilibration model are solved again for the new temperature and this way the fluid phase compositions are updated accordingly. When the resulting mole fractions of the solid former in the fluid phase of the two different calculations become equal, the solution has been found.

The derivative of Eq. (3.52) with respect to temperature is calculated by using a forward difference scheme. The resulting temperature corrections from Newton's method, especially in early iterations, may produce large steps that can lead to conditions where the flash calculation returns one stable phase (rather than a liquid and a vapor phase at equilibrium), or to conditions very far away from the solution. This has as a result divergence of the method and subsequent crash of the code. To remedy this behavior, it is a good choice to give as feed composition ($\mathbf{z}$) to the flash, initially at least, 0.5 mole fraction to every component in the mixture. This has a result that the isopleth VL phase envelope will be wider and there are better chances for the flash not to encounter one phase conditions. Moreover, to avoid overstepping, a successive under relaxation scheme is applied to the temperature corrections and has the form:

$$\begin{gathered} \hat{T}^{(k+1)} = T^{(k)} - f\left(T^{(k)}\right) \cdot \left(\frac{df}{dT}\right)^{-1} \\ T^{(k+1)} = q \cdot \hat{T}^{(k+1)} + (1-q) \cdot T^{(k)} \\ 0 < q \leq 1 \end{gathered} \tag{3.53}$$

The flash calculation may encounter one phase conditions during the iterations even if the initial feed composition is 0.5 for every component. If this is the case, a good choice is to

equate the feed phase composition with the resulting fluid phase composition given by the solid – fluid equilibration of the previous iteration. Figure 3-4 represents a flow diagram of the implementation algorithm when the solution is going to be performed using Eq. (3.51), although the same principle is applied to Eq. (3.50).

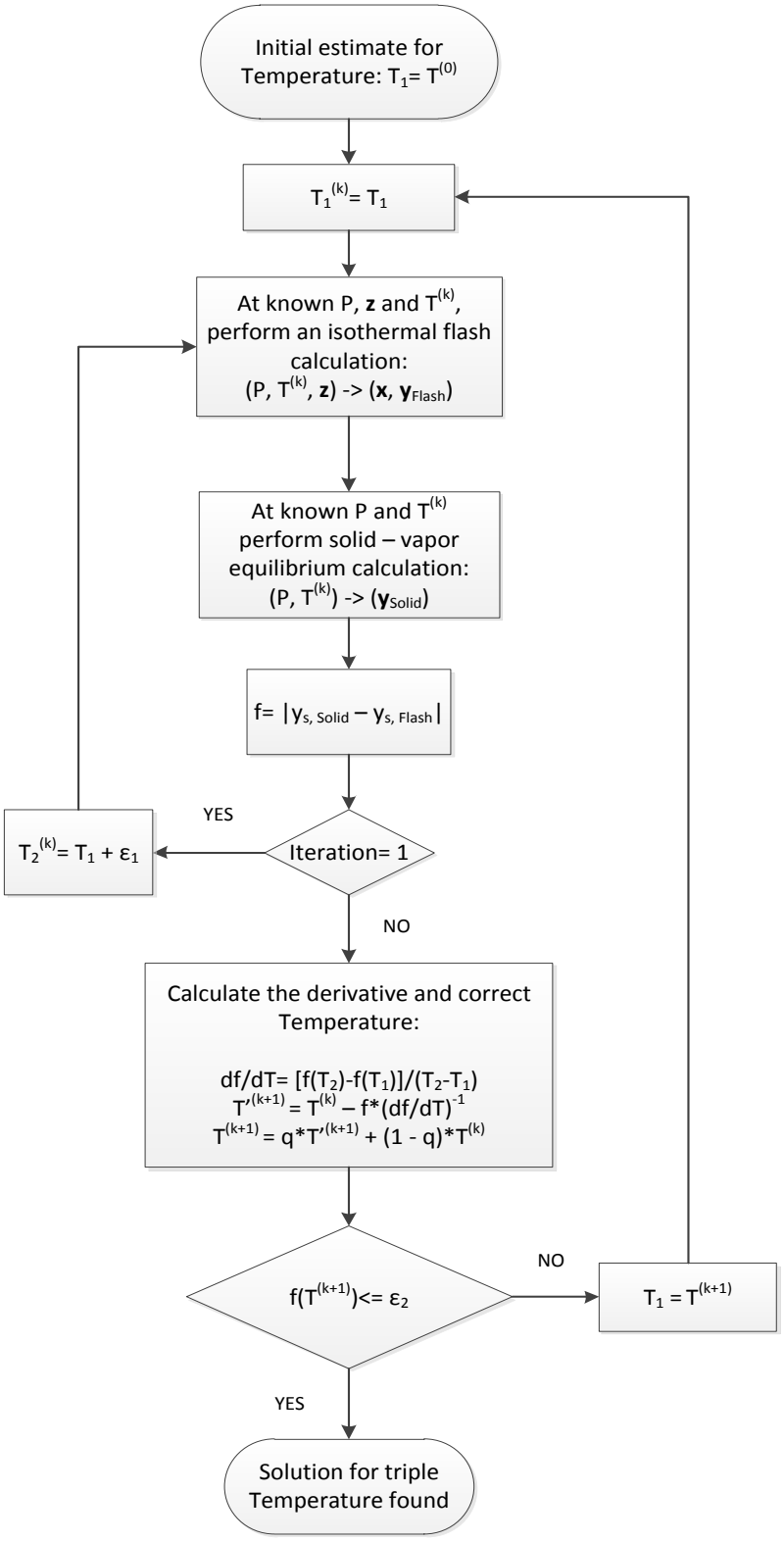

Figure 3-4: Flow diagram for the solid – liquid – vapor equilibrium calculation algorithm

4. The "Bead Spring" Method

4.1. Introduction

Accurate and robust prediction of the phase equilibrium boundaries of multicomponent mixtures is important for the design, simulation and optimization of various processes in oil & gas and chemical industry. A plethora of approaches to tackle the problem have been proposed, which differ in the formulation of the problem, the numerical scheme used and the details of the implementation.[36,41-43]

In this case where we are interested in tracing a coexistence line, it is a common practice to start from an equilibrium point and then use the information at this point to extend the boundary curve. A characteristic example of such a calculation is the use of the Clausius-Clapeyron differential equation resulted from the Gibbs-Duhem relation in the evaluation of a pure component pressure – temperature phase diagram.[44]

Although it is possible to device a numerical scheme that solves Gibbs-Duhem based differential equations for specific phase equilibrium problems, most of the methods proposed in the literature[41-43,45-47] perform a direct computation of the equilibrium for the thermodynamic conditions of interest (equilibrium point). For the multi-component problem, usually a pre-calculated equilibrium point is used to get a reasonable estimate of the thermodynamic variables for the next equilibrium point and in this stepwise fashion the phase envelope is traced. The main problem still is that unlike the case of a pure component, in multi-component mixtures the pressure - temperature phase boundary is non-monotonic and in many cases is characterized by the presence of local extremes of temperature as a function of pressure and the pressure as a function of temperature, i.e. the cricondentherm and the cricondenbar points. Tracing the phase boundary in the vicinity of these points needs special attention due to the divergence of some of the thermodynamic derivatives.

In this work, a variation of the algorithm introduced by Michelsen[41] for tracing the pressure - temperature isoplethic phase diagrams has been developed. In the proposed scheme, one of the equations of the original method has been modified, where the value of one independent variable was set using an extrapolation scheme, based on a "spring" that sets the slope value of the modified tangent plane distance in respect to either temperature or pressure and guides the estimation of the equilibrium curve extension.

4.2. Problem formulation

The equifugacity relation has been used extensively for the mathematical construction of methods that iteratively solve the non-linear two phase equilibrium problem. The most well- known method is the one proposed by Michelsen[41] where $C + 2$ non-linear equations are solved simultaneously with Newton's method. The equations which are utilized are the C equifugacity relations and two more equations, namely the explicit elimination of the constraint that mole fractions have to add to 1 and the *specification equation*. The non-linear equation set is:

$$f_i = \ln K_i + \ln\hat{\varphi}_i^v - \ln\hat{\varphi}_i^l = 0, \qquad i = 1, 2 \dots C \tag{4.1}$$

$$f_{C+1} = \sum_{i=1}^{C} (y_i - x_i) = 0 \tag{4.2}$$

$$f_{C+2} = X_S - S = 0 \tag{4.3}$$

It should be noted that in this type of calculation (tracing a coexistence line), Eq. (4.2) is ensured to be fulfilled only if the mole fractions y_i and x_i add up to one, because at every point one of the two composition vectors is set. When a constant phase fraction line is calculated other than the boundary ones, the composition vectors are connected through Eq. (B4). As a result, these two vectors are not simultaneously independent. The independent variables are chosen to be $\ln K_i \left(K_i = \frac{y_i}{x_i}\right)$, lnT and lnP, so that negative values of mole fractions are avoided and the specification variable (X_S), which is one of the elements of the unknown variables' vector (**X**), is set to a specified value (S). To produce initial estimates for the next equilibrium point, an Euler-Newton predictor – corrector continuation procedure is applied. At each calculated point, the derivatives of every variable with respect to the specification variable ($\frac{\partial \mathbf{X}}{\partial S}$) are computed, so that a linear extrapolation (Euler predictor) scheme can be utilized to produce initial estimates for the next point:

$$\frac{\partial \mathbf{f}}{\partial \mathbf{X}} \frac{\partial \mathbf{X}}{\partial S} + \frac{\partial \mathbf{f}}{\partial S} = 0 \tag{4.4}$$

$$\mathbf{X}(S + \Delta S) = \mathbf{X}(S) + \frac{\partial \mathbf{X}}{\partial S} \Delta S \tag{4.5}$$

After the initial estimates have been produced, the Newton's method (Newton corrector) is used for final convergence. The sensitivity vector $\frac{\partial \mathbf{X}}{\partial S}$ is obtained as the solution of the linear system defined in Eq. (4.4), where $\frac{\partial \mathbf{f}}{\partial \mathbf{X}}$ is the Jacobian for the system of equations (4.1) to (4.3) and hence available since Newton's method is used for solving the equations set.

The method used in this work to solve the linear systems is the LU decomposition method, where a matrix is decomposed to an upper and a lower triangular and this way a factorization of the initial matrix is possible. The LU decomposition method is particularly effective in this calculation because the Jacobian is already factorized at the solution of the non-linear problem and a second inversion of the matrix to solve Eq. (4.4) is avoided. As a result, the solution of Eq. (4.4) requires only a forward and a backward substitution.

When at least two equilibrium points have been computed, a third degree polynomial can be used for accurate interpolation and extrapolation. The specification variable is chosen to be at every point the variable with the largest sensitivity, so that turning points (infinite derivatives) in phase space are avoided.

Michelsen[48] has shown that phase equilibrium points of a C component system can be calculated by finding the stable roots of the modified tangent plane distance equation:

$$Q[\mathbf{w}, P, T] = 1 - \sum_{i=1}^{C} w_i + \sum_{i=1}^{C} w_i\{\ln(w_i) + \ln(\hat{\varphi}_i[\mathbf{w}, P, T]) - \ln(z_i) - \ln(\hat{\varphi}_i[\mathbf{z}, P, T])\} = 0 \qquad (4.6)$$

where **z** is the composition of the feed phase, and **w** is the composition of the incipient phase. Alternatively, the conditions of the phase boundary can be recovered by setting a similar Q* function equal to zero:

$$Q^*(\mathbf{w}, P, T) = 1 - \sum_{i} \frac{z_i \hat{\varphi}_i[\mathbf{z}, P, T]}{\hat{\varphi}_i[\mathbf{w}, P, T]} \qquad (4.7)$$

The condition of equal fugacity in both phases is equivalent to the condition that the functions Q or Q* are set to zero and at the same time the root is a stationary point. Furthermore, it is possible to construct a variety of similar functions to formulate the phase equilibrium problem, by combining basic equilibrium relations. Since Q is always zero along the coexistence curves, it follows that the pressure - temperature relation will satisfy the expressions:

$$\left.\frac{dP}{dT}\right|_{Q=0} = -\frac{\partial Q/\partial T}{\partial Q/\partial P} \qquad (4.8)$$

$$\frac{\partial Q}{\partial P} = \sum_{i=1}^{C} w_i \left(\frac{\partial \ln \hat{\varphi}_i(\mathbf{w})}{\partial P} - \frac{\partial \ln \hat{\varphi}_i(\mathbf{z})}{\partial P} \right) \tag{4.9}$$

$$\frac{\partial Q}{\partial T} = \sum_{i=1}^{C} w_i \left(\frac{\partial \ln \hat{\varphi}_i(\mathbf{w})}{\partial T} - \frac{\partial \ln \hat{\varphi}_i(\mathbf{z})}{\partial T} \right) \tag{4.10}$$

The use of the tangent plane criterion has also been extended to the calculation of saturation pressures or temperatures of a homogeneous phase by Nghiem and Heidemann.[42] The necessary equations describing the cricondenbar and cricondentherm in terms of the distance from the Gibbs free energy surface to the tangent plane were also derived, and a scheme for computing these points of interest was given.

Another well-known approach for calculating constant composition phase envelopes of multicomponent mixtures is the one proposed by Ziervogel and Poling.[47] The method consists of calculating dew and bubble points throughout the critical and retrograde regions by stepping around the envelope in suitably small increments of T or P. These dew and bubble points are calculated by applying Newton iterations on a single variable, namely the temperature or the pressure and the compositions are updated with successive substitution. The authors presented also the criteria which allow determination of whether the iteration variable should be T or P. The performance of this method was demonstrated with only closed loop phase envelopes. Nichita[49] constructed a reduction method for calculating multicomponent mixtures phase envelopes and used for his calculations the approach of Ziervogel and Poling, but also proposed specific sequences of choosing the iteration variable for mixtures with open-ended dew lines with one critical point or zero critical points.

Ortiz-Vega et al.[45] extended the method proposed by Iglesias-Silva et al.[50] which is a Gibbs minimization technique that requires only the solution of a set of algebraic equations to determine phase boundaries. The calculation of the coexistence curve in this method is also driven by the dimensionless criterion proposed by Ziervogel and Poling.[47]

At this point, it is important to note that most EoS do not provide a direct relationship for the fugacity coefficient as a function of pressure and temperature, but as a function of density and temperature. This results in extra complexity in the implementation of the phase equilibrium scheme since the calculation of density as a function of pressure is required for each phase.

Alternatively, Quiñones-Cisneros and Deiters[43] proposed to solve the multi-component phase equilibrium problem by using a density (ρ) representation, where the condition for equalization of pressure is given from the expression:

$$\sum_{i=1}^{N}\left(\frac{\partial\Psi^{v}}{\partial\rho_i}\right)\rho_i^{v}-\sum_{i=1}^{N}\left(\frac{\partial\Psi^{l}}{\partial\rho_i}\right)\rho_i^{l}=\Psi^{v}-\Psi^{l} \tag{4.11}$$

while the equilibration of chemical potentials is expressed as:

$$\mu_i^{v}=\left.\frac{\partial\Psi^{v}}{\partial\rho_i}\right|_{T,\rho_{j\neq i}}=\left.\frac{\partial\Psi^{l}}{\partial\rho_i}\right|_{T,\rho_{j\neq i}}=\mu_i^{l},\quad i=1,2\ldots C \tag{4.12}$$

, where Ψ^{v} and Ψ^{l} are the Helmholtz free energies per unit volume for the two coexisting phases.

In this work, a variation of the procedure introduced by Michelsen[41] for tracing the isoplethic bubble and dew lines has been proposed, by performing minimization of the modified tangent plane distance along the phase boundary line. As shown by Venkatarathnam,[46] it is potentially preferable to alter the specification equation and use instead a variable that is not present in the independent variables vector (**X**) in order to achieve monotonic behavior during the tracing of the phase boundary. In contrast to the method proposed in the literature, in our implementation the extrapolation of the phase boundary is achieved by setting one of the thermodynamic state variables to an extrapolated value driven with the help of a "spring" that sets the slope value of the modified tangent plane distance with respect to either temperature or pressure.

4.3. Tracing the phase boundary with the bead spring method

The discussion in the previous section elaborated the most well-known methods for calculating constant composition phase envelopes of multicomponent mixtures and also, the fundamental mathematical relations that apply to the calculation of phase boundary lines. In this section, the proposed scheme called bead spring method will be presented in detail. The non-linear set of equations that has to be solved for a C component mixture consists of Eqs. (4.1), (4.2) and:

$$f_{C+2}=\frac{\partial Q}{\partial P}+\theta\cdot\left(S_{l+1}^{est}-2S_l+S_{l-1}\right)=0 \tag{4.13}$$

, where $S=T$ or P. A detailed description of the derivation of Eq. (4.13) is given in Appendix A. The independent variables' vector (**X**) consists of the natural logarithms of the K-values, the temperature and the pressure, so that negative values of these variables are avoided. Generally, calculations can be initiated either from the bubble or the dew line. Cases of phase behavior where one of the two choices is better behaved are going to be discussed. In the case

where the calculation is initiated from the dew line, the feed phase **z** is set equal to the vapor phase **y** and the incipient phase **w** is set equal to the liquid phase **x**. The opposite holds for the bubble point. Depending on the input value of the vapor fraction (β), in the proposed scheme the calculation may start either from a bubble or a dew point. When β is set equal to 0, the calculation starts from a bubble point and when it is set equal to 1, the calculation starts from a dew point. The value of the vapor fraction is kept constant along the entire isoplethic phase envelope trace.

The proposed replacement of the specification equation that is used in this scheme is Eq. 15, where S_{l-1} is the calculated specification of the previous point (l-1), S_l is the unknown specification of the current point (l) , θ is a parameter regulated by the user, and S_{l+1}^{est} is an implicit specification (estimate), given by:

$$S_{l+1}^{est} = S_{l-1} \pm \delta S \tag{4.14}$$

Figure 4-1 represents a flow diagram of the implementation algorithm for the proposed method when the calculation of the phase envelope starts from the dew point branch.

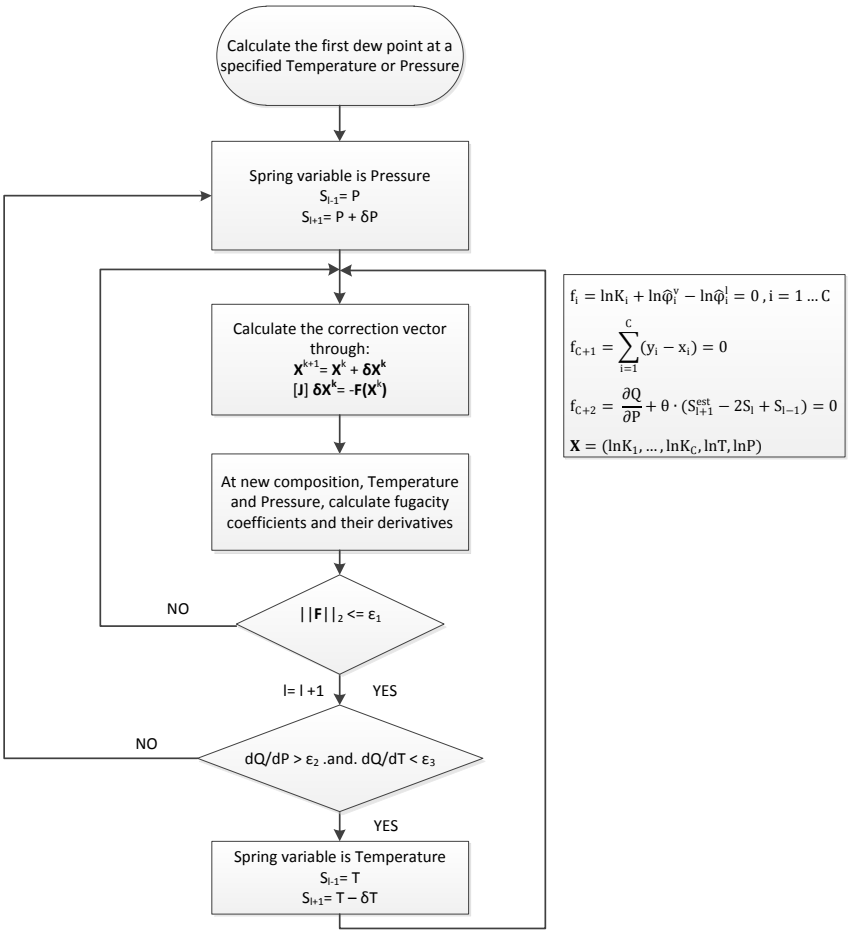

Figure 4-1: Flow diagram of the implementation algorithm for the proposed method.

The sequence of calculations is initiated by specifying a dew point at a specified temperature or pressure where convergence is easily achieved. This point is calculated by performing a number of steps with the successive substitution method, followed by the full Newton's method for final convergence.[12] Once the initial point is calculated, every next point is calculated using as initial estimates the composition, the temperature and the pressure of the previous point and the coexistence curve is further extended using the bead spring method.

In the proposed scheme, using S_{l-1} for the converged pressure or temperature of the previous calculated equilibrium point and S_{l+1}^{est} for a pressure or temperature estimate, the unknown specification S_l is bounded. In this way, the final specification value of the current point after convergence will lie between the two specifications, S_{l-1} and S_{l+1}^{est}. The specifications used in the proposed method are the temperature or the pressure of every equilibrium point, while the use of either of those as specification variables depends on the location of every point. When the calculations are initiated from the dew line, pressure is used initially as specification and it is increased, so that $S_{l+1}^{est} = S_{l-1} + \delta S$, up until the cricondenbar of the mixture. Then, the specification variable is changed to temperature and is decreased until the entire retrograde region and the bubble line are calculated.

If the calculations were to be initiated from the bubble line, temperature would be used as the first specification variable and it would be increased up until the cricondentherm point. Then, S would change to pressure and would decrease until the entire dew line is traced. In general, starting the calculations from the dew line is very useful for mixtures other than those which exhibit Type I phase behavior[51] and have open ended dew lines. For Type I mixtures, the calculations can be initiated either from the dew line or the bubble line.

For the calculation of every equilibrium point, Newton iterations are performed where the calculation of the Jacobian of the $C + 2$ nonlinear equations is needed. The first $C + 1$ equations are identical to those of the method proposed by Michelsen[41] and as a result, the $(C + 1) \times (C + 1)$ part of the Jacobian is the same. The elements of the last row of the matrix are different and the derivatives of the f_{C+2} equation with respect to the natural logarithm of K-values, temperature and pressure are needed. A comprehensive presentation of the Jacobian of the aforementioned equations can be found in Appendix B. On the k^{th} iteration of the Newton method for the calculation of every equilibrium point, the independent variables vector $\mathbf{X}$ is updated using the correction formula:

$$\mathbf{X}^{k+1} = \mathbf{X}^{k} + \delta\mathbf{X}^{k} \tag{4.15}$$

$$\delta \mathbf{X}^{k} = -\left[\frac{\partial \mathbf{F}}{\partial \mathbf{X}}\right]^{-1} \mathbf{F}(\mathbf{X}^{k}) \tag{4.16}$$

When a correction is applied on the **X** vector, the K-values of the components, pressure and temperature are updated and as a result, fugacity coefficients and their derivatives with respect to temperature, pressure and composition have to be reevaluated.

The corrections are repeated until final convergence using as convergence criterion the Euclidean norm of the non-linear equations vector ($\|\mathbf{F}\|_2$). The precision used for the calculations in this work was 10^{-9}. When an equilibrium point is calculated, the criterion for the spring variable is tested and if it is satisfied, the spring variable is changed and an appropriate implicit step is taken. If the criterion is not satisfied, the calculations proceed with the same spring variable.

Every equilibrium point can be considered as a bead connected with springs with the two immediate neighboring beads. The θ parameter represents the stiffness of the springs and its value affects the resulting position of every calculated point on the phase envelope, as well as the convergence rate of the method. Moreover, choosing correctly the implicit step δS and the criterion for changing the spring variable from pressure to temperature and vice versa tunes the number of calculated points as well as the distance from the adjacent points. Indicative values for these parameters are given in the results and discussion section.

4.4. Step characteristics in the bead spring method

Using Eq. (4.13) as the specification equation enables the method to converge in the retrograde region with pressure or temperature being implicitly specified. In the existing method of Michelsen, specifying either of these two variables in the vicinity of the critical point or in the retrograde region causes the iterative procedure to diverge or lead to a trivial solution and as a result, a subsequent breakdown.[12] To fix this problem, the specified variable is chosen to be the one for which the magnitude of the sensitivity is the largest. In this manner, all elements of the sensitivity vector are limited in magnitude to about 1. A disadvantage in this approach is that incomparable quantities like pressure and K-values have to be compared. The automatic selection in most cases leads to selection of lnK for the least or the most volatile component in the mixture.[12] In the proposed method, the need to specify the most sensitive variable is eliminated. As a result, there is no need to calculate and compare the sensitivities between pressure, temperature and K-values which results in the tedious work of setting specific step magnitudes according to the different possible specifications. One more complicating factor about setting the steps is that when many

different mixtures need to be studied, the K-values may be very different and as result, a small step for a particular mixture may be large enough for another mixture.

The method of taking implicit steps on temperature and pressure as described so far implies that the proposed method uses as initial estimates for the calculation of every point, the solution from the previous converged equilibrium point. This means that the calculations can be performed without the need of extrapolations as a prerequisite like the other methods that have been proposed so far. The only exception is the density marching method proposed by Venkatarathnam,[46] which is able to trace the vapor – liquid phase envelope with or without the use of extrapolations.

4.5. Convergence approach at near critical conditions and for double retrograde calculations

All the different methods for calculating the phase envelope of fluid mixtures share a common characteristic related to the treatment of near critical calculations to avoid breakdown. A widely adopted approach is to bypass the critical point based on an indication for a potential breakdown. One common indicator is the number of iterations needed for convergence of the method at an equilibrium point. Depending on the quality of the initial estimates, 2 to 4 iterations are efficient to achieve convergence far from the critical point. If the number of iterations needed for convergence exceeds a predefined lower limit, this is an early indication that the current point is in the vicinity of the critical point and so a larger step for the next point may be tried in order to avoid the problematic region. In addition, if the number of iterations during convergence becomes larger than a pre-set upper limit, the current point is abandoned and a different step is taken to trace the phase envelope. In this way, all types of phase envelopes can be traced starting from a dew point line, passing through the critical point and proceeding to the bubble line. Moreover, the handling described above also works for open-ended dew lines and multiple critical points. Nevertheless, the values for the lower and higher limits are rather empirical since every method has different convergence behavior and, moreover, it obviously depends on the quality of initial estimates.

In the proposed scheme, a different indicator is used to identify and handle possible failures i.e. the reduction of the residual during convergence. Away from the critical point, the method converges after 3 to 4 iterations when the solution of the previous converged point is used as an initial estimate while the implicit steps are mentioned in Table 4-1. Depending on the fluid mixture and the shape of the P-T diagram, larger steps can be taken and still the method will converge within 3 or 4 iterations. Close to the critical point the number of iterations becomes larger (usually varying from 10 to 70) with the residual performing significant oscillations. To control this behavior and to avoid breakdown, the proposed

implementation tracks the residual along the iterations enforcing its reduction. If the value of the residual is increased compared with the residual of the previous iteration, the current point is abandoned and a smaller step is taken on the implicitly specified variable. If three smaller steps are tried successively and still the residual oscillates, the calculation continues until convergence. In this way, the method will converge at 10 to 15 iterations and the next step will be larger to skip the critical point and continue the tracing of the phase boundary.

Taking implicit steps on temperature or pressure, based on the values of $\frac{\partial Q}{\partial P}$ and $\frac{\partial Q}{\partial T}$, does not guarantee that a breakdown will not occur if wrong values away from the path of the phase envelope are used. The criteria listed in Table 4-1 ensured convergence for many types of phase envelopes, especially those which present a very wide two phase region, but resulted in breakdowns for very narrow phase envelopes like those presented by binary mixtures of similar components and double retrograde cases. The case of very narrow envelopes can be addressed by modifying the values in the criterion for the spring variable change but this makes the implementation less general and more importantly doesn't address the case of double retrograde mixtures. A more robust solution was based on the observation that when an implicit step was specified outside the two-phase region, the convergence behavior is the same with the one obtained close to the critical point, meaning oscillations of the residual. As a result, a similar type of error handling was applied. In this case, if smaller steps do not solve the convergence problem, the spring variable is forced to change. With this approach, even phase envelopes of mixtures that present double retrograde behavior can be calculated. To identify if the case of oscillating behavior is a false specification or a critical point, the values of $\frac{\partial Q}{\partial P}$ and $\frac{\partial Q}{\partial T}$ are used once more. Normally, very close to the critical point, the values of these parameters are very small (in the range of 10^{-7} and even lower). Moreover, the compressibility factors of the two phases can be compared and also the K-values of the components.

4.6. Results and discussion

The new method was applied to binary, ternary and multicomponent mixtures that exhibit different types of phase envelopes. Although the main focus of this work is not to compare calculations against experimental data, for the cases where such data exist, they are added to the relevant figures for comparison.

4.6.1. Closed loop phase envelopes

The proposed method was initially implemented and tested for closed loop vapor – liquid equilibria (VLE) phase envelopes. Figure 4-2 shows a typical phase envelope for a natural gas mixture (7 components) that has been studied previously.[38,51] The calculation was initiated from a low temperature bubble point and the entire phase envelope was calculated

using the Soave-Redlich-Kwong (SRK) EoS with binary interaction parameters from literature.[52]

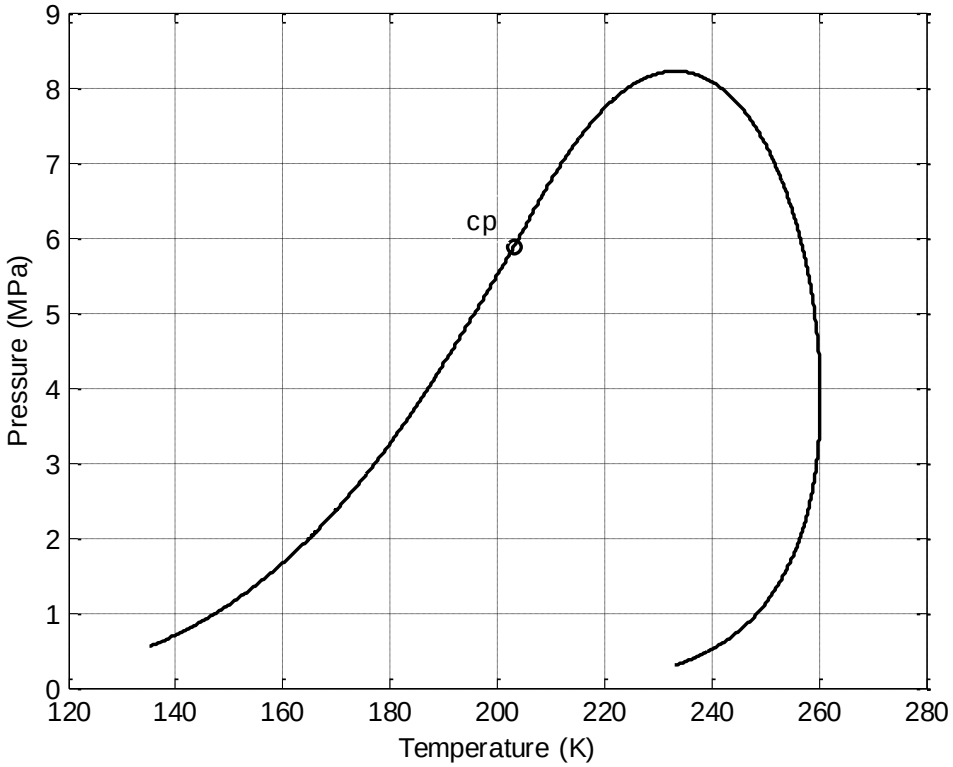

Figure 4-2: Phase envelope of a mixture of 94.3% methane - 2.7% ethane - 0.74% propane - 0.49% n-butane - 0.27% n-pentane - 0.10% n-hexane - 1.4% nitrogen (mole) calculated with the SRK EoS.

The θ parameters used in our implementation, the implicit temperature, pressure steps and the criteria for the spring variable change are reported in Table 4-1.

Table 4-1: Implicit steps, θ parameter values and spring variable change criteria used in this work.

	Calculation is initiated from bubble line		Calculation is initiated from dew line	
	Spring variable is temperature	Spring variable is pressure	Spring variable is temperature	Spring variable is pressure
θ	2	1000	5	9000
δP (MPa)	10^{-2}	10^{-2}	10^{-2}	10^{-2}
δT (K)	10^{-1}	10^{-1}	10^{-1}	10^{-1}
Spring change criterion	$\frac{\partial Q}{\partial P} < \varepsilon_2$ .and. $\frac{\partial Q}{\partial T} > \varepsilon_3$		$\frac{\partial Q}{\partial P} > \varepsilon_2$ .and. $\frac{\partial Q}{\partial T} < \varepsilon_3$	
ε_1	10^{-9}			
ε_2	10^{-2}		10^{-3}	
ε_3	10^{-5}		10^{-3}	

The temperature and pressure steps are chosen so that the resulting phase envelope has a satisfactory number of calculated equilibrium points. Taking into account that in the proposed scheme, no extrapolation is used to create initial estimates for the independent variables at each point, and instead the solution of the previous converged equilibrium point is used, the pressure and temperature increments (or decrements) have to be chosen so that convergence is ensured. Moreover, there is freedom in the way the step values can be chosen. A proportional increase (or decrease) in pressure or temperature is a valid choice also. All the values reported in Table 1 are not restrictive and can be modified, depending on the system(s) under consideration. In the current work, they provided robust results in all different cases examined.

Another closed loop phase envelope that exhibits slightly different geometry than the one presented before is the one shown in Figure 4-3. To trace the specific phase envelope, calculations were initiated from a low temperature dew point and proceeded through the critical point to the bubble line. Calculations were generated using the SRK EoS with all binary interaction coefficients set equal to zero.

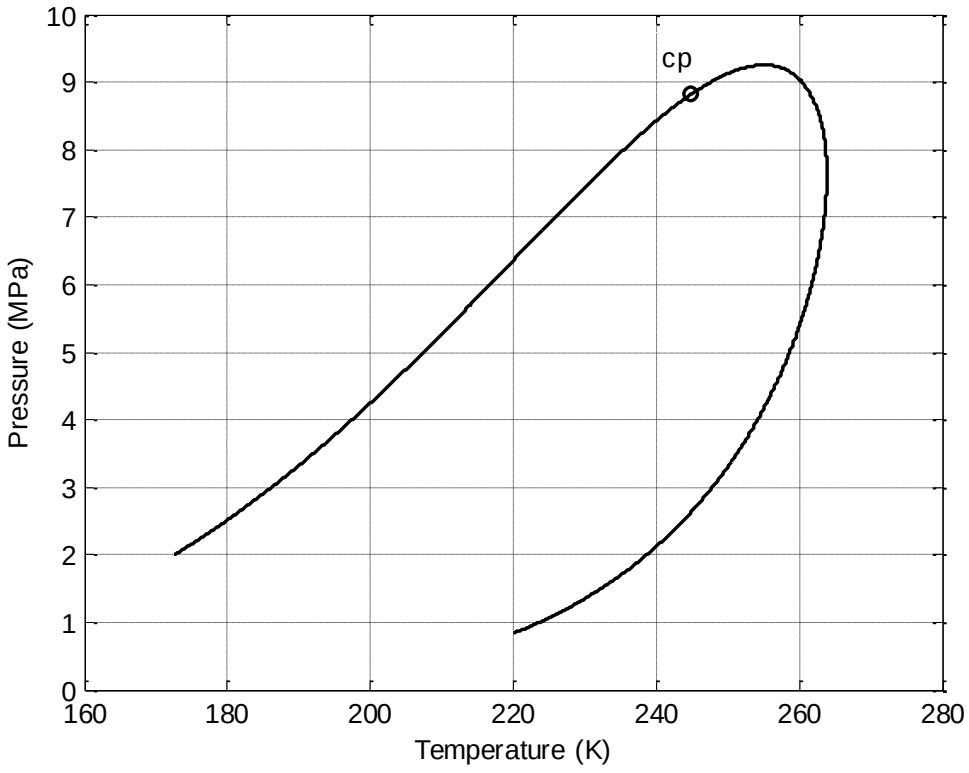

Figure 4-3: Phase envelope of a mixture of 70% methane - 15% carbon dioxide - 15% hydrogen sulfide (mole) calculated with the SRK EoS.

4.6.2. Open ended and double retrograde phase envelopes

The proposed method has also been tested for the calculation of phase envelopes that consist of open ended dew lines and multiple critical points. A mixture that exhibits this behavior is a 50 % methane – 50 % hydrogen sulfide mixture (mole percentages), which is classified as Type III mixture according to Van Konynenburg and Scott.[53] Calculations shown in Figure 4-4 were performed using the SRK EoS and the same binary interaction coefficients as for Figure 4-2.

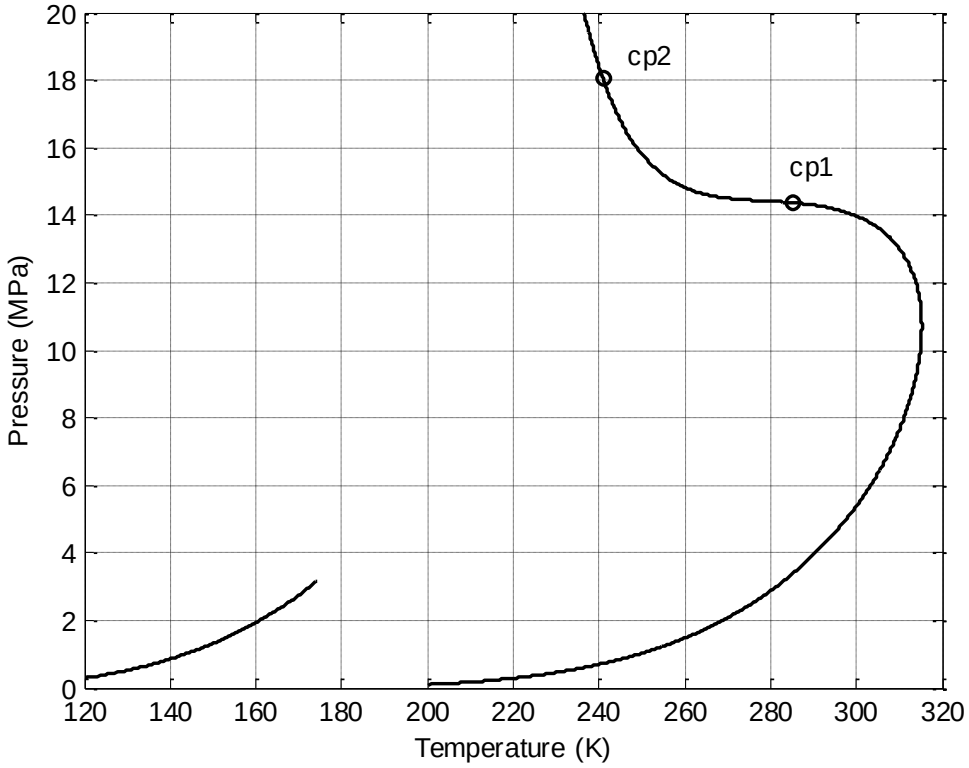

Figure 4-4: Phase envelope of a mixture of 50% methane - 50% hydrogen sulfide (mole) calculated with the SRK EoS.

This mixture has an open ended dew line with more than two inflection points and a separate bubble line at low temperatures.[45] On the dew line, for the pressure range that is presented in Figure 4-4, two critical points have been determined. The two lines were calculated separately, initially starting from a low temperature dew point and then from a low temperature bubble point. It has to be noted that the EoS calculates the coexistence lines even at very low temperatures without taking into account the appearance of a solid phase. To account for this, an appropriate model should be used. As a result, the low temperature bubble point shown here crosses the conditions where a solid phase appears. Moreover, experimental measurements from Kohn et al.[54] indicate that this mixture at temperatures ranging from approximately 180 to 200 K exhibits vapor – liquid – liquid equilibrium (VLLE) and there is

also a quadruple point at lower temperatures where the VLLE, SLVE and SLLE lines intersect. These phase equilibria cannot be calculated with the proposed method.

Another case of an open ended dew line that has been studied previously[38,46] is the mixture shown in Figure 4-5. This mixture has three critical points on the two phase coexistence curve which is comprised of vapor – liquid, liquid – liquid and high pressure fluid – fluid regions. This mixture also has two separate three phase regions,[38] which are not calculated in this work. Moreover, it has to be noted that for the calculation of these open ended dew lines, the use of k_{ij} interaction parameters[52] was necessary for the SRK equation to predict the phase behavior.

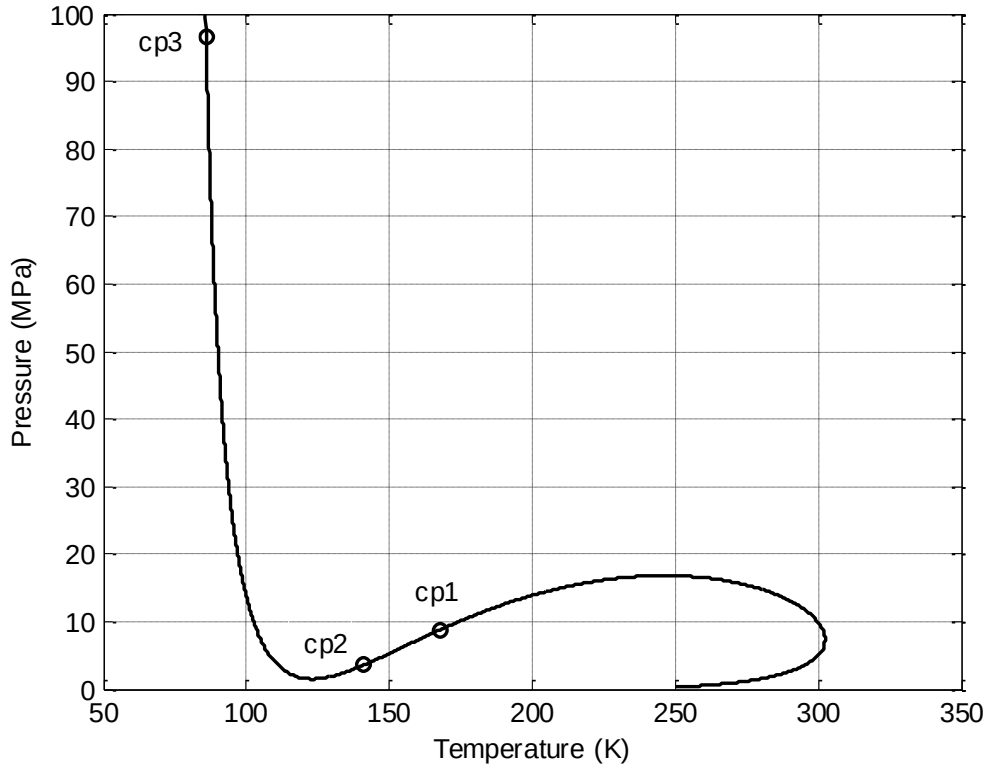

Figure 4-5: Phase envelope of a mixture of 30.4% nitrogen - 54.8% methane - 7.1% ethane - 3.7% propane - 2% n-butane - 2% n-pentane (mole) with the SRK EoS.

The cases of unusual phase envelopes are not limited to open ended dew lines and multiple critical points though. Another, interesting case is the phenomenon of double retrograde vaporization (DRV). DRV occurs in mixtures having high molecular dissimilarity in terms of differences in size, shape and interaction energy between like and unlike molecules. The result is an anomalous retrograde dew point curve at small solute concentrations and at temperatures close to the critical temperature of the solvent.[55] Many binary hydrocarbon mixtures that present this type of behavior have been studied.[55-58] In this work the bead spring method has been used to calculate the isopleth phase envelope of a

mixture containing 99.95% methane – 0.05% n-pentane, using the SRK EoS with zero binary interaction coefficients. Calculations are shown in Figure 4-6.

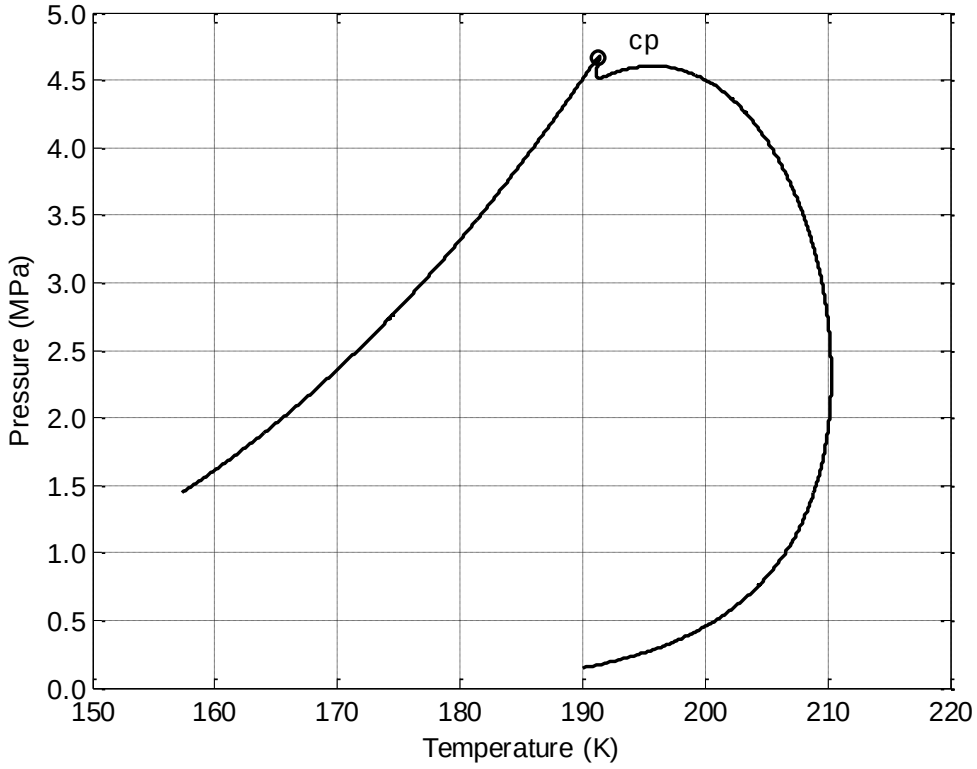

Figure 4-6: Phase envelope of a mixture of 99.95% methane - 0.05% n-pentane (mole) with the SRK EoS.

Clearly, for the calculation of a phase envelope of this type, the spring variable has to be changed more than once. If the calculation is initiated from a low pressure – low temperature dew point, the pressure is used as the first specification variable and is increased until the first pressure maximum is reached. At this point, the automated selection will switch the spring variable from pressure to temperature which subsequently will be decreased. Because of the irregular behavior of double retrograde phase envelopes, the continuous decrease of temperature will drive the specification variable outside the two phase region. When the spring variable is set to a value that pulls the solution to a non-feasible region, the residual oscillates. This behavior is an indication of false convergence, as described above. Consequently, when the specification variable is set outside the two phase region, it will be forced to change and the entire phase diagram will be calculated without any problems.

4.6.3. Constant phase fraction lines

The proposed method has also been successfully tested for calculating constant phase fraction lines in addition to the boundary ones. The calculation of a phase envelope can start either from a low temperature – pressure dew or bubble point. The calculation is conducted

by setting the vapor fraction (β) equal to 0 or 1. If β is set equal to 1, the dew point branch is calculated first. Once the critical point is passed, the value of the vapor fraction is kept fixed, but the x-phase now becomes the lighter phase and the y-phase the heavier one.[12]

Similar to the phase boundary calculation, tracing a constant phase fraction line other than 0 or 1 will start by setting the vapor fraction to a value between 0 and 1 and calculate the whole branch up to the critical point. After passing the critical point, the phase fraction now represents the liquid phase. In Figure 4-7, one can see the results from the calculation of constant phase fraction lines with the SRK EoS, for the same mixture as in Figure 4-3. As expected, all the lines intersect at the critical point of the mixture.

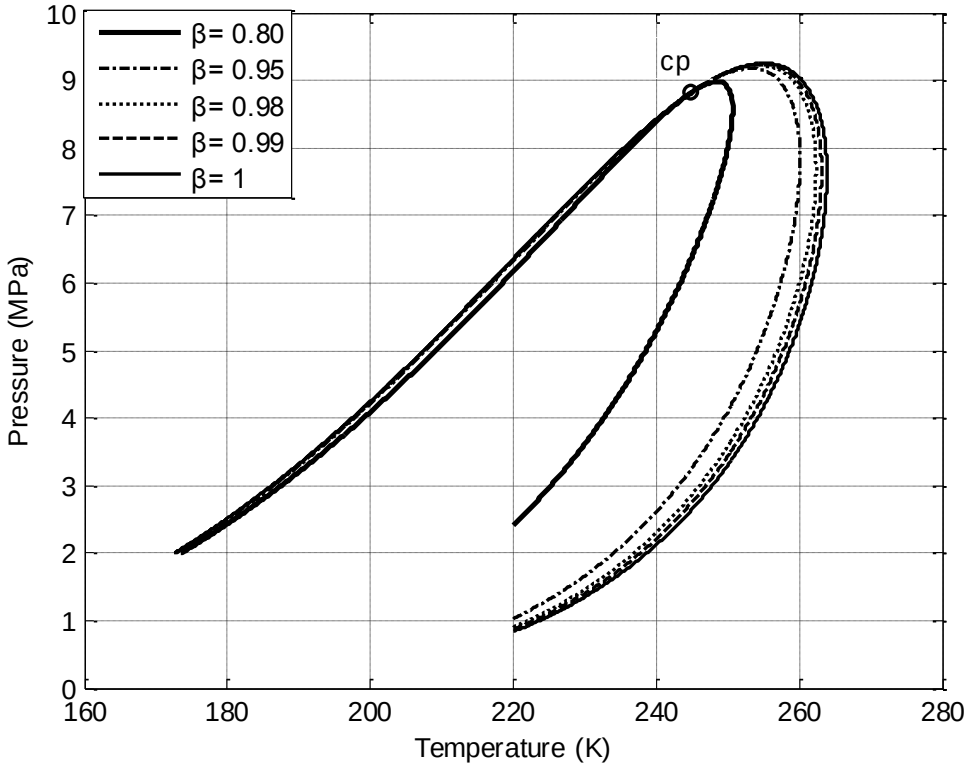

Figure 4-7: Constant phase fraction lines of a mixture of 70% methane - 15% carbon dioxide - 15% hydrogen sulfide (mole) with the SRK EoS.

4.6.4. Higher order equations of state

The performance of the bead spring method has also been tested with the use of more complex EoS like SAFT and PC-SAFT. Using SAFT type EoS for the calculation of fugacity coefficients and their derivatives significantly increases the computational time needed for the calculation of a phase envelope. The iterations needed for convergence of a single equilibrium point, when PC-SAFT was used remained the same, varying in the range of 2 – 4 iterations without extrapolations to generate initial estimates. The need of a density solver to calculate the properties from the EoS significantly increased the computational cost though. Moreover,

calculations near the critical point become even more time consuming because convergence of the density solver is slower.

Figure 4-8 shows the predictions (k_{ij} = 0) of SRK, PR and PC-SAFT EoS for a ternary mixture of 96.09% CO_2 – 1.93% Ar – 1.98% O_2. This mixture has a closed loop isoplethic phase envelope with only one critical point. Experimental data for this mixture are taken from Coquelet et al.[59] The CPU times for the calculation of approximately 3200 phase equilibrium points using SRK and PR equations of state were in the order of around 0.4 seconds in each case. The total CPU time needed for the calculation of approximately 3400 equilibrium points on the phase envelope using PC-SAFT EoS in an Intel – Haswell architecture - core i7 (2.7 GHz base frequency) mobile processor was approximately more than an order of magnitude higher. The procedure used to calculate density with PC-SAFT was based on Topliss et al. method.[60] The CPU time needed per state point when a cubic EoS was used, approximately matches the one reported by Quiñones-Cisneros and Deiters[43], who also observed a 10-fold larger CPU time with PC-SAFT when a Gibbs energy based method was used. A density based method was computationally faster when PC-SAFT was used.

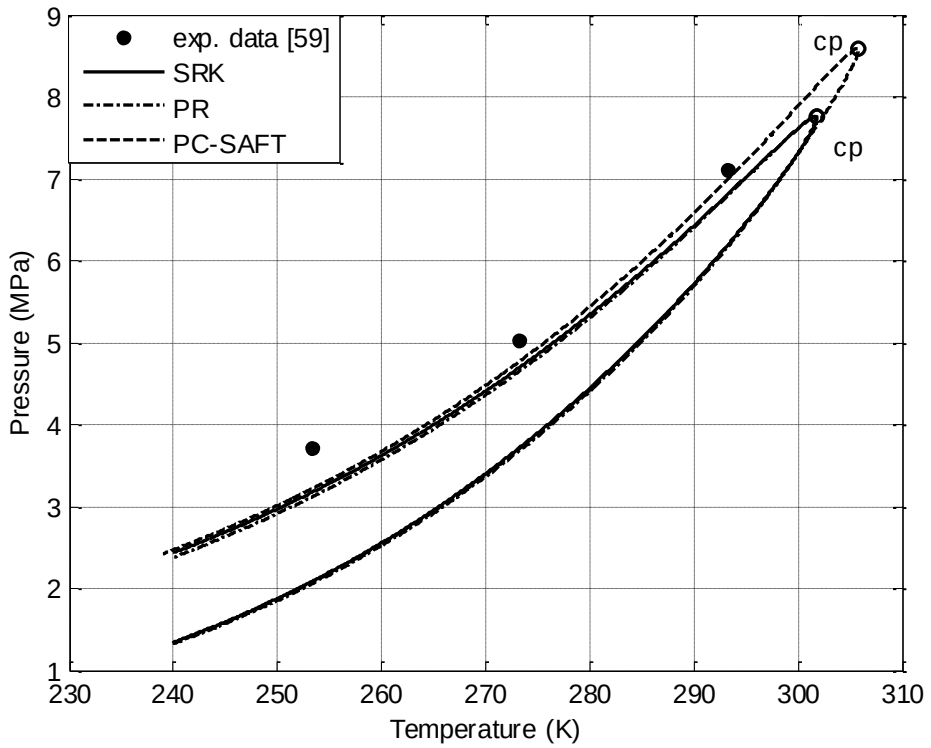

Figure 4-8: Phase envelopes of a mixture of 96.09% carbon dioxide - 1.93% argon - 1.98% oxygen (mole) with the SRK, PR and PC-SAFT EoS.

In order to further test the performance of the method with PC-SAFT, an additional case of a double retrograde behavior reported by Espinosa et al.[55] of 99.85% methane – 0.15% n-butane mixture was examined. Experimental data were taken from Chen et al.[61]

Calculations included the SRK and PC-SAFT EoS with zero binary interaction coefficients and the GERG-2008 EoS. Calculations with GERG EoS were performed using REFPROP 9.1. All three EoS reproduce qualitatively correct the behavior, with GERG-2008 being more accurate (see Figure 4-9). The critical points of the three equations are very close to each other and they are depicted as open circles in Figure 4-9.

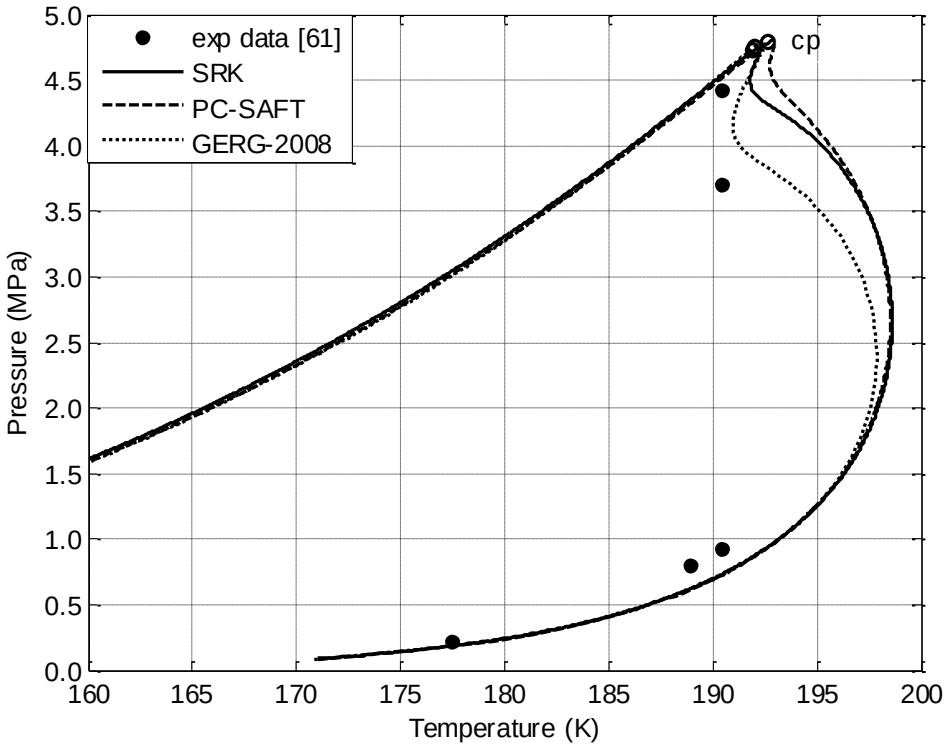

Figure 4-9: Phase envelope of a mixture of 99.85% methane - 0.15% n-butane (mole) with the SRK, PC-SAFT and GERG-2008 EoS.

4.6.5. Relation to the cricondentherm and cricondenbar calculation

Michelsen[48] was the first to show that the slope of the phase boundary of a multicomponent mixture can be calculated exactly, using only pressure and temperature derivatives of the fugacity coefficients, through Eq. (4.8). Moreover, he has shown that this equation can be used to provide the necessary relations for the direct determination of the pressure and temperature maxima of a phase boundary. At the temperature maximum:

$$\left.\frac{dT}{dP}\right|_{Q=0} = 0 \tag{4.17}$$

And using Eq. (4.8) yields:

$$\left.\frac{\partial Q}{\partial P}\right|_{T} = 0 \tag{4.18}$$

A similar relation for the cricondenbar is also applicable:

$$\left.\frac{\partial \mathrm{Q}}{\partial \mathrm{T}}\right|_{\mathrm{P}} = 0 \tag{4.19}$$

Comparing Eq. (4.18) with Eq. (4.13) which is the core equation of the bead spring method, it is easily understood that by setting the θ "stiffness" parameter equal to zero, the proposed method becomes the direct determination of the cricondentherm method. Using a value of θ other than zero - taking also into account the convergence properties – will result in moving the calculated beads (equilibrium points) away from the cricondentherm. If a calculation starts from a low pressure - low temperature point on the dew point branch, setting a low value to θ will gather the beads close to the cricondentherm.

This property of the bead spring method, namely the very smooth conversion of a method that sequentially traces the isoplethic phase envelope to a method that directly determines the cricondentherm, makes the method a general framework for different equilibrium calculations without the need of programming separate algorithms. Moreover, the calculation can also be easily converted to the direct determination of the cricondenbar point, just by substituting $\frac{\partial \mathrm{Q}}{\partial \mathrm{P}}$ term in the $\mathrm{f}_{\mathrm{C+2}}$ equation with $\frac{\partial \mathrm{Q}}{\partial \mathrm{T}}$. Altering the elements of the last row of the Jacobian matrix is also trivial in the sense that only specific pressure derivatives of the fugacity coefficients have to be substituted with temperature derivatives and vice versa. It has to be noted though that the direct determination of the cricondenbar is not as well behaved as the cricondentherm one.[48,62]

The proposed version of the bead spring method can be also altered by substituting the $\frac{\partial \mathrm{Q}}{\partial \mathrm{P}}$ term in Eq. (4.13) with $\frac{\partial \mathrm{Q}}{\partial \mathrm{T}}$. As a result the core equation will become:

$$\mathrm{f}_{\mathrm{C+2}} = \frac{\partial \mathrm{Q}}{\partial \mathrm{T}} + \theta \cdot \left(\mathrm{S}_{\mathrm{l+1}}^{\mathrm{est}} - 2\mathrm{S}_{\mathrm{l}} + \mathrm{S}_{\mathrm{l-1}}\right) = 0 \tag{4.20}$$

For this new version the θ parameter will have to be regulated again.

In Figure 4-10 and Figure 4-11, convergence of the cricondentherm direct determination method is shown in P-T space for the mixtures presented in Figure 4-2 and Figure 4-8 respectively. In Figure 4-10, calculations using the SRK EoS are initiated from a low temperature, low pressure dew point and convergence is achieved in 12 iterations with 10^{-9} tolerance in the residual of the equations. In Figure 4-11, calculation using the PR EoS starts again from a low temperature, low pressure dew point and convergence is achieved in 16 iterations.

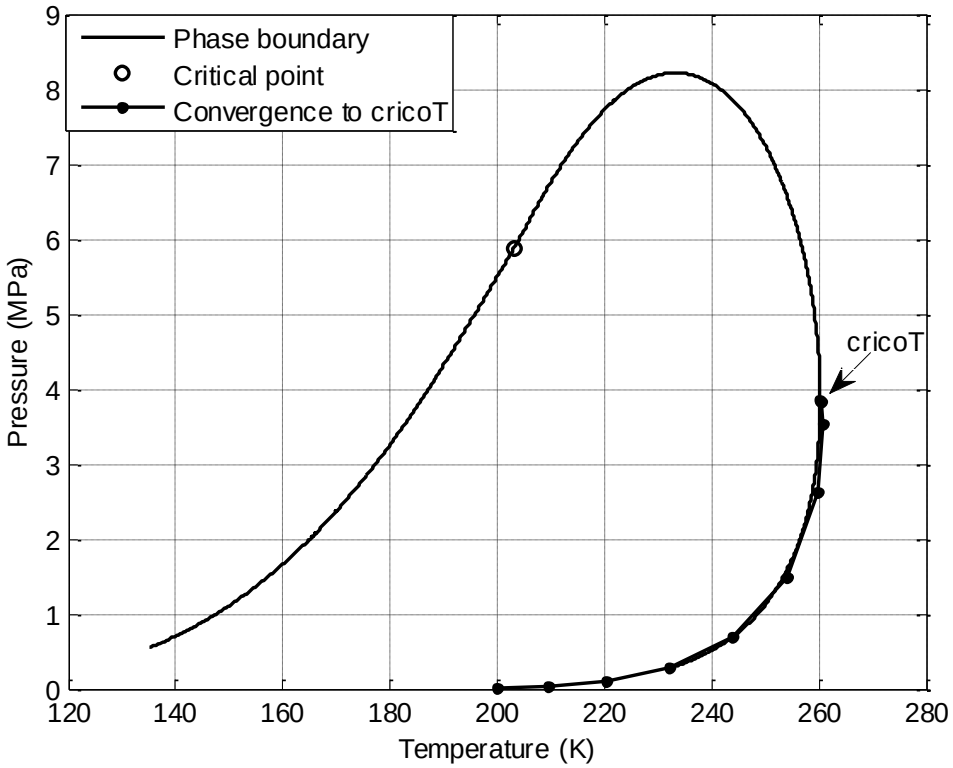

Figure 4-10: Direct determination of cricondentherm of a mixture of 94.3% methane - 2.7% ethane - 0.74% propane - 0.49% n-butane - 0.27% n-pentane - 0.10% hexane - 1.4% nitrogen (mole) with the SRK EoS.

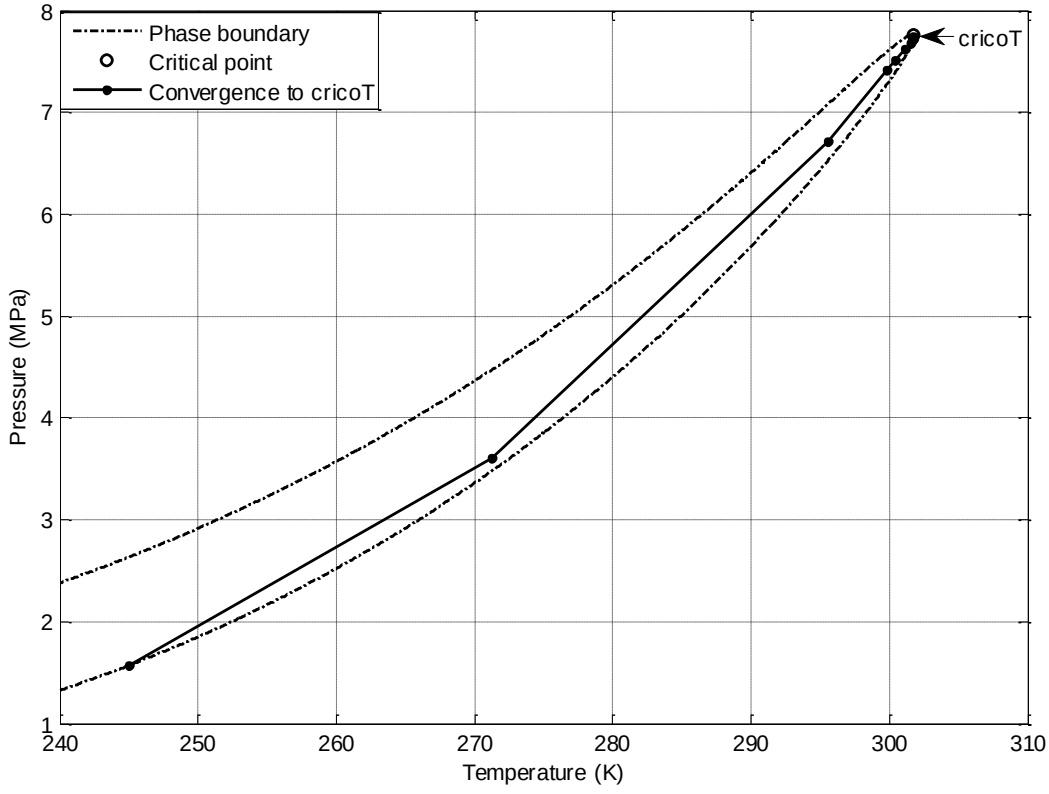

Figure 4-11: Direct determination of cricondentherm of a mixture of 96.09% carbon dioxide - 1.93% argon - 1.98% oxygen (mole) with the PR EoS.

4.7. Conclusions

A new method for the construction of constant composition phase envelopes of multicomponent mixtures has been proposed. The method traces the vapor – liquid coexistence lines using a “spring” that sets the slope value of the modified tangent plane distance in respect to either temperature or pressure.

Extensive tests have been performed on various binary, ternary and multicomponent mixtures for calculating phase envelopes of different types and at different phase fractions. We have shown that the method is capable of tracing common types of phase envelopes as well as more unusual cases like open ended dew lines with multiple critical points and double retrograde behaviors. The calculation of closed loop phase envelopes can be initiated either from the bubble or the dew line. The capabilities of the method also extend to the calculation of coexistence lines other than the boundary ones, i.e. phase fractions between 0 and 1.

The method converges in the vicinity of critical points and also in the retrograde region when pressure or temperature is implicitly specified and as initial estimate, the solution of the previous point is used. Extrapolating the solution of every equilibrium point to create initial estimates for the next is not a prerequisite for the method to be implemented. The calculations presented here have also shown that the method is capable of handling both cubic equations of state as well as higher order ones such as the PC-SAFT EoS.

The proposed method is easily converted to the direct determination of the cricondentherm and cricondenbar point method. Thus, the method serves as a general framework for calculating constant composition phase envelopes and also directly determining the pressure and temperature maxima without the need of programming separate algorithms.

5. Vapor – Liquid Equilibrium Modeling of CO_2 mixtures

5.1. Binary Mixtures of CO_2 with Other Gases

Modeling the vapor – liquid equilibrium (VLE) behavior of CO_2 with other components relevant to CCS applications is particularly important for CO_2 pipeline transport and subsequent sequestration. The gas stream which is going to be transported through the pipeline is highly unlikely to be comprised of pure CO_2 and other compounds such as N_2, CH_4, O_2, Ar, SO_2, H_2S and H_2O are going to be present at different concentrations, based on the source of the flue gas and the capture process. The effect of these impurities on the phase behavior is very important for the design and operation of the pipeline.

In this work, the SRK, PR, SAFT and PC-SAFT equations of state have been used to model the phase behavior of binary, ternary and multicomponent mixtures of CO_2 with other gases. In this section, the pure component parameters used by every EoS will be presented and the calculations for the binary CO_2 mixtures are going to be discussed.

Tables 5-1, 5-2 and 5-3 summarize the pure component parameters used by the cubic and the SAFT EoS in this work.

Table 5-1: Critical Temperature (T_c), Critical Pressure (P_c) and Acentric Factor (ω) values for the components studied in this work.[63]

Component	T_c (K)	P_c(MPa)	ω
CO_2	304.20	7.376	0.225
CH_4	190.60	4.600	0.008
N_2	126.20	3.394	0.040
Ar	150.86	4.859	0.0010
O_2	154.58	5.040	0.0220
SO_2	430.80	7.880	0.2510
H_2S	373.20	8.936	0.100

Table 5-2: SAFT EoS parameters for the components studied in this work.

Component	m	v^{00} (Å^3)	u/k (K)	e/k (K)	ε^{AB}/k (K)	κ^{AB}	Ref.
CO_2	1.4170	13.578	216.08	40	-	-	14
CH_4	1.0000	21.576	190.29	1	-	-	14
N_2	1.000	19.457	123.53	3	-	-	14
Ar	1.0000	16.290	150.86	0	-	-	14
O_2	1.0000	16.056	154.72	0	-	-	64
SO_2	1.1330	22.611	335.84	88	-	-	14
H_2S	2.3482	7.801	207.86	10	-	-	64

Table 5-3: PC-SAFT EoS parameters for the components studied in this work.

Component	m	σ (Å)	ε/k (K)	ε^{AB}/k (K)	κ^{AB}	Ref
CO_2	2.6037	2.555	151.04	-	-	64
CH_4	1.0000	3.704	150.03	-	-	64
N_2	1.2053	3.313	90.96	-	-	64
Ar	0.9285	3.478	122.23	-	-	16
O_2	1.1217	3.210	114.96	-	-	64
SO_2	2.8611	2.683	205.35	-	-	16
H_2S	1.7163	3.009	224.96	-	-	64

The phase envelopes of CO_2 binary mixtures with 5% mole fraction of different gases have been calculated with the PR and the PC-SAFT EoS by Diamantonis et al.[65] and the resulting phase behavior has been discussed. The authors observed that Ar, N_2, CH_4, and O_2 shift both the bubble and dew point curves to pressures higher than the saturation curve of pure CO_2. Another important observation was that the dew point curves of the mixtures almost overlap each other, leading to the conclusion that their effect on the vapor phase is weaker than on the liquid phase. The only component that lowers the saturation pressure and shifts the envelope lower than the pure CO_2 curve is the SO_2. The addition of H_2S to CO_2 has practically no effect on the phase behavior. The bubble and dew curves of the binary mixture almost overlap, leaving a very narrow two phase region, and the whole envelope is attached on the pure CO_2 saturation curve.

Except for the qualitative effect of the impurities on the phase behavior, the authors did not present experimental data to evaluate the performance of the two EoS on predicting or correlating the isoplethic phase diagrams. In this work, the constant composition vapor – liquid phase envelopes of 6 binary CO_2 mixtures at various compositions have been calculated. The calculations have been conducted with zero binary interaction parameters (predictions) and with binary interaction parameters (correlations) fitted to experimental binary VLE data. The interaction parameters (k_{ij}) used in this work are taken from Diamantonis et al.[66] who regressed their values on isothermal phase equilibrium data over a wide temperature range. The experimental data sets modeled in this work are presented in Table 5-4.

In Tables 5-5 to 5-10, the percentage average absolute deviation (AAD %) between experimental data and model calculations for each binary mixture at different compositions and the corresponding k_{ij} values are presented. The AAD % between model calculations and experimental data for a mixture is calculated as the difference between the calculated and the experimental equilibrium pressure at specific temperature using the following form:

$$\text{AAD \%} = \frac{100}{\text{NP}} \sum_{i=1}^{\text{NP}} \left| \frac{P_i^{\text{calculated}} - P_i^{\text{experimental}}}{P_i^{\text{experimental}}} \right| \quad (5.1)$$

The average AAD % of a model over the entire set of mixtures is calculated as a weighted average of the summation of AAD % of every single mixture, using as weight factor the number of experimental points available for a single mixture.

Table 5-4: Experimental binary VLE data from Literature modeled in this work.

CO_2 Composition (mole %)	**Temperature (K)**	**Ref**
	$CO_2 - N_2$	
97.50	278.15 – 298.15	Ahmad et al.[67]
94.50	278.15 – 298.15	Ahmad et al.[67]
	$CO_2 - CH_4$	
99.02	253.15 – 298.15	Rivas et al.[68]
98.09	253.15 – 298.15	Blanco et al.[68]
97.50	277.75 – 302.15	Ahmad et al.[67]
97.19	253.15 – 298.15	Blanco et al.[68]
94.70	277.95 – 298.95	Ahmad et al.[67]
85.25	253.15 – 283.15	Blanco et al.[68]
	$CO_2 - O_2$	
97.45	277.35 – 298.15	Ahmad et al.[67]
94.93	277.65 – 297.65	Ahmad et al.[67]
	$CO_2 - Ar$	
97.45	278.35 – 300.35	Ahmad et al.[67]
97.45	288.23 – 299.21	Coquelet et al.[69]
94.48	278.35 – 296.65	Ahmad et al.[67]
94.48	295.01 – 299.21	Coquelet et al.[69]
	$CO_2 - SO_2$	
92.68	299.15 – 312.15	Caubet[70]
88.71	314.35 – 322.95	Caubet[70]
	$CO_2 - H_2S$	
93.94	248.09 – 295.13	Stouffer et al.[71]
93.92	250.99 – 304.06	Stouffer et al.[71]
90.45	257.21 – 307.16	Stouffer et al.[71]
70.67	261.32 – 315.86	Stouffer et al.[71]

Table 5-5: AAD% between experimental VLE data and EoS calculations for $CO_2 - N_2$ mixtures and corresponding k_{ij} values.

EoS		$CO_2 - N_2$		
			CO_2 Composition (mole %)	
		k_{ij}	97.50	94.50
			AAD%	AAD%
SRK	Pr.	0	1.57	7.26
	Cor.	-0.018	1.53	7.82
PR	Pr.	0	1.29	7.62
	Cor.	-0.007	1.27	7.94
SAFT	Pr.	0	5.10	11.90
	Cor.	0.018	4.70	11.18
PC-SAFT	Pr.	0	1.38	7.06
	Cor.	*		

"Pr." refers to predictions (k_{ij}= 0), whereas "Cor." refers to correlations (calculations with $k_{ij} \neq 0$).

*Optimum kij value was zero.

Table 5-6: AAD% between experimental VLE data and EoS calculations for $CO_2 - CH_4$ mixtures and corresponding k_{ij} values.

EoS		$CO_2 - CH_4$						
			CO_2 Composition (mole %)					
		k_{ij}	99.02	98.09	97.50	97.19	94.70	85.25
			AAD%	AAD%	AAD%	AAD%	AAD%	AAD%
SRK	Pr.	0	1.69	2.19	2.19	3.04	1.67	9.37
	Cor.	0.103	0.72	0.39	0.69	0.52	1.58	1.43
PR	Pr.	0	2.40	2.90	1.94	3.82	2.29	10.20
	Cor.	0.100	1.15	0.78	0.75	0.96	1.46	1.69
SAFT	Pr.	0	5.94	6.82	7.95	7.94	8.07	39.05
	Cor.	0.100	4.15	3.58	5.15	3.53	3.48	6.27
PC-SAFT	Pr.	0	1.88	2.57	1.56	3.56	1.90	10.73
	Cor.	0.061	0.73	0.74	1.06	0.85	2.39	1.66

"Pr." refers to predictions (k_{ij}= 0), whereas "Cor." refers to correlations (calculations with $k_{ij} \neq 0$).

Table 5-7: AAD% between experimental VLE data and EoS calculations for $CO_2 - O_2$ mixtures and corresponding k_{ij} values.

EoS		**$CO_2 - O_2$**		
			CO_2 Composition (mole %)	
		k_{ij}	**97.45**	**94.93**
			AAD%	**AAD%**
PR	Pr.	0	3.61	8.93
	Cor.	0.111	1.91	6.13
PC-SAFT	Pr.	0	2.37	7.35
	Cor.	0.049	2.00	5.96

"Pr." refers to predictions (k_{ij}= 0), whereas "Cor." refers to correlations (calculations with $k_{ij} \neq 0$).

Table 5-8: AAD% between experimental VLE data and EoS calculations for $CO_2 - Ar$ mixtures and corresponding k_{ij} values.

EoS		**$CO_2 - Ar$**		
			CO_2 Composition (mole %)	
		k_{ij}	**97.45**	**94.48**
			AAD%	**AAD%**
PR	Pr.	0	1.88	7.24
	Cor.	0.141	2.62	3.76
PC-SAFT	Pr.	0	1.56	4.67
	Cor.	0.028	2.36	3.38

"Pr." refers to predictions (k_{ij}= 0), whereas "Cor." refers to correlations (calculations with $k_{ij} \neq 0$).

Table 5-9: AAD% between experimental VLE data and EoS calculations for $CO_2 - SO_2$ mixtures and corresponding k_{ij} values.

EoS		**$CO_2 - SO_2$**		
			CO_2 Composition (mole %)	
		k_{ij}	**92.68**	**88.71**
			AAD%	**AAD%**
PR	Pr.	0	11.12	3.82
	Cor.	0.052	1.09	7.70
PC-SAFT	Pr.	0	13.13	5.76
	Cor.	0.030	1.77	6.03

"Pr." refers to predictions (k_{ij}= 0), whereas "Cor." refers to correlations (calculations with $k_{ij} \neq 0$).

Table 5-10: AAD% between experimental VLE data and EoS calculations for $CO_2 - H_2S$ mixtures and corresponding k_{ij} values.

EoS		$CO_2 - H_2S$				
			CO_2 Composition (mole %)			
		k_{ij}	93.94	93.92	90.45	70.67
			AAD%	AAD%	AAD%	AAD%
PR	Pr.	0	8.14	6.19	6.97	15.99
	Cor.	0.098	0.78	0.89	0.71	0.85
PC-SAFT	Pr.	0	9.46	7.33	7.59	17.39
	Cor.	0.067	0.69	0.91	0.97	0.94

"Pr." refers to predictions ($k_{ij}= 0$), whereas "Cor." refers to correlations (calculations with $k_{ij} \neq 0$).

Cubic (SRK, PR), SAFT and PC-SAFT EoS have been used to model the phase behavior of $CO_2 - N_2$ and $CO_2 - CH_4$ mixtures. SAFT predictions fail to provide satisfactory description of the phase behavior for these two mixtures, with the average AAD% being 10.54. The most accurate predictions for these two mixtures are provided by PC-SAFT (AAD% = 2.79), while SRK and PR are slightly less accurate, giving very similar results. Based on these observations, all the remaining mixtures have been modeled only with the PC-SAFT and PR equations of state.

PC-SAFT predictions are the most accurate on the average for all 6 binary mixtures studied with AAD% = 5.55, while PR is slightly less accurate with the predictions giving an average AAD%= 5.61. PC-SAFT is more accurate for most mixtures except for the 85.25% CO_2 – 14.75% CH_4 (mole) mixture and the $CO_2 - SO_2$, $CO_2 - H_2S$ mixtures where PR predictions are more accurate. These observations are consistent with the results of Diamantonis et al.[66], who also reported PC-SAFT being the most accurate model overall and PR being slightly less accurate in terms of predictions. It should be emphasized though that at near critical conditions, PR is systematically more accurate than PC-SAFT. This is due to the fact that SAFT-type EoS are mean field theories that fail to predict correctly the near critical behavior of pure components and mixtures.

The use of BIPs improves the correlation of the experimental data for the two EoS for most cases. On average, PC-SAFT gives an AAD% = 2.02 when the k_{ij} values from Diamantonis et al.[66] are used, while PR gives an AAD% = 2.37. As a result, the overall description of the phase behavior is improved, but there are specific mixtures where the use of BIPs deteriorates the performance of the EoS compared to the predictive results. Specifically, both PR and PC-SAFT correlate ($k_{ij} \neq 0$) worse the phase behavior of 97.45% CO_2 – 2.55% Ar and 88.71% CO_2 – 11.29% SO_2 mixtures when compared to their predictive performance. PR also presents worse correlating than predictive performance for the 94.50% CO_2 – 5.50%

N_2 mixture and PC-SAFT for the 94.70% CO_2 – 5.30% CH_4 mixture. Representative results for some of the mixtures discussed are given in Figures 5-1 to 5-6. The figures that are not presented in this section can be found in Appendix C.

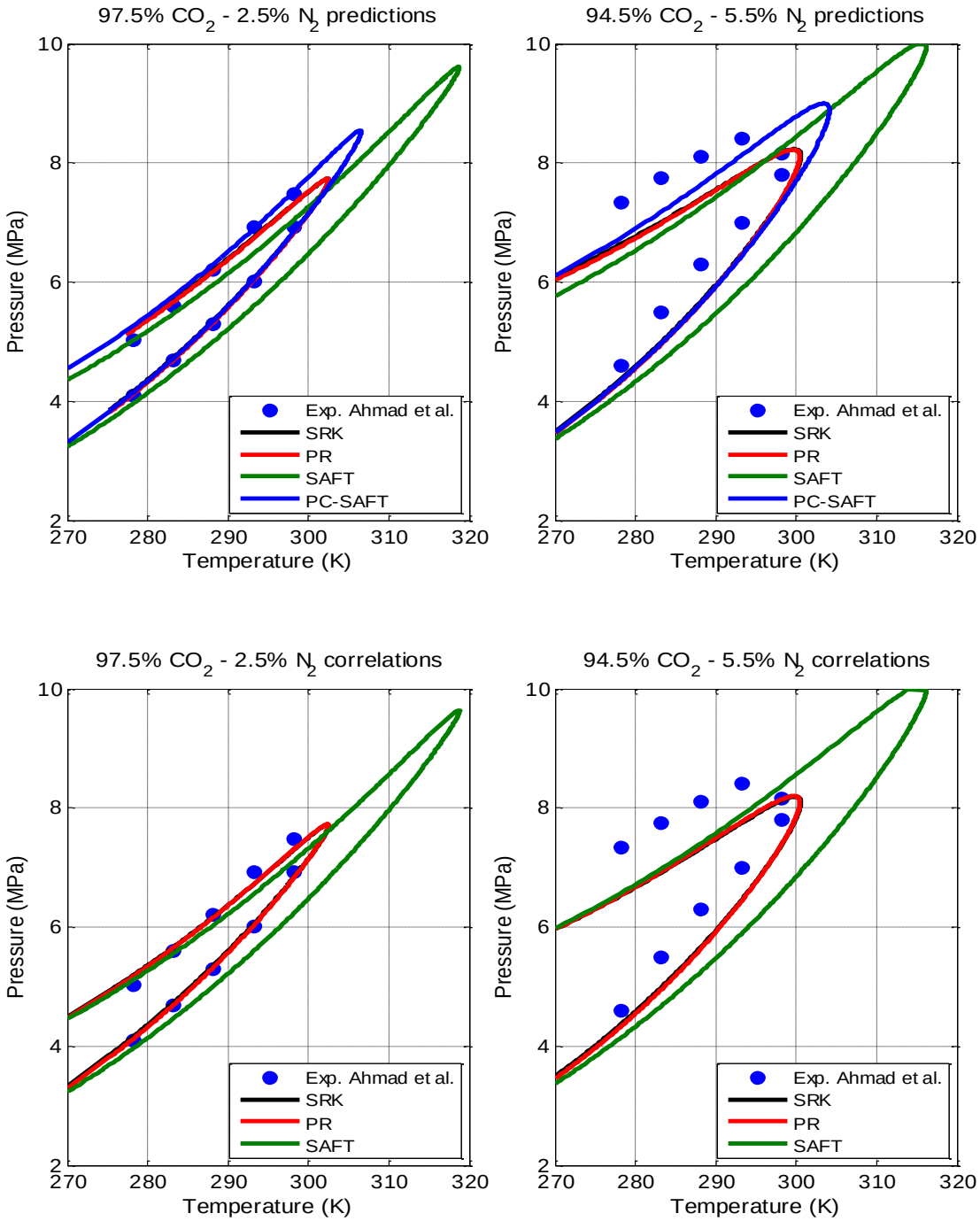

Figure 5-1: Phase envelopes of 97.5% carbon dioxide – 2.5% nitrogen, 94.5% carbon dioxide – 4.5% nitrogen (mole) mixtures. Top panels show predictions ($k_{ij} = 0$), whereas bottom panels show correlations ($k_{ij} \neq 0$).

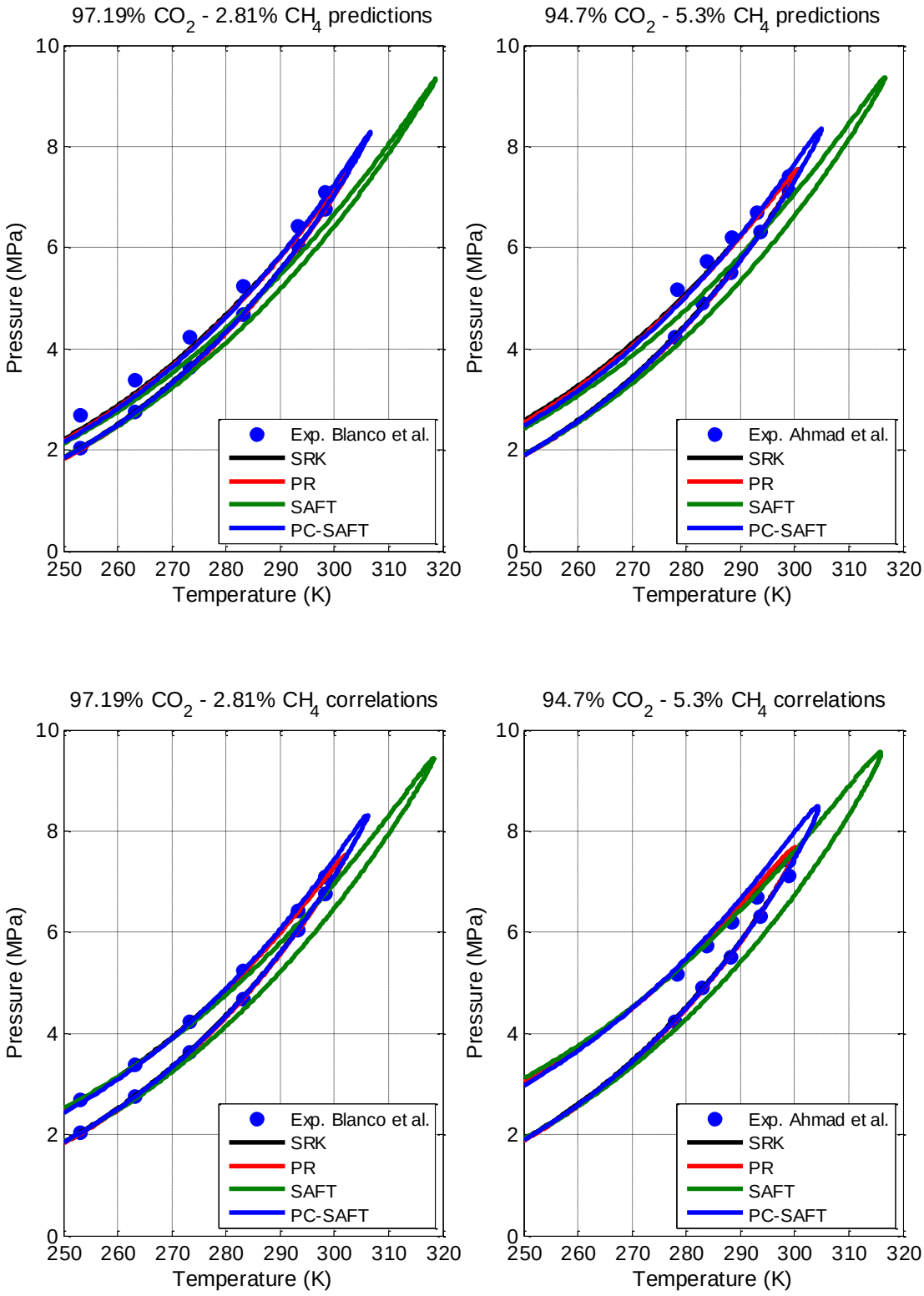

Figure 5-2: Phase envelopes of 97.19% carbon dioxide – 2.81% methane, 94.7% carbon dioxide – 5.3% methane (mole) mixtures. Top panels show predictions ($k_{ij} = 0$), whereas bottom panels show correlations ($k_{ij} \neq 0$).

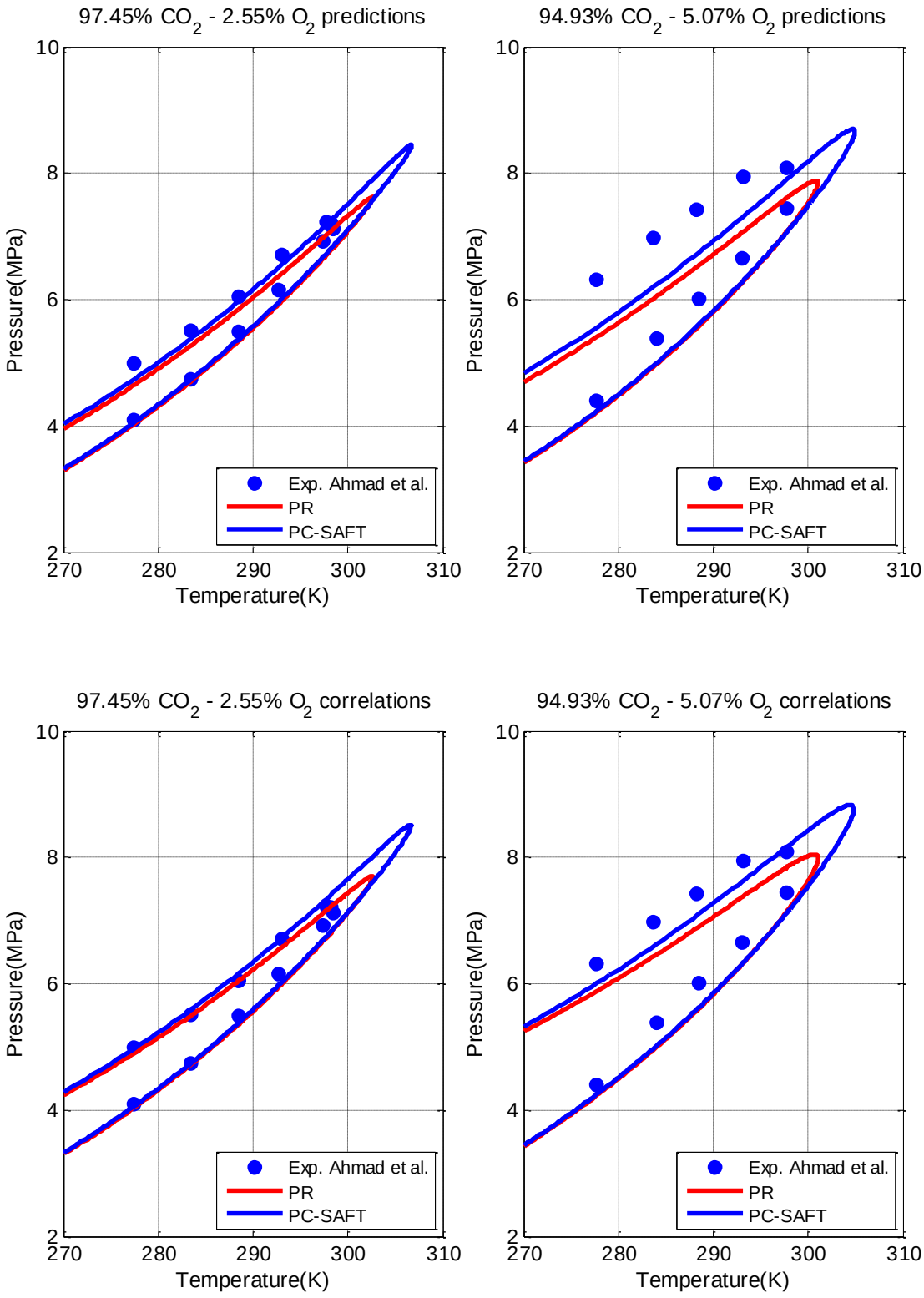

Figure 5-3: Phase envelopes of 97.45% carbon dioxide – 2.55% oxygen, 94.93% carbon dioxide – 5.07% oxygen (mole) mixtures. Top panels show predictions ($k_{ij} = 0$), whereas bottom panels show correlations ($k_{ij} \neq 0$).

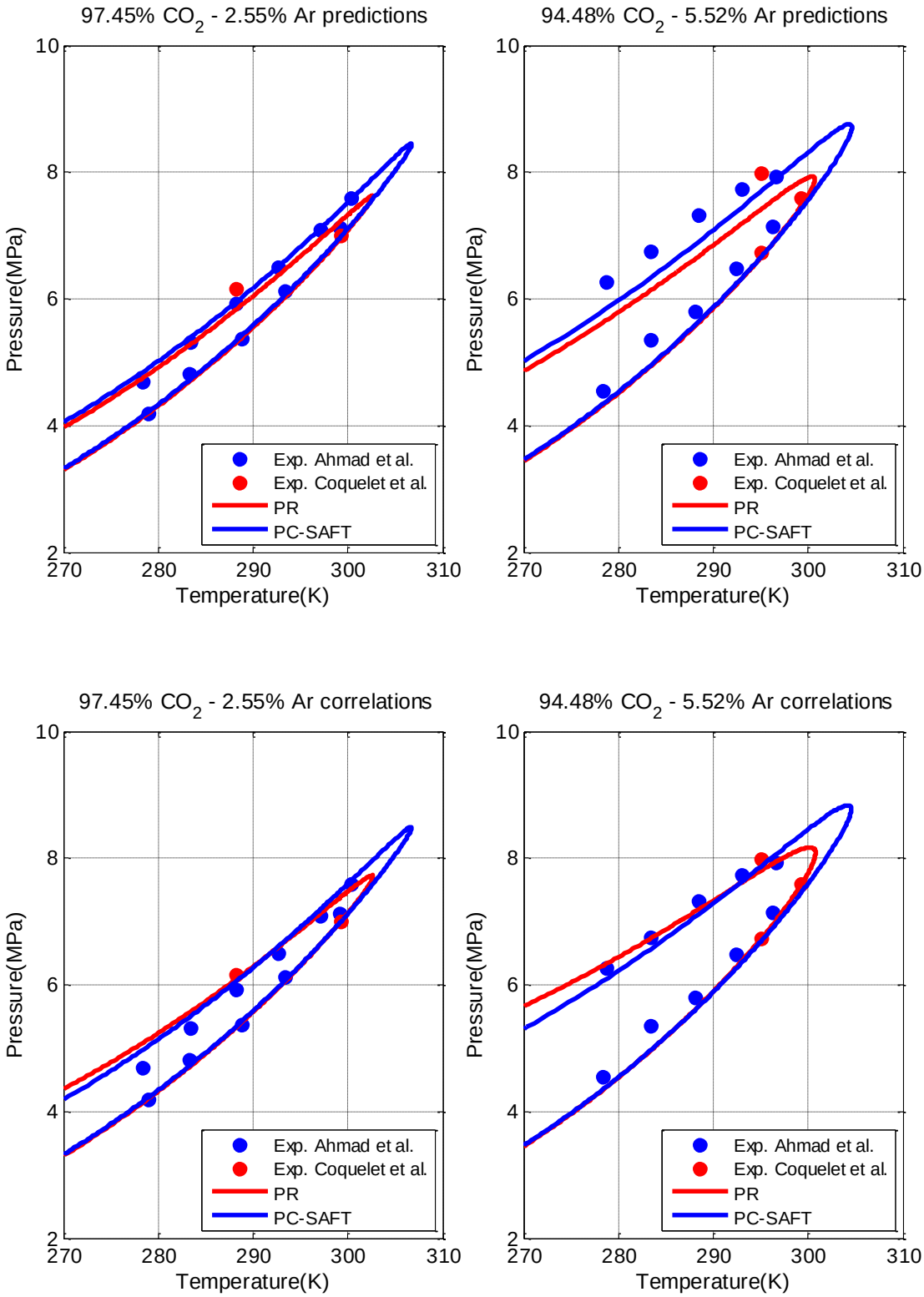

Figure 5-4: Phase envelopes of 97.45% carbon dioxide – 2.55% argon, 94.48% carbon dioxide – 5.52% argon (mole) mixtures. Top panels show predictions ($k_{ij} = 0$), whereas bottom panels show correlations ($k_{ij} \neq 0$).

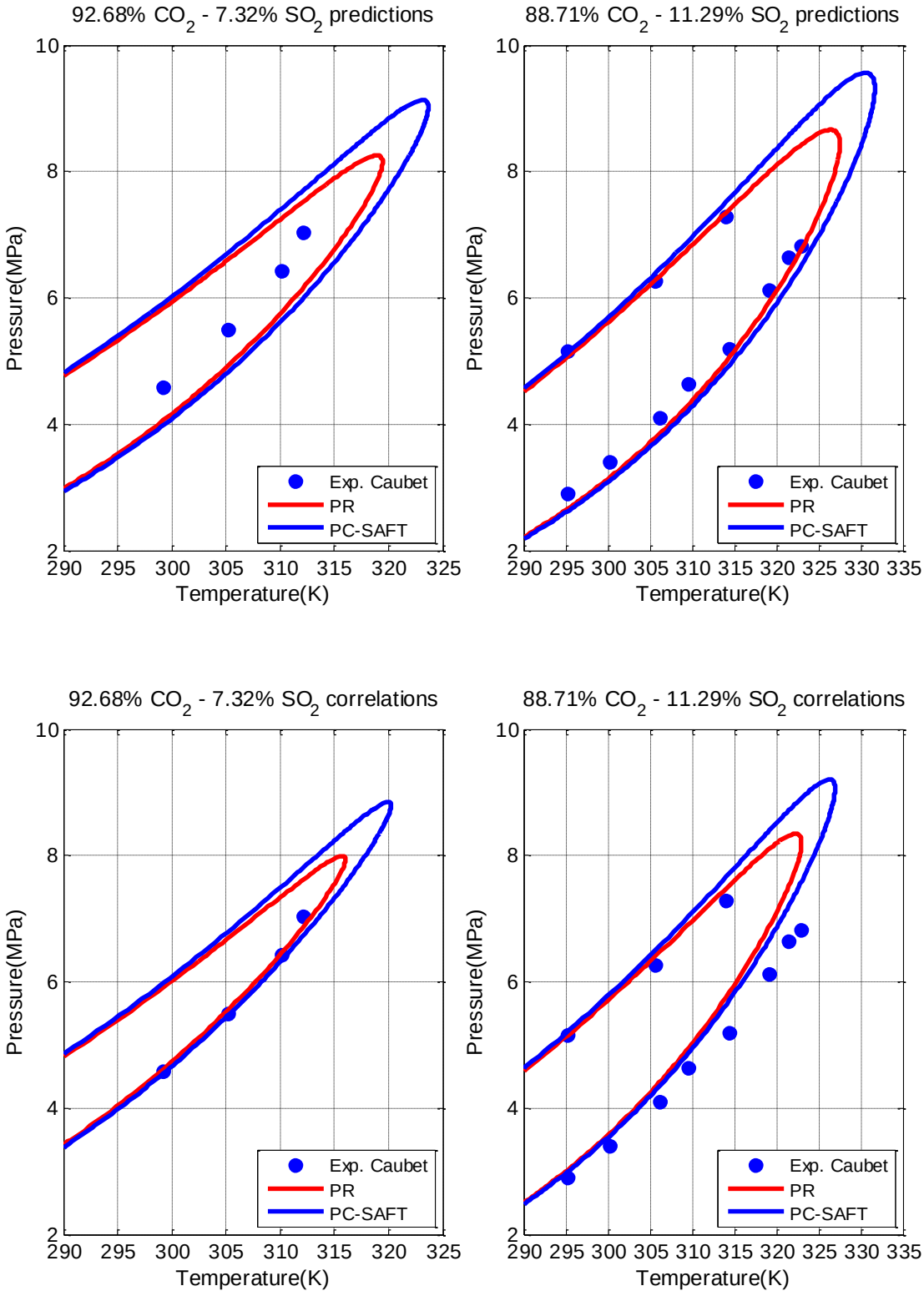

Figure 5-5: Phase envelopes of 92.68% carbon dioxide – 7.32% sulfur dioxide, 88.71% carbon dioxide – 11.29% sulfur dioxide (mole) mixtures. Top panels show predictions ($k_{ij} = 0$), whereas bottom panels show correlations ($k_{ij} \neq 0$).

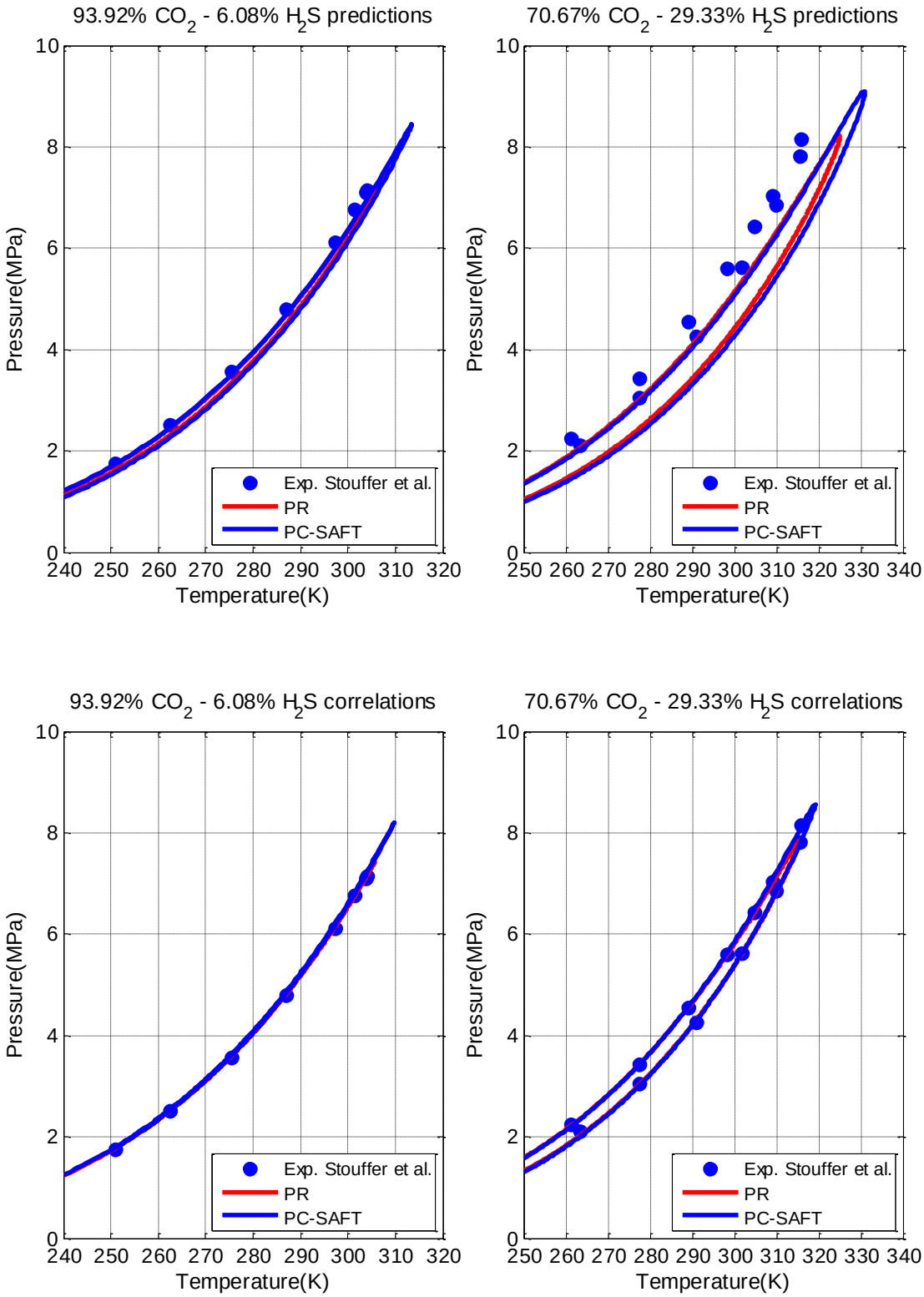

Figure 5-6: Phase envelopes of 93.92% carbon dioxide – 6.08% hydrogen sulfide, 70.67% carbon dioxide – 29.33% hydrogen sulfide (mole) mixtures. Top panels show predictions ($k_{ij} = 0$), whereas bottom panels show correlations ($k_{ij} \neq 0$).

5.2. Ternary and Multicomponent Mixtures of CO_2

Evaluation of the performance of the models on predicting or correlating the phase behavior of ternary and multicomponent mixtures of CO_2 related to CCS processes can be a very good basis for their application in real process calculations.

In this work, experimental data available in the literature for 2 ternary with various compositions and 1 quaternary mixtures of CO_2 with N_2, O_2, Ar and SO_2 have been modeled using the PC-SAFT and PR equations of state. The pure component parameters used are the same with the ones presented in section 5.1 and two types of predictive calculations have been conducted. In the first case, all BIPs have been set equal to zero and in the second the BIPs fitted to experimental binary VLE data (see section 5.1) have been used.

The experimental data sets modeled in this work are presented in Table 5-11. Table 5-12 and Table 5-13 summarize the percentage average absolute deviation between experimental data and model calculations for every mixture.

Table 5-11: Experimental ternary and multicomponent VLE data from Literature modeled in this work.

Composition (mole %)	Temperature (K)	Ref
	CO_2 – Ar - O_2	
97.51 – 1.22 – 1.27 (Mix1)	253.28 – 293.21	Coquelet et al.[59]
96.09 – 1.93 – 1.98 (Mix2)	253.27 – 293.22	Coquelet et al.[59]
95.30 – 2.33 – 2.37 (Mix3)	253.27 – 293. 21	Coquelet et al.[59]
94.51 – 2.71 – 2.78 (Mix4)	253.27 – 291.21	Coquelet et al.[59]
	CO_2 – O_2 – SO_2	
92.70 – 1.90 – 5.40	253.28 – 293.23	Coquelet et al.[59]
	CO_2 – O_2 – Ar – N_2	
89.83 – 5.05 – 2.05 – 3.07	252.65 – 293.35	Chapoy et al.[72]

Table 5-12: AAD% between experimental VLE data and EoS calculations for $CO_2 – Ar – O_2$ mixtures.

EoS			**$CO_2 – Ar - O_2$**			
		k_{ij}	**Mix 1**	**Mix 2**	**Mix 3**	**Mix 4**
			AAD%	**AAD%**	**AAD%**	**AAD%**
PR	Pr.	0	5.29	9.22	10.34	11.04
	Prk.	Binaries	2.68	1.32	1.68	3.78
PC-SAFT	Pr.	0	3.10	6.64	6.95	8.08
	Prk.	Binaries	1.58	1.89	2.05	0.78

"Pr." refers to predictions when k_{ij}= 0, whereas "Prk." refers to predictions when k_{ij} fitted to experimental binary VLE data are used.

Table 5-13: AAD% between experimental VLE data and EoS calculations for $CO_2 – O_2 – SO_2$ and $CO_2 – O_2 – Ar - N_2$ mixtures.

EoS			**$CO_2 – O_2 – SO_2$**	**$CO_2 – O_2 – Ar – N_2$**
		k_{ij}	**AAD%**	**AAD%**
PR	Pr.	0	8.73	12.57
	Prk.	Binaries	3.25	3.67
PC-SAFT	Pr.	0	6.72	9.29
	Prk.	Binaries	2.74	4.50

"Pr." refers to predictions when k_{ij}= 0, whereas "Prk." refers to predictions when k_{ij} fitted to experimental binary VLE data are used.

PC-SAFT predictions when all BIPs are set equal to zero are the most accurate on the average for all 3 mixtures studied with AAD% = 7.05, while PR is less accurate with the predictions giving an average AAD%= 9.84. Moreover, it has to be noted that PC-SAFT is consistently more accurate than PR for every mixture studied when all BIPs are zero.

The use of non-zero BIPs significantly improved the performance of the two models on average, with PC-SAFT giving an AAD% = 2.48 and PR giving an AAD% = 2.82. Contrary to some cases of binary mixtures where the use of BIPs deteriorated the performance of the two EoS, in the case of the multicomponent mixtures studied in this work, the use of non-zero k_{ij} values systematically improved the predictions for every system. In this case, PC-SAFT is again more accurate than PR on average, but for the half of the mixtures studied, PR calculations result in more accurate prediction of the phase behavior.

Representative results for some of the mixtures discussed are given in Figures 5-7 to 5-9. The figures that are not presented in this section can be found in Appendix C.

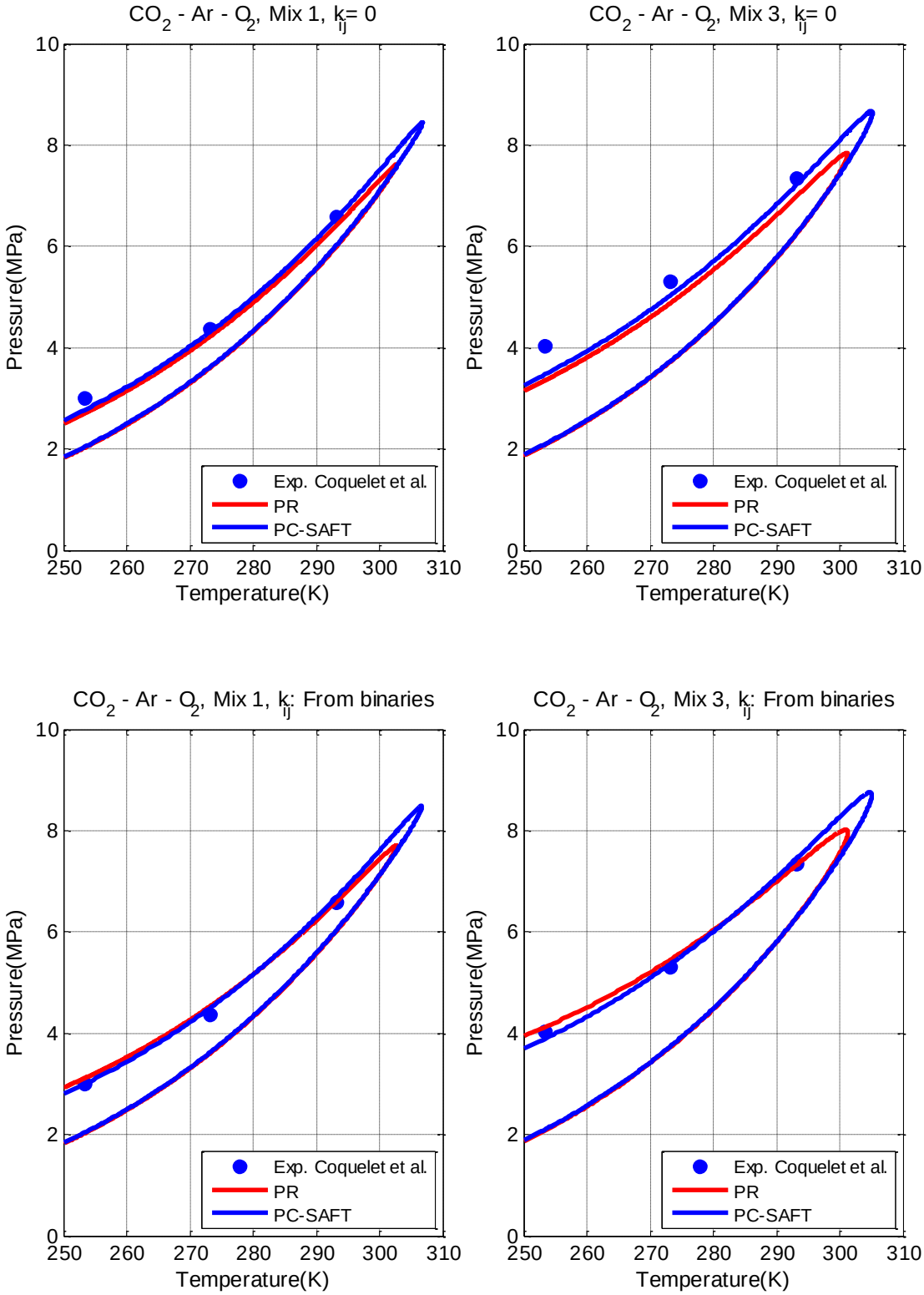

Figure 5-7: Phase envelopes of carbon dioxide – argon - oxygen, mixtures 1 and 3 (see Table 5-11). Top panels show predictions ($k_{ij} = 0$), whereas bottom panels show calculations with k_{ij} fitted to experimental binary VLE data.

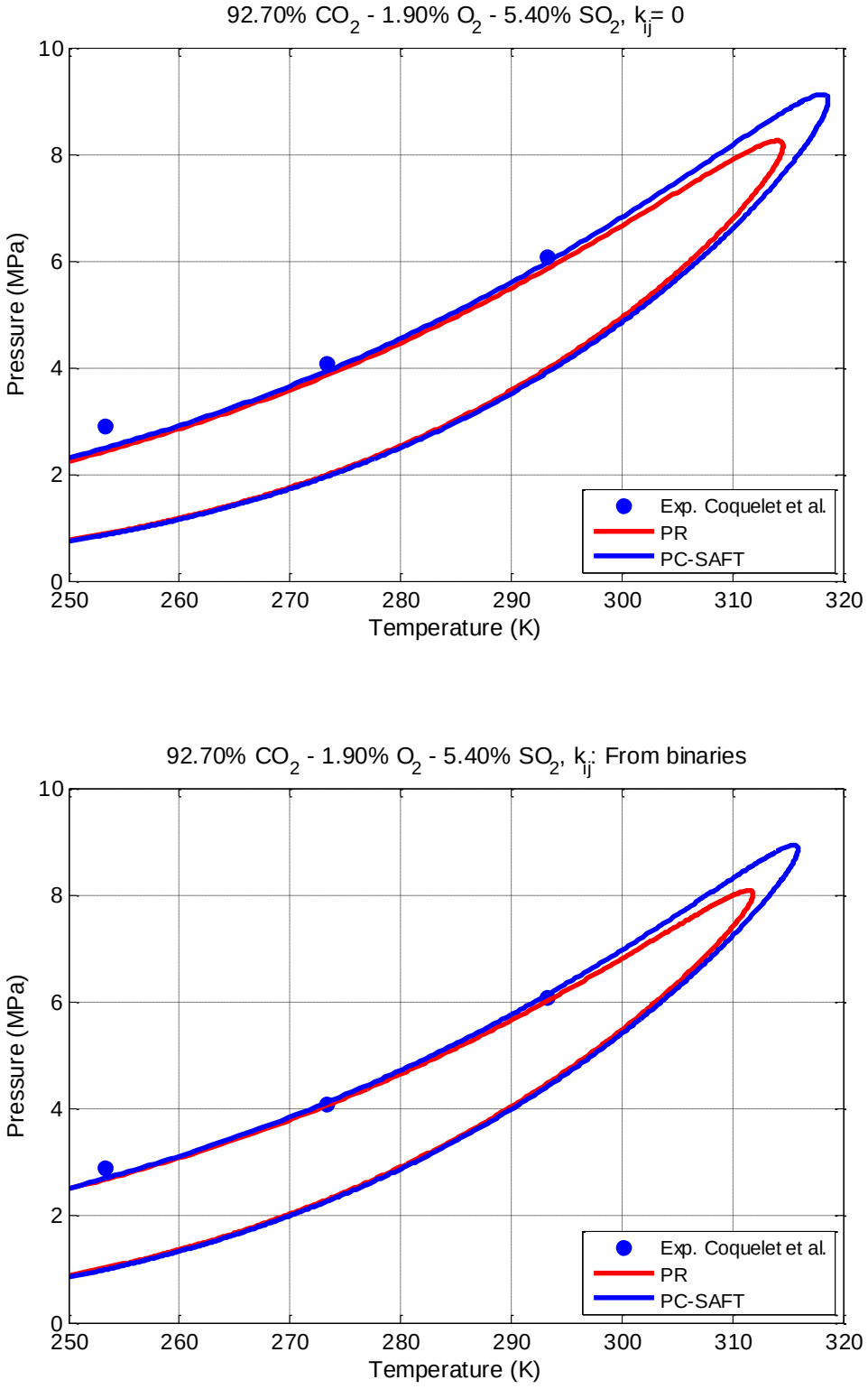

Figure 5-8: Phase envelope of a 92.70% carbon dioxide – 1.90% oxygen – 5.40% sulfur dioxide (mole) mixture. Top panel shows predictions ($k_{ij} = 0$), whereas bottom panel shows calculations with k_{ij} fitted to experimental binary VLE data.

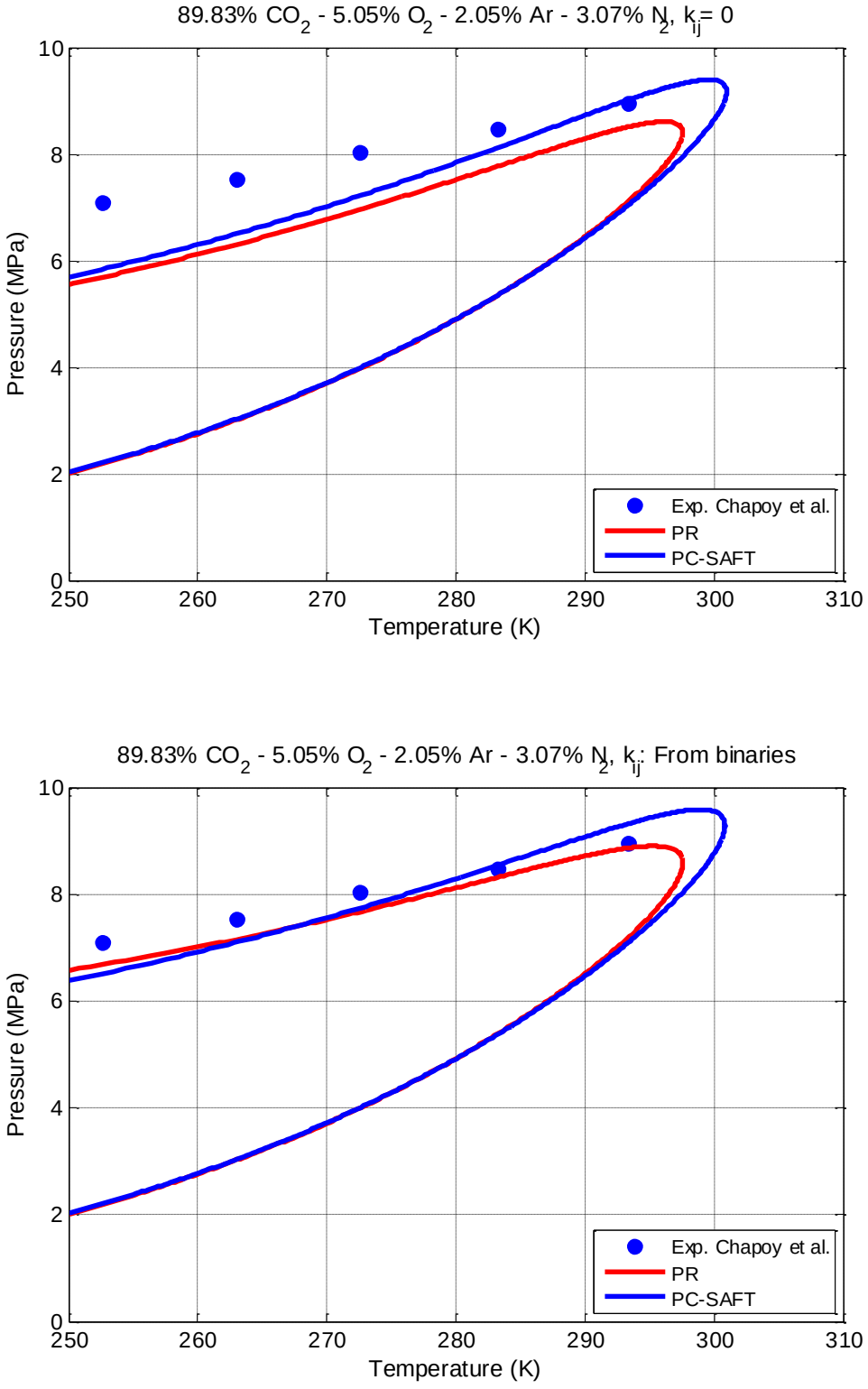

Figure 5-9: Phase envelope of a 89.83% carbon dioxide – 5.05% oxygen – 2.05% argon – 3.07% nitrogen (mole) mixture. Top panel shows predictions ($k_{ij} = 0$), whereas bottom panel shows calculations with k_{ij} fitted to experimental binary VLE data.

5.3. Conclusions

Both cubic and higher order EoS have been used to model the phase behavior of binary and multicomponent mixtures of CO_2 with other gases relevant to CCS applications. The most accurate predictive results for binary mixtures have been provided by PR and PC-SAFT equations of state with the first giving an absolute average deviation over the entire set of mixtures of 5.61% and the latter 5.55%. The use of temperature independent binary interaction parameters resulted in improvement of the modeling results with PR giving an AAD% = 2.37 and PC-SAFT giving an AAD% = 2.02.

The two EoS also provided reliable prediction of the vapor – liquid equilibrium of ternary and quaternary mixtures with the average deviation over the entire set of mixtures for PR being equal to 9.84%, while PC-SAFT being equal to 7.05%. The use of the interaction parameters fitted to binary VLE data significantly improved the performance of the two models on average, with PC-SAFT giving an AAD% = 2.48 and PR giving an AAD% = 2.82.

6. Two phase and Multiphase Solid – Fluid Equilibrium

6.1. Introduction

Identifying solid - fluid equilibria conditions of pure carbon dioxide and also their dependence on impurities are critical to the design and operation of CO_2 pipelines and storage facilities. Since, scenarios with sharp expansion are conceivable, phase equilibria involving solid - liquid as well as solid - gas may occur. Because of CO_2 possessing a relatively high Joule–Thomson expansion coefficient, the rapid expansion of an accidental release may reach temperatures below 180 K. Due to this effect, solid formation following a pipeline puncture or rupture is to be expected, and subsequently, at atmospheric pressure, the solid CO_2 will sublime into gas. In assessing the hazards posed by releases of CO_2, it is important to take account of the fact that the CO_2 gas will be much denser than air, due to both its higher molecular weight and very low temperature. This could lead to a gravity-driven flow of high CO_2-concentration gas, which would tend to flow down slopes and accumulate in low-lying areas.[7] Taking this into account, it is easily understood that the formation of dry-ice resulting from solid - fluid equilibrium can largely affect the safety of CCS facilities during equipment depressurization, process shutdown or other process upsets.

In this work, solid models of different complexity (see section 2.2) have been developed to model the solid – fluid phase behavior of pure CO_2 and also mixtures of CO_2 with other compounds. The solid models have been coupled with different fluid equations of state and the performance of each resulting model has been assessed. The Correlation and Thermodynamic Integration models have been coupled with SRK, PR and PC-SAFT EoS and the Jager and Span EoS has been coupled with PC-SAFT. As a result, 7 different models have been used and been evaluated for different mixtures.

The first step has been the evaluation of every model for the description of pure carbon dioxide in solid – vapor (SV) and solid – liquid (SL) equilibrium conditions. This way, the performance of every solid model, coupled with different EoS, could be tested and also the agreement between the different models could be assessed. Moreover, an accurate description of the solid – fluid (SF) equilibrium behavior of the pure solid former is a good basis for subsequent two phase mixture modeling and three phase SLG equilibrium calculations. As it is going to be shown later, accurate description of the triple point of the pure solid forming compound is crucial for the overall performance of a model when SLG equilibrium calculations for binary mixtures are concerned.

Furthermore, the effect on the SF equilibrium behavior of CO_2 when impurities like N_2 are added and a mixture is formed has been tested. Because of the lack of experimental

data for two phase solid – fluid equilibrium for these mixtures, the performance of the different models has been evaluated on SLG equilibrium behavior, using experimental data available in the literature. Two mixtures of CO_2 (relevant with CCS applications) with N_2 and H_2 have been modeled where CO_2 forms a pure solid phase at SLG equilibrium conditions. Moreover, three other binary mixtures, where naphthalene and phenanthrene form the solid phase have been modeled to further assess the accuracy of the solid models.

6.2. Two phase Solid – Fluid Equilibrium modeling

Table 6-1 and Table 6-2 summarize the pure component parameters of the cubic and the PC-SAFT EoS used to model the fluid phases studied in this work. Tables 6-3 to 6-7 summarize the parameters used by every solid model, for the different solid forming compounds studied in this work.

Table 6-1: Critical Temperature (T_c), Critical Pressure (P_c) and Acentric Factor (ω) values for the components studied in this work.[73]

Component	T_c (K)	P_c(MPa)	ω
H_2	33.19	1.313	-0.216
C_2H_4	282.34	5.04	0.0865
Naphthalene	748.35	4.05	0.3022
Phenanthrene	869.25	2.90	0.4949

Table 6-2: PC-SAFT EoS parameters for the components studied in this work.

Component	m	σ (Å)	ε/k (K)	ε^{AB}/k (K)	κ^{AB}	Ref
H_2	1.0	2.9860	19.2775	-	-	74
Ethylene	1.5930	3.4450	176.47	-	-	16
Naphthalene	3.0047	3.9133	353.63	-	-	75
Phenanthrene	3.8494	4.1477	377.1719	-	-	This work

Table 6-3: Thermodynamic integration model parameters for solid – vapor equilibrium.[73]

Component	Thermodynamic Integration Model				
	Solid - Vapor				
	T_{0i}^{SV}(K)	Δh_{0i}^{SV}(J/mol)	v_{0i}^{S}(cm^3/mol)	$\Delta c_{P,0i}^{SV^*}$(J/mol K)	P^+ (MPa)
CO_2	194.5	26300[a]	29.091	-23.611	0.1

[a] Δh_{0i}^{SV} value taken from Chickos and Acree.[76]

Table 6-4: Thermodynamic integration model parameters for solid – liquid equilibrium.[73]

Component	Thermodynamic Integration Model					
	Solid - Liquid					
	$T_{0i}^{SL}(K)$	$\Delta h_{0i}^{SL}(J/mol)$	$v_{0i}^{S}(cm^3/mol)$	$v_{0i}^{L^*}(cm^3/mol)$	$\Delta c_{P,0i}^{SL^*}(J/mol\,K)$	P^+ (MPa)
CO_2	216.58	8875[a]	29.091	37.347	20.205	0.6
Naphthalene	353.43	19318[b]	112.0	131.0	-[c]	0.1
Phenanthrene	372.38	16463	155.0	167.0	-[c]	0.1

[a] Δh_{0i}^{SL} value for CO_2 has been taken from Jager and Span[22], who used it as an adjustable parameter.

[b] Δh_{0i}^{SL} value for Naphthalene has been taken from Corrazza et al.[77]

[c] For the cases of Naphthalene and Phenanthrene, the two terms involving the difference between solid and liquid heat capacities have been truncated.

Table 6-5: DIPPR[73] correlations for CO_2 SV and SL saturation pressures.

Equilibrium Type	Correlation Model
	CO_2
Solid - Vapor	$P^{sat}(MPa) = \exp\left[14.57893 \cdot \left(1 - \frac{T_{tr}}{T}\right) - 14.48067 \cdot \ln\left(\frac{T}{T_{tr}}\right) + 65.35685 \cdot \left(\frac{T}{T_{tr}} - 1\right) - 47.14593 \cdot \left(\left(\frac{T}{T_{tr}}\right)^2 - 1\right) + 14.53922 \cdot \left(\left(\frac{T}{T_{tr}}\right)^3 - 1\right) + \ln(P_{tr})\right]$
Solid - Liquid	$P^{sat}(MPa) = P_{tr} \cdot \left[1 - 648.13886 + \exp\left(3 \cdot \ln\left(\frac{T}{T_{tr}}\right) + \ln(648.13886)\right)\right]$
	$T_{tr} = 216.58\ K$
	$P_{tr} = 0.51867\ MPa$

Table 6-6: Antoine equations for naphthalene and phenanthrene SV saturation pressures.

Component	Correlation Model		
	Solid - Vapor		
	A[a]	B[a]	C[a]
Naphthalene	9.4144	2603.4	-49.52
Phenanthrene	11.4200	4567.7	0
	$\log(P^{sat}\,[mmHg]) = A - \frac{B}{T[K] + C}$		

[a] Antoine constants for Naphthalene are taken from Bertakis et al.[78] and for Phenanthrene from Spiliotis et al.[79]

Table 6-7: Jager and Span solid EoS parameters, adjusted for PC-SAFT EoS.

Jager and Span EoS for solid CO_2		
PC-SAFT		
g_0	**g_1**	**Ref**
7.447399	-2.19139	This work

In Figure 6-1, a comparison of three different solid models for the pure CO_2 solid – vapor equilibrium is presented. The DIPPR correlation is fitted on experimental SVE data of pure CO_2 and as a result it can be used as a basis to assess the performance of the other two models. The results presented in Figure 6-1 show that the correlation and the Jager – PCSAFT models completely coincide, whereas the thermodynamic integration model coupled with PC-SAFT deviates at temperatures higher than 200 K. In Figure 6-2, the effect on the solid – vapor equilibrium line when 5% N_2 (mole) is added in pure CO_2, is presented. The addition of N_2 in CO_2 shifts the equilibrium curve to higher pressures and again there is excellent agreement between the correlation and Jager and Span EoS, whereas the thermodynamic integration model deviates from the other two at high temperatures.

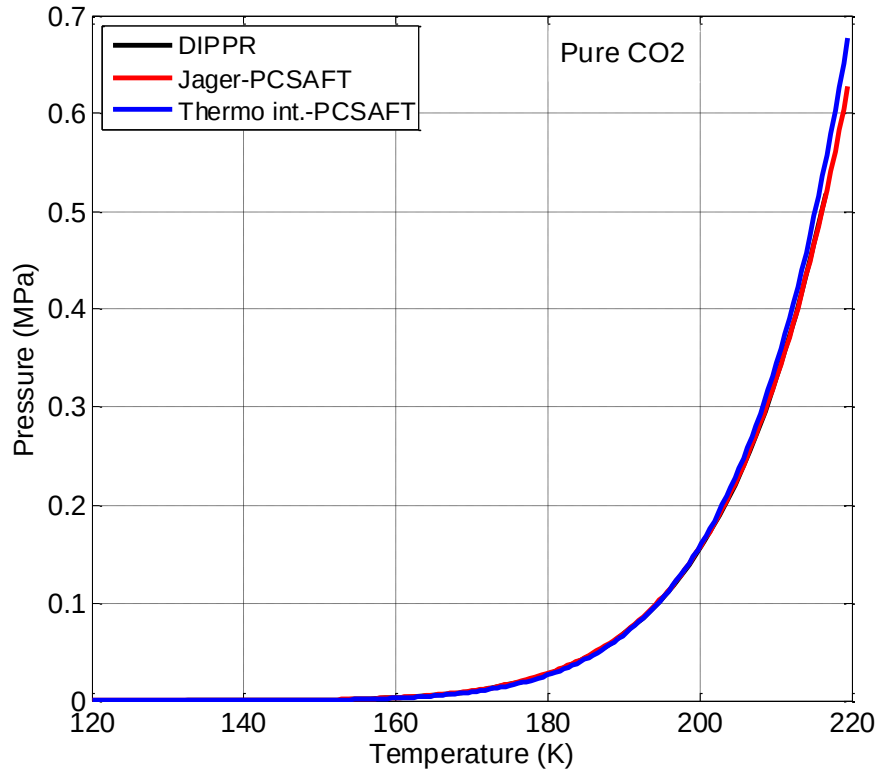

Figure 6-1: Comparison of the DIPPR correlation, the thermodynamic integration model and the Jager and Span EoS, coupled with PC-SAFT for pure CO_2 solid – vapor equilibrium.

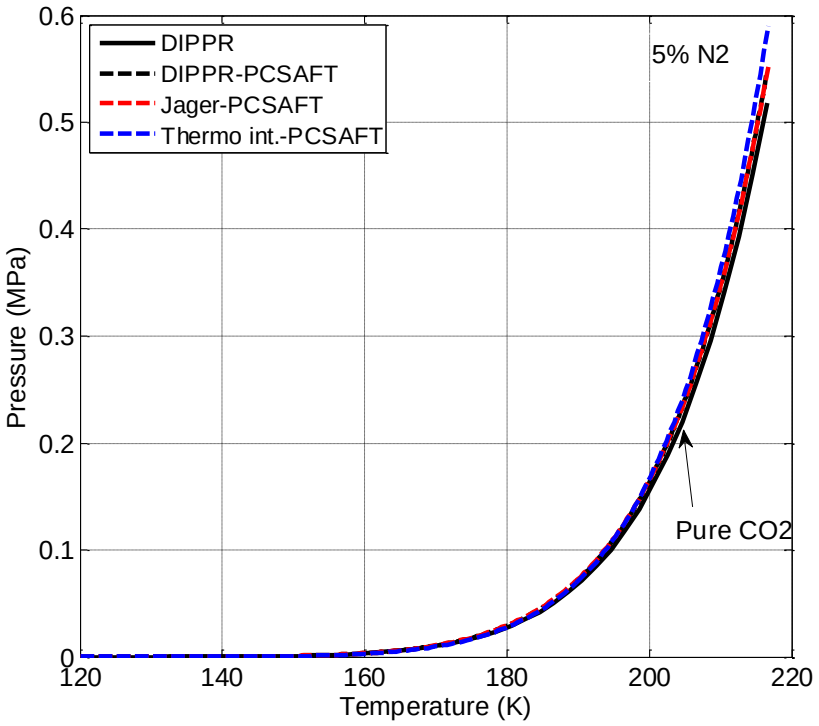

Figure 6-2: Comparison of the correlation, the thermodynamic integration and the Jager and Span EoS models, coupled with PC-SAFT, when 5% N_2 (mole) is added in pure CO_2 at solid – vapor equilibrium.

The same comparison has been performed between the solid models also for the SLE of pure CO_2. The results are presented in Figure 6-3. In this case, all three models present very good agreement at low temperatures until 226 K, where Jager – PCSAFT model starts to deviate from the other two. It is interesting to note at this point that the thermodynamic integration and the correlation models present very good agreement for the entire temperature range, even at very high pressures. Addition of 5% N_2 (mole) in pure CO_2 (Figure 6-4), shifts the equilibrium solid – liquid line to higher pressures, but the effect in this case is much more prevalent than the solid – vapor case. The three solid models, coupled with PC-SAFT EoS present relatively good agreement for low temperatures until 226 K, where they start to deviate from each other. In this case, the thermodynamic integration and the correlation models present very good agreement, but the deviation between them is greater at high pressures than the pure carbon dioxide case.

The effect of coupling different fluid equations of state with the same solid model has been also investigated. In Figure 6-5 and Figure 6-6 the effect of coupling SRK, PR and PC-SAFT EoS with the correlation model for a 95% CO_2 – 5% N_2 (mole) mixture at SVE and SLE respectively is presented. As expected, the different fluid EoS alter the predictions significantly at SLE rather than at SVE, as the deviations from ideality are more pronounced in the liquid phase and at high pressures.

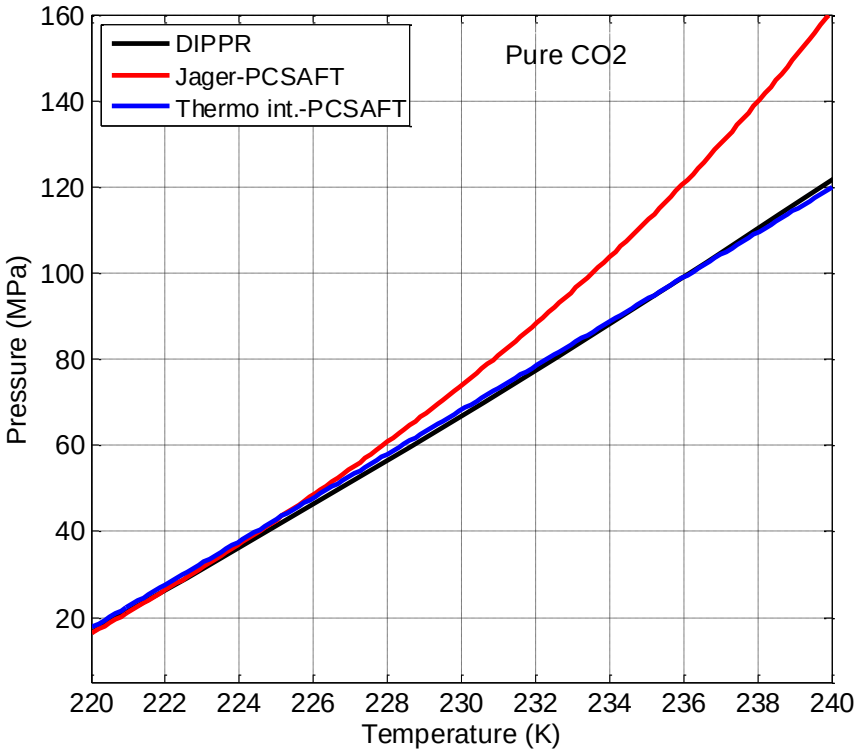

Figure 6-3: Comparison of the DIPPR correlation, the thermodynamic integration model and the Jager and Span EoS, coupled with PC-SAFT for pure CO_2 solid – liquid equilibrium.

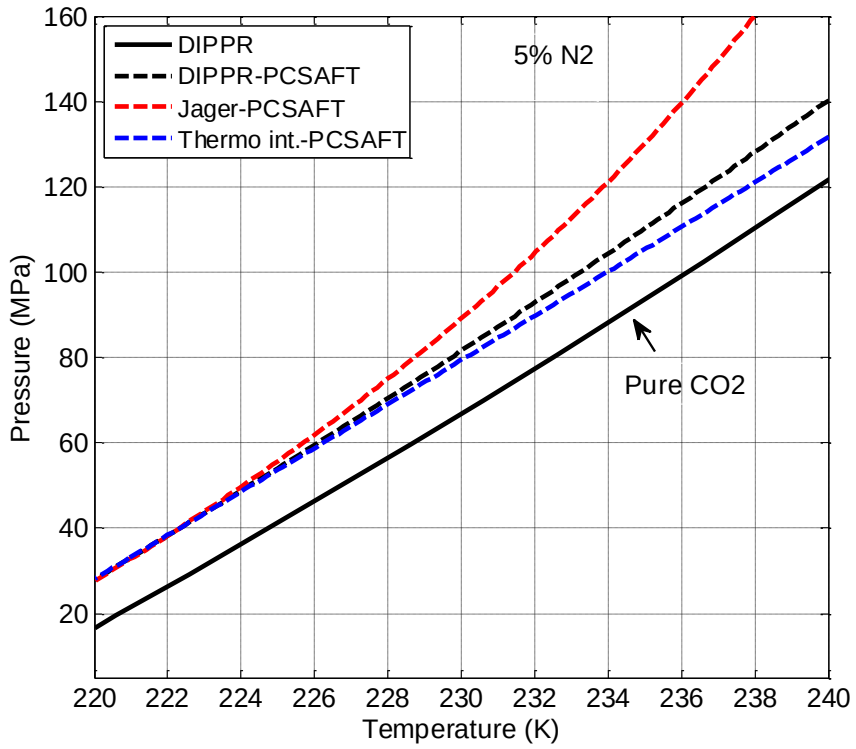

Figure 6-4: Comparison of the correlation, the thermodynamic integration and the Jager and Span EoS models, coupled with PC-SAFT, when 5% N_2 (mole) is added in pure CO_2 at solid – liquid equilibrium.

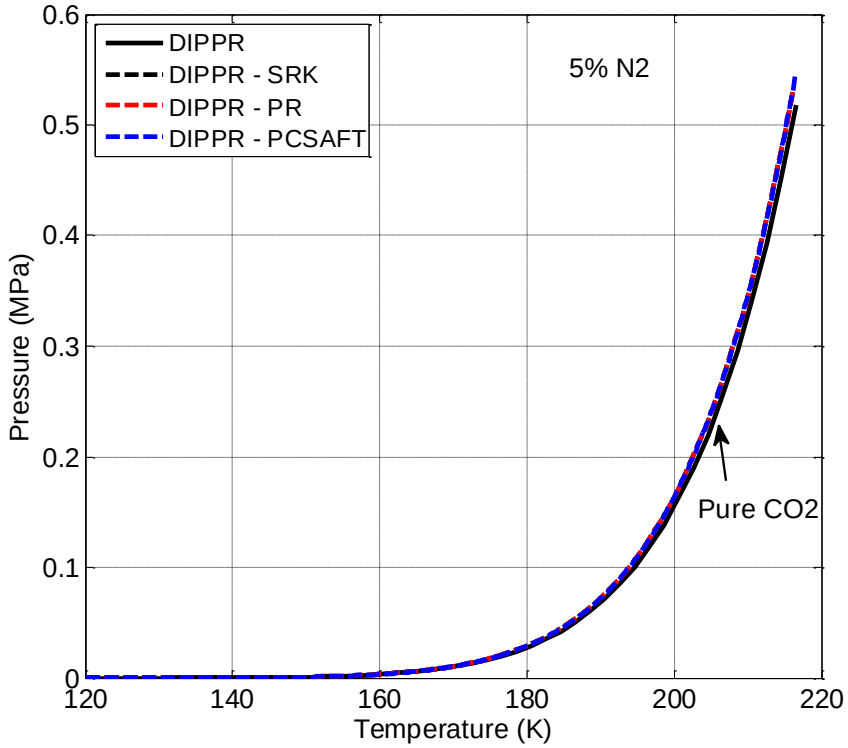

Figure 6-5: Effect of different fluid equations of state, coupled with the correlation model, on the predicted solid – vapor equilibrium of 95% CO_2 – 5% N_2 (mole) mixture.

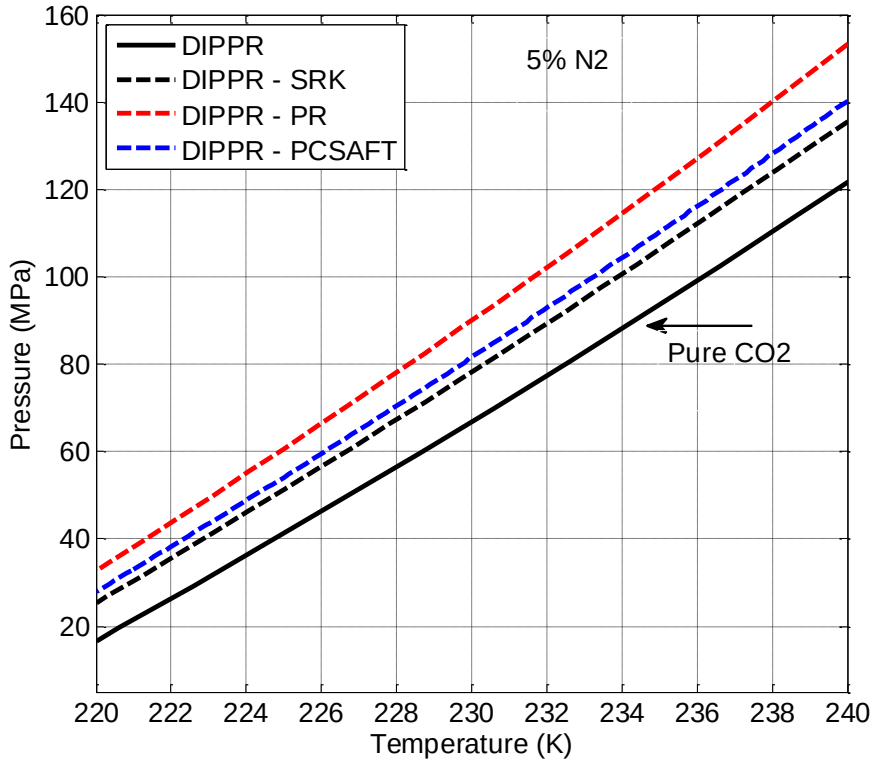

Figure 6-6: Effect of different fluid equations of state, coupled with the correlation model, on the predicted solid – liquid equilibrium of 95% CO_2 – 5% N_2 (mole) mixture.

6.3. Multiphase Solid – Fluid Equilibrium modeling

As it has already been mentioned, there is scarcity of experimental data for the mixtures of interest in this work, particularly at two phase SFE conditions. To validate the models, experimental data measured at SLGE conditions, available in the literature have been used. The same models have been implemented to calculate the three phase coexistence curves of binary mixtures of CO_2 with other compounds, where CO_2 forms the pure solid phase. To further test the results of the implemented models, the calculations have been extended to other mixtures, where compounds like naphthalene and phenanthrene solidify in presence of another compound.

Table 6-8: Experimental binary SLG data from Literature modeled in this work.

Pressure (MPa)	**Ref**
CO_2 – N_2	
4.8 – 13.01	80
CO_2 – H_2	
4.3 – 13.7	80
Naphthalene – CO_2	
0.1 – 23.17	78
2.2 - 24.25	81
10.64 – 26.35	82
14.19 – 25.60	83
8.84 – 26.30	84
0.10 – 20.00	85
Naphthalene – Ethylene	
1.1 – 7.61	86
Phenanthrene – CO_2	
1.40 – 28.00	78

In Tables 6-9 to 6-13, the percentage average absolute deviation (AAD %) between experimental SLG data and model calculations for each system and corresponding k_{ij} values are presented. The AAD % between model calculations and experimental data in this case is calculated as the difference between the calculated and the experimentally measured equilibrium temperature at specific pressure using the following form:

$$\text{AAD } \% = \frac{100}{\text{NP}} \sum_{i=1}^{\text{NP}} \left| \frac{T_i^{\text{calculated}} - T_i^{\text{experimental}}}{T_i^{\text{experimental}}} \right| \tag{6.1}$$

Table 6-9: AAD% between experimental SLG data and model calculations for the $CO_2 - N_2$ system and corresponding k_{ij} values.

EoS		$CO_2 - N_2$			
		k_{ij}	Thermodynamic Integration model	Correlation model	Jager and Span EoS
			AAD%	AAD%	AAD%
SRK	Pr.	0	0.14	0.25	-
	Cor.	-	-	-	-
PR	Pr.	0	0.025	0.33	-
	Cor.	-	-	-	-
PC-SAFT	Pr.	0	0.075	0.11	0.08
	Cor.	0.00575	0.040	0.03	0.02

"Pr." refers to predictions ($k_{ij} = 0$), whereas "Cor." refers to correlations (calculations with $k_{ij} \neq 0$).

Table 6-10: AAD% between experimental SLG data and model calculations for the $CO_2 - H_2$ system and corresponding k_{ij} values.

EoS		$CO_2 - H_2$			
		k_{ij}	Thermodynamic Integration model	Correlation model	Jager and Span EoS
			AAD%	AAD%	AAD%
SRK	Pr.	0	0.118	0.02	-
	Cor.	-	-	-	-
PR	Pr.	0	0.217	0.58	-
	Cor.	-	-	-	-
PC-SAFT	Pr.	0	0.131	0.07	0.05
	Cor.	0.05984	0.053	0.02	0.003

"Pr." refers to predictions ($k_{ij} = 0$), whereas "Cor." refers to correlations (calculations with $k_{ij} \neq 0$).

Table 6-11: AAD% between experimental SLG data and model calculations for the Naphthalene - CO_2 system and corresponding k_{ij} values. AAD% is calculated based on the experimental data of Bertakis et al.[78]

EoS		**Naphthalene – CO_2**			
		Thermodynamic Integration model		**Correlation model**	
		k_{ij}	**AAD%**	**k_{ij}**	**AAD%**
SRK	Pr.	0	-	0	-
	Cor.	0.130	0.182	0.118	0.163
PR	Pr.	0	-	0	-
	Cor.	0.129	0.167	0.10	1.05
PC-SAFT	Pr.	0	-	0	-
	Cor.	0.167	0.124	0.172	0.510

Table 6-12: AAD% between experimental SLG data and model calculations for the Naphthalene - Ethylene system and corresponding k_{ij} values.

EoS		**Naphthalene – Ethylene**			
		Thermodynamic Integration model		**Correlation model**	
		k_{ij}	**AAD%**	**k_{ij}**	**AAD%**
SRK	Pr.	0	0.684	0	0.709
	Cor.	0.02	0.103	-	-
PR	Pr.	0	1.06	0	1.01
	Cor.	0.03	0.080	-	-
PC-SAFT	Pr.	0	1.42	0	1.67
	Cor.	0.024	0.035	-	-

Table 6-13: AAD% between experimental SLG data and model calculations for the Phenanthrene - CO_2 system and corresponding k_{ij} values.

EoS		**Phenanthrene – CO_2**	
		Thermodynamic Integration model	
		k_{ij}	**AAD%**
SRK	Pr.	0	-
	Cor.	0.190	0.312
PR	Pr.	0	-
	Cor.	0.182	0.331
PC-SAFT	Pr.	0	-
	Cor.	0.225	0.189

The coexistence of three phases at SLG equilibrium conditions implies that the chemical potential of the solid former in the solid phase has to be equilibrated with its chemical potential in the two fluid phases. As it has already been discussed in section 3.2.2, this leads to satisfaction of two independent equations. As a result, to calculate the specific type of equilibrium, one can choose to solve either Eqs. (3.50) or Eqs. (3.51). In the first case the solid chemical potential will be equilibrated with the liquid chemical potential, whereas in the second case with the vapor chemical potential.

When the Thermodynamic integration model has been used for the SLG equilibrium calculations in this work, the calculation was performed by solving Eqs. (3.50). Judging by the results of the model for the pure CO_2, the model is more accurate in the solid – liquid case, because the fitted enthalpy is used and the enthalpic term has the major impact on the results.[21] If the SV thermodynamic integration model was used, the calculations would be less accurate because the model fails to describe very accurately the pure CO_2 SVE curve. Of course, if the two models had the same performance in describing the pure CO_2 saturation curves, the choice would be insignificant. Finally, the terms that include the difference between isothermal heat capacities between the solid and the liquid had been truncated because they cancel out each other, thus having practically no impact on the result.[21]

When SLG calculations with the use of a correlation that provides the saturation pressure are concerned, one has to choose between using a correlation for the solid – vapor or the solid – liquid equilibrium curves. Normally, these correlations are accurate only within the range of fitting which means that an SVE correlation should be used for temperatures lower and until the triple temperature of the pure solid former, whereas an SLE correlation should be used for temperatures greater than the triple temperature. The P-T projection of the SLG equilibrium curve for many compounds is located at temperatures lower than the triple temperature of the pure solid former. For these cases, using an SVE correlation and solving the set of equations (3.51) is the valid choice. There are systems though, where the SLG equilibrium curve lies at temperatures greater than the triple temperature of the pure solid former. In this case, an SLE correlation should be used. All the systems studied in this work, present SLG curves that lie at lower temperatures than the pure solid former triple temperature, except for the case of the $CO_2 – H_2$ mixture. The same approach used for fitted correlations is also used when SLG calculations with the Jager and Span solid EoS are concerned.

For the case of the $CO_2 – N_2$ system, the thermodynamic integration model coupled with PR EoS gives the most accurate predictive results with an AAD% = 0.025, while PC-SAFT is slightly less accurate (AAD% = 0.075). Coupling all the fluid EoS with the correlation model results in higher deviations, ranging from 0.11 – 0.33 AAD%. The higher deviations in this case for the cubic EoS are due to their inaccuracy to reproduce the pure CO_2

triple point. PC-SAFT in this case successfully predicts it, giving the most accurate results with this model, but in general less accurate than the thermodynamic integration model. At this point is has to be noted that all fluid EoS reproduce accurately the pure CO_2 triple point when coupled with the thermodynamic integration model because the triple temperature is an input parameter in this modeling approach, since the reference pressure is very close to the triple point of the pure solid former and as a result all the input parameters are taken at this point. Finally, the Jager and Span EoS coupled with PC-SAFT results in very similar predictions with the thermodynamic integration model (AAD% = 0.08).

To improve the performance of the models, k_{ij} parameters have been regressed. Instead of implementing the traditional approach and regress BIPs straight on the SLG data, a different methodology has been adopted. For this system isothermal VLE data at low temperature (T= 218.15 K) are available in the literature.[80] In Table 6-14, the AAD% between experimental VLE data and modeling results at T= 218.15 K, using SRK, PR and PC-SAFT EoS are presented. The AAD% have been calculated as the deviations of the calculated and the experimentally measured vapor and liquid compositions at specific temperature and pressure. The PR predictions are the most accurate, while PC-SAFT is slightly less accurate, which is in agreement with the SLG modeling results when a solid model that accurately predicts the pure solid former triple point is used. Moreover, if the assumption of a pure solid phase is valid, the SLG prediction of a model is a combination of the accuracy of the solid model to describe the pure solid former SVE or SLE and the accuracy of the EoS to describe the fluid phases. As a result, k_{ij} parameters were regressed using low temperature isothermal CO_2 – N_2 VLE data, with the PC-SAFT EoS. The corresponding BIPs and the AAD% between experiments and correlations are also summarized in Table 6-14. The use of the regressed BIPs resulted in a more accurate description of the SLG behavior with every solid model coupled with PC-SAFT. The most accurate model in this case is the Jager and Span EoS (AAD% = 0.02).The deviations from experimental data are summarized in Table 6-9. In Figure 6-7 and Figure 6-8, the SLG calculation results with the different solid models and fluid equations of state are presented, while Figure 6-9 presents the predictions and correlations of the different EoS for the binary VLE data of CO_2 – N_2 mixture at T= 218.15 K.

The same approach has been adopted also for the CO_2 – H_2 system. In this mixture, the correlation model is generally more accurate than the thermodynamic integration model, except for the case of the PR EoS. In both models, SRK gives the most accurate prediction of the SLG behavior, while PC-SAFT is slightly less accurate. The Jager and Span EoS coupled with PC-SAFT predicts very accurately the SLG equilibrium (AAD% = 0.05), but still the correlation model coupled with SRK is slightly more accurate (AAD%= 0.02). In this system, k_{ij} values were also regressed on experimental binary VLE data[80] at low temperature (T=

218.15 K) with PC-SAFT. The use of BIPs, improved the description of the SLG equilibrium, leading to very low deviations, especially with the Jager and Span EoS (AAD% = 0.003). Figures 6-10 to 6-12 present the SLG and VLE modeling results for the $CO_2 – H_2$ system.

The calculation of the SLG equilibrium has been also extended to three other binary mixtures - where naphthalene and phenanthrene form the pure solid phase - with the thermodynamic integration and the correlation models. The Jager and Span EoS is specifically developed for solid CO_2 and as a result it cannot be used for other compounds.

For the naphthalene – CO_2 system, the use of binary interaction parameters was complementary for the models to describe the SLG behavior. Calculations with k_{ij} values set equal to zero, resulted in high deviations from the experimental data and also P-T lines with the wrong trend. In this mixture, the correlation model fails to accurately reproduce the normal melting point of naphthalene with PR and PC-SAFT EoS. More specifically, PC-SAFT over predicts the equilibrium temperature at 0.1 MPa by 3.3 K and PR by 7.4 K. SRK presents a much better behavior as it over predicts the normal melting point by only 0.9 K. As a result, SRK EoS correlates the phase behavior better than the other EoS with an AAD% = 0.163, while PC-SAFT and PR present deviations of 0.51% and 1.05% respectively. The thermodynamic integration model significantly improves the overall performance of the fluid EoS as it successfully describes the normal melting point of the solid compound. PC-SAFT in this case is the most accurate model with AAD% = 0.124 and PR presents an AAD% = 0.167. The performance of SRK is slightly worse than before with AAD% = 0.182, because when compared to the other two EoS fails to describe very accurately the high pressure region of the SLG curve. The AAD% mentioned are calculated using the experimental data of Bertakis et al.[78], but there are plenty of other experimental data and a relative scattering occurs. Figure 6-13 presents the calculations using the two solid models for the naphthalene – CO_2 system and Figure 6-14 presents a comparison between the thermodynamic integration model coupled with PC-SAFT and many different experimental data sets available.

Another system where naphthalene forms the solid phase is the naphthalene – ethylene mixture. In this case, the use of BIPs was not a prerequisite so that a relatively good agreement between experimental data and model calculations could be achieved. The correlation model again fails to satisfactory reproduce the normal melting point of the solid compound with PC-SAFT and PR, while SRK presents a better behavior and as a result it provides a more accurate prediction of the equilibrium curve. The use of the thermodynamic integration model improves the predictive results and a very good agreement between experiments and calculations is achieved when binary interaction parameters are used. More specifically, PC-SAFT coupled with the thermodynamic integration model results in a deviation of 0.035%, while PR and SRK present deviations of 0.080% and 0.103% respectively. The results for this system are presented in Figure 6-15 and Figure 6-16.

The last system examined, was the phenanthrene – CO_2 mixture. Similarly to the naphthalene – CO_2, the use of BIPs was complementary for the models to present the correct trend. The overall fit with the correlation model with all three fluid equations of state was very poor and the results are not presented at all. The use of the thermodynamic integration model results in good agreement between experimental data and model calculations with PC-SAFT being the most accurate EoS (AAD% = 0.189). PR and SRK present deviations of 0.331% and 0.312%. All three EoS correlate really well the low pressure region of the SLG curve, but the deviations become greater in the high pressure region, where PC-SAFT presents the best performance. The calculations for this system are shown in Figure 6-17.

Table 6-14: AAD% between experimental VLE data and EoS calculations for $CO_2 – N_2$ and $CO_2 – H_2$ mixtures at T= 218.15 K and corresponding k_{ij} values.

EoS			**$CO_2 – N_2$**		**$CO_2 – H_2$**	
		Phase	**k_{ij}**	**AAD%**	**k_{ij}**	**AAD%**
SRK	Pr.	Liquid	0	7.18	0	23.38
		Vapor	0	1.15	0	0.430
	Cor.	Liquid	-	-	-	-
		Vapor	-	-	-	-
PR	Pr.	Liquid	0	4.26	0	50.90
		Vapor	0	0.91	0	0.865
	Cor.	Liquid	-	-	-	-
		Vapor	-	-	-	-
PC-SAFT	Pr.	Liquid	0	6.95	0	13.25
		Vapor	0	0.85	0	1.87
	Cor.	Liquid	0.00575	4.59	0.05984	2.59
		Vapor	0.00575	1.06	0.05984	1.97

"Pr." refers to predictions (k_{ij}= 0), whereas "Cor." refers to correlations (calculations with $k_{ij} \neq 0$).

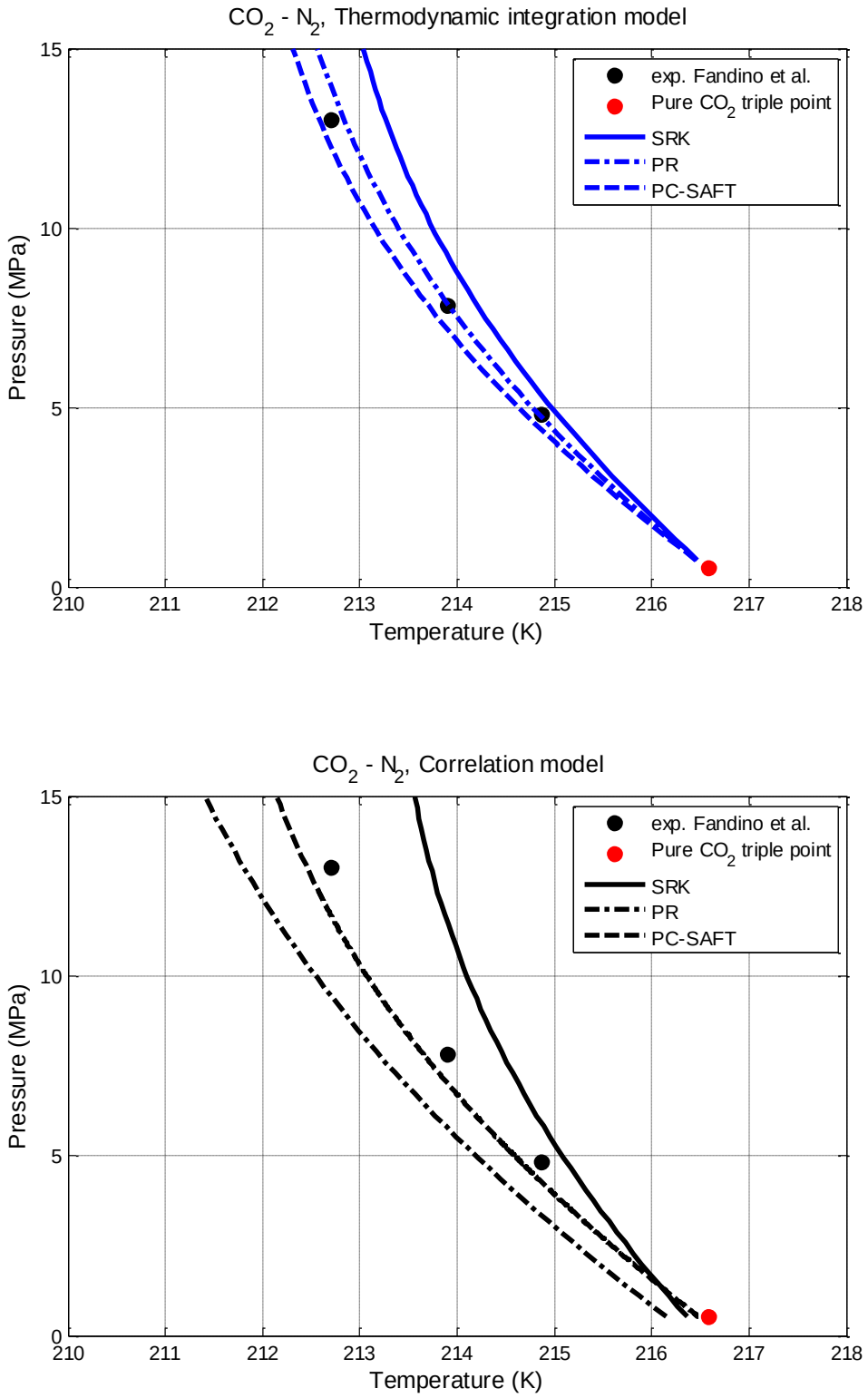

Figure 6-7: P-T projections of the SLG equilibrium curve of the CO_2 – N_2 system. Top panel shows the results with the Thermodynamic Integration model and bottom panel with the Correlation model.

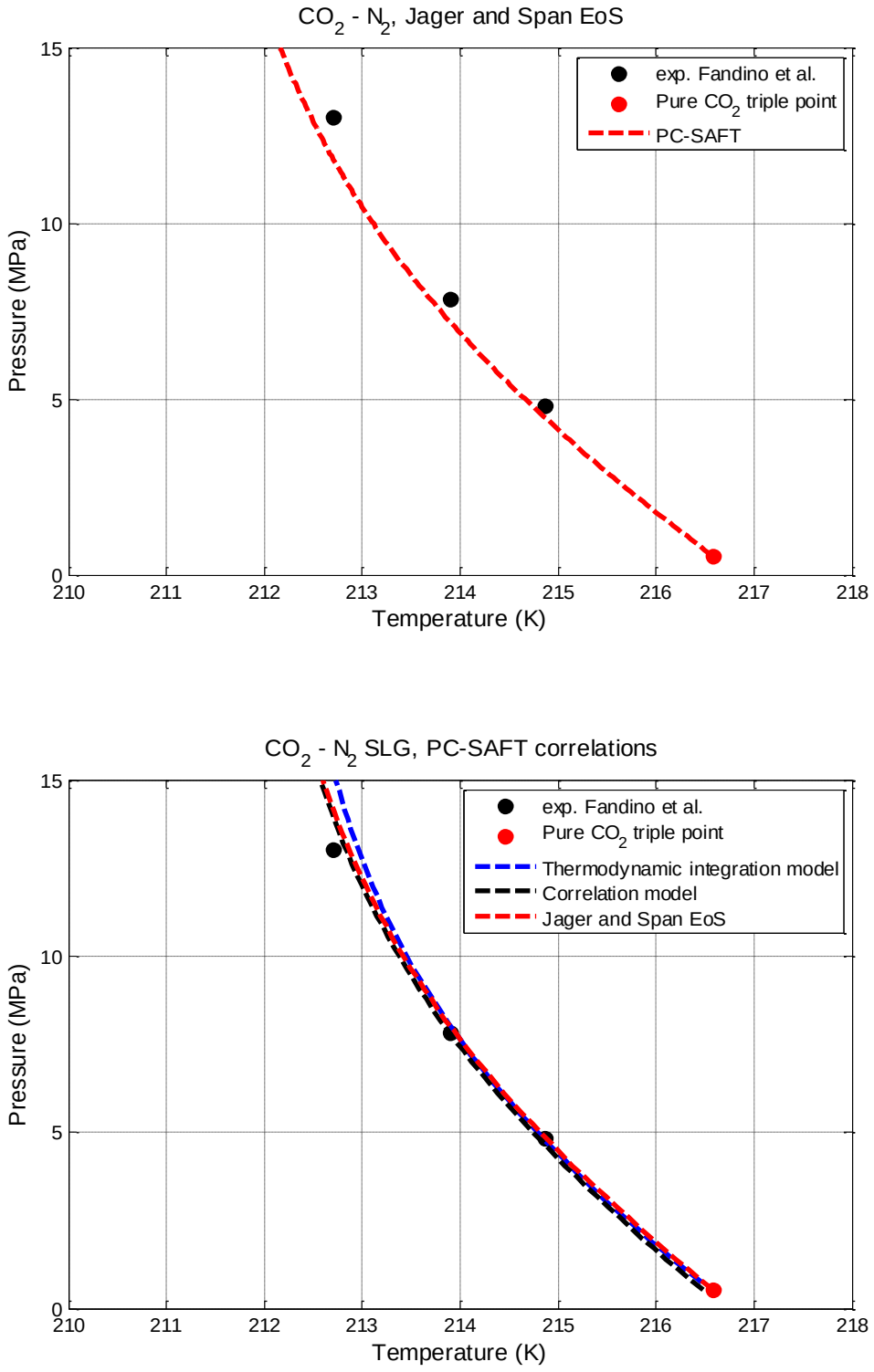

Figure 6-8: P-T projections of the SLG equilibrium curve of the CO_2 – N_2 system. Top panel shows the results with the Jager and Span EoS and bottom panel shows the results of all solid models coupled with PC-SAFT, when k_{ij} parameters fitted to experimental binary VLE data are used.

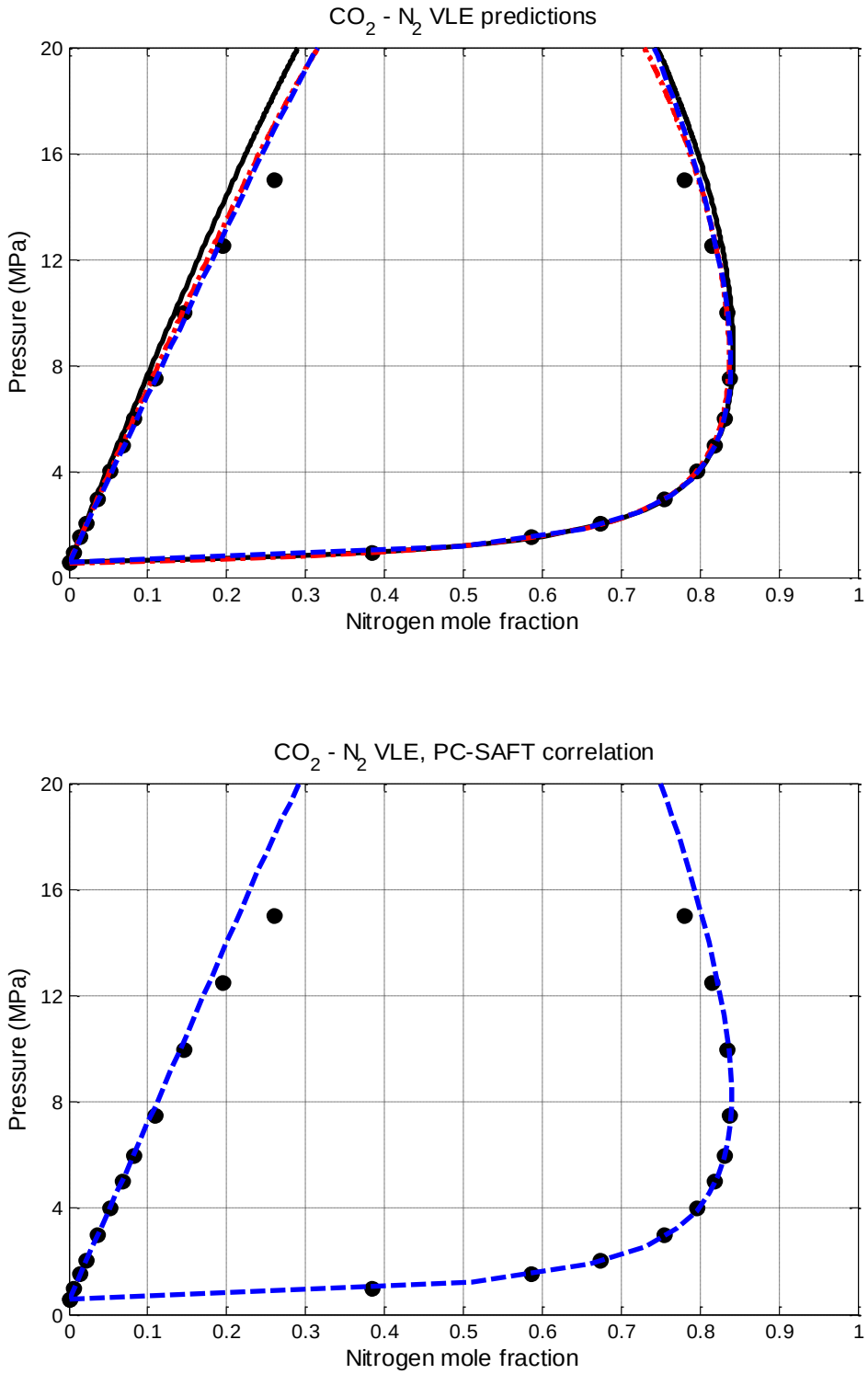

Figure 6-9: Pressure – composition phase diagram for the CO_2 – N_2 mixture, at T= 218.15 K. Experimental data[80] are represented by data points and calculations are represented by lines (–) SRK, (– · –) PR, (– – –) PC-SAFT. Top panel shows predictions ($k_{ij} = 0$), whereas bottom panel shows correlations ($k_{ij} \neq 0$).

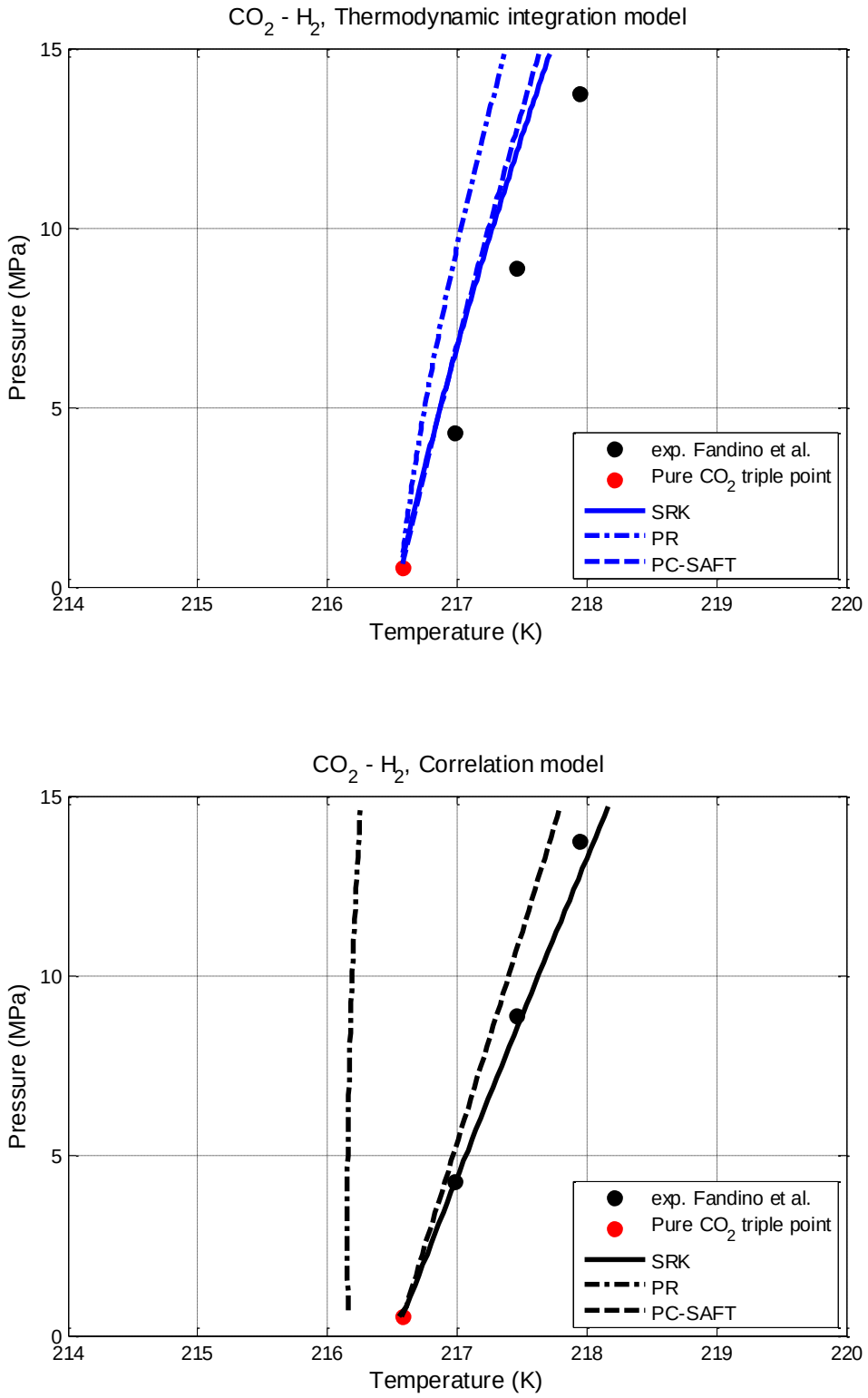

Figure 6-10: P-T projections of the SLG equilibrium curve of the CO_2 – H_2 system. Top panel shows the results with the Thermodynamic Integration model and bottom panel with the Correlation model.

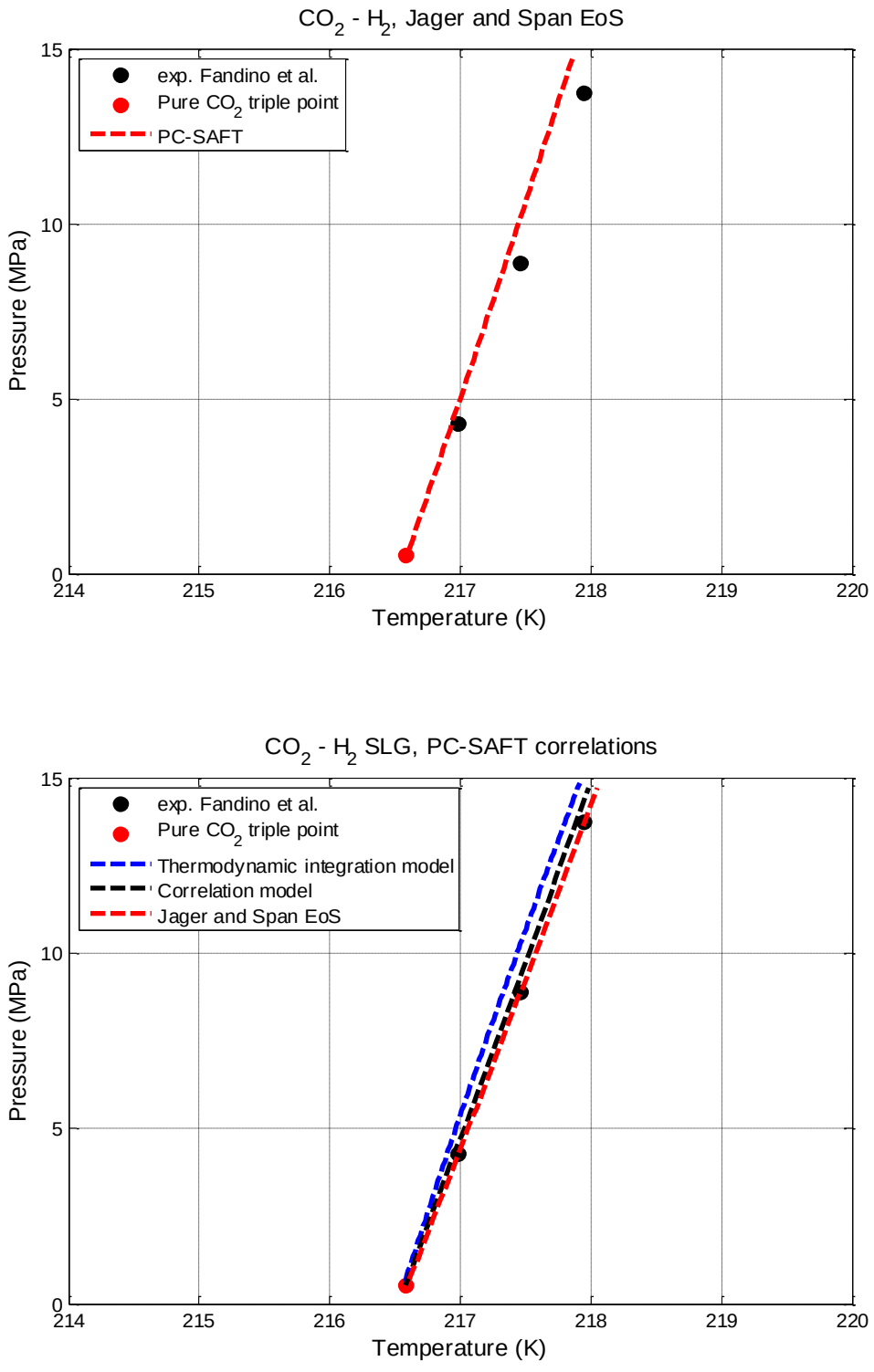

Figure 6-11: P-T projections of the SLG equilibrium curve of the CO_2 – H_2 system. Top panel shows the results with the Jager and Span EoS and bottom panel shows the results of all solid models coupled with PC-SAFT, when k_{ij} parameters fitted to experimental binary VLE data are used.

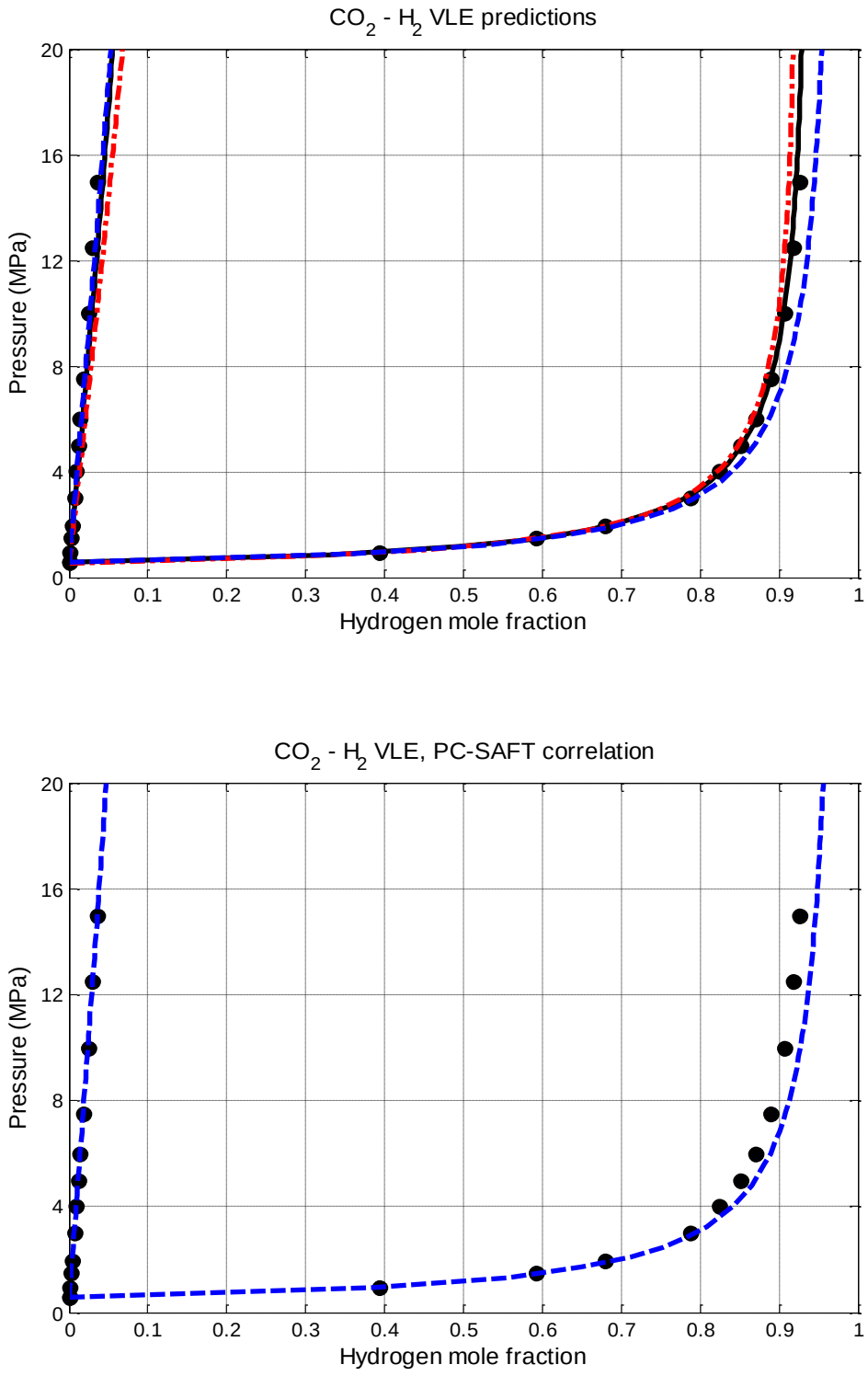

Figure 6-12: Pressure – composition phase diagram for the CO_2 – H_2 mixture, at T= 218.15 K. Experimental data[80] are represented by data points and calculations are represented by lines (–) SRK, (– · –) PR, (– – –) PC-SAFT. Top panel shows predictions ($k_{ij} = 0$), whereas bottom panel shows correlations ($k_{ij} \neq 0$).

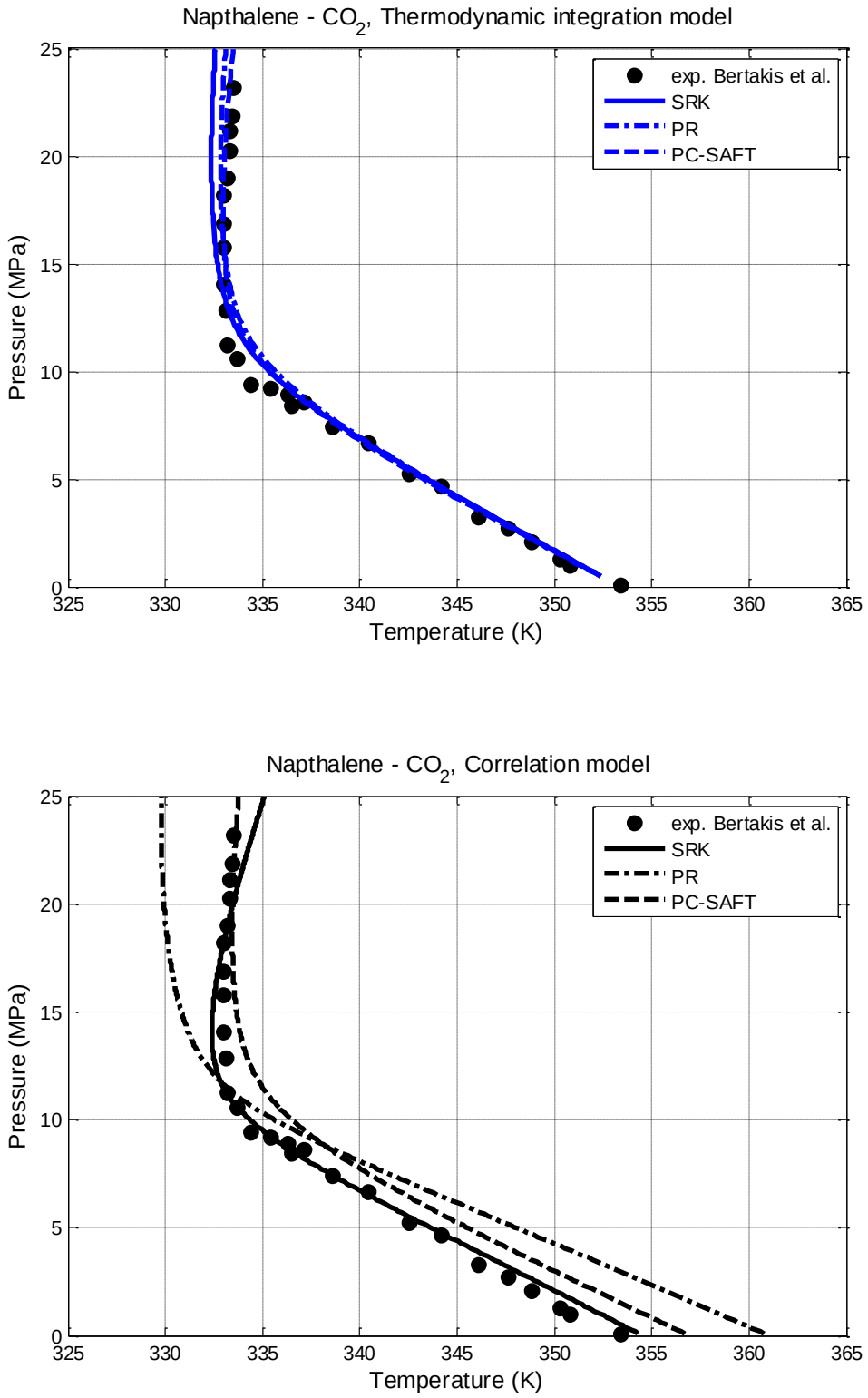

Figure 6-13: P-T projections of the SLG equilibrium curve of the Naphthalene - CO_2 system. Top panel shows the results with the Thermodynamic Integration model and bottom panel with the Correlation model. The use of BIPs is complementary for the specific system.

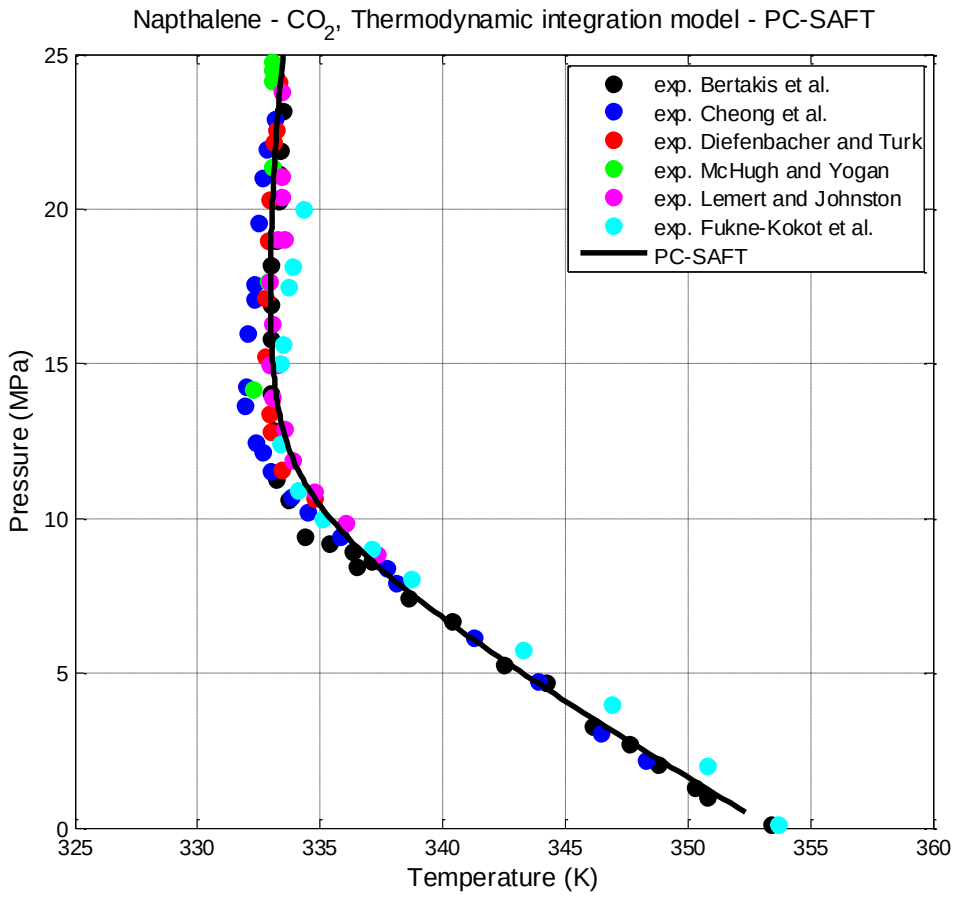

Figure 6-14: P-T projection of the SLG equilibrium curve of the Naphthalene - CO_2 system. Calculations with the Thermodynamic Integration model, coupled with PC-SAFT EoS. The scattering of available experimental is presented.

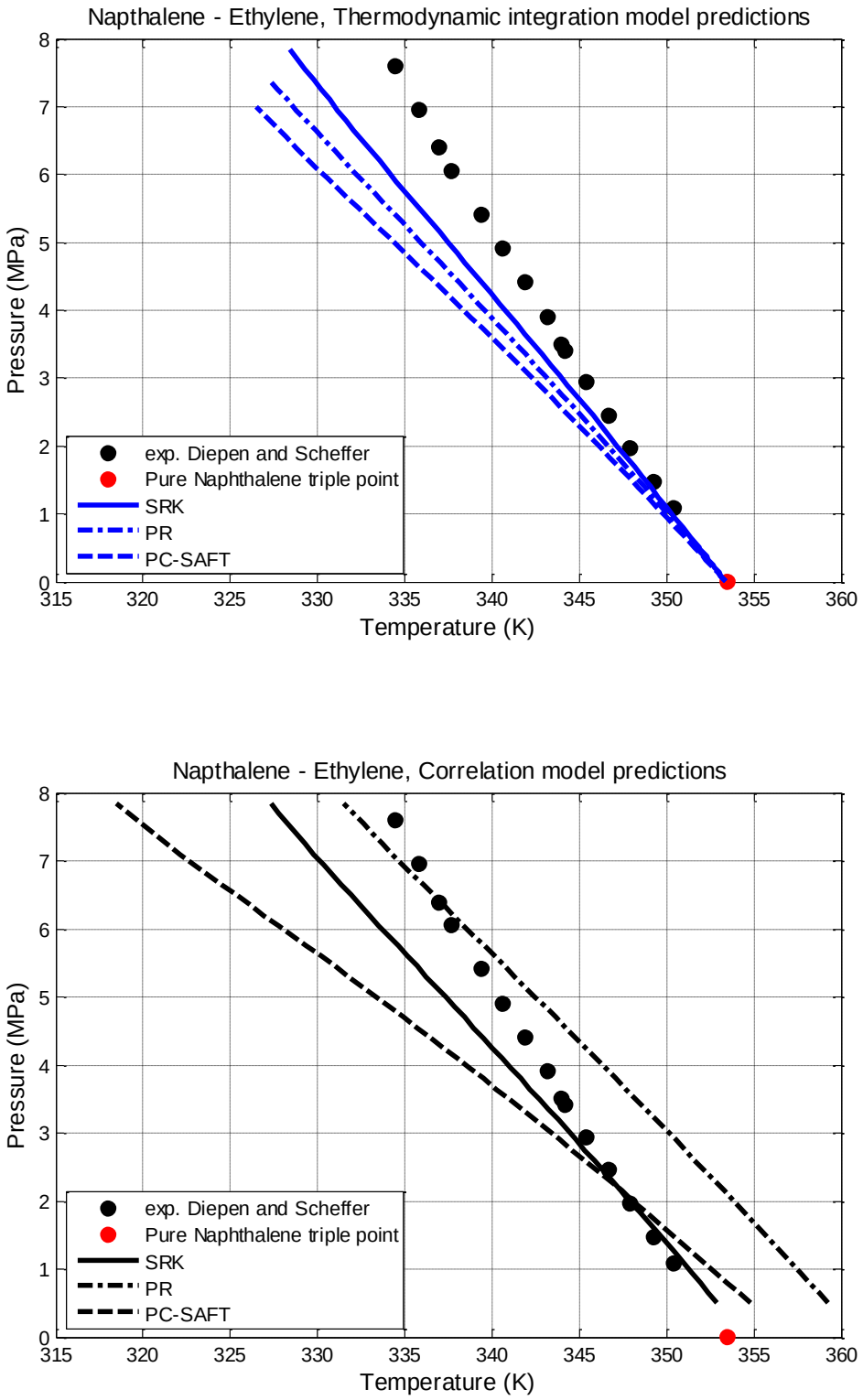

Figure 6-15: P-T projections of the SLG equilibrium curve of the Naphthalene - Ethylene system. Top panel shows the results with the Thermodynamic Integration model and bottom panel with the Correlation model.

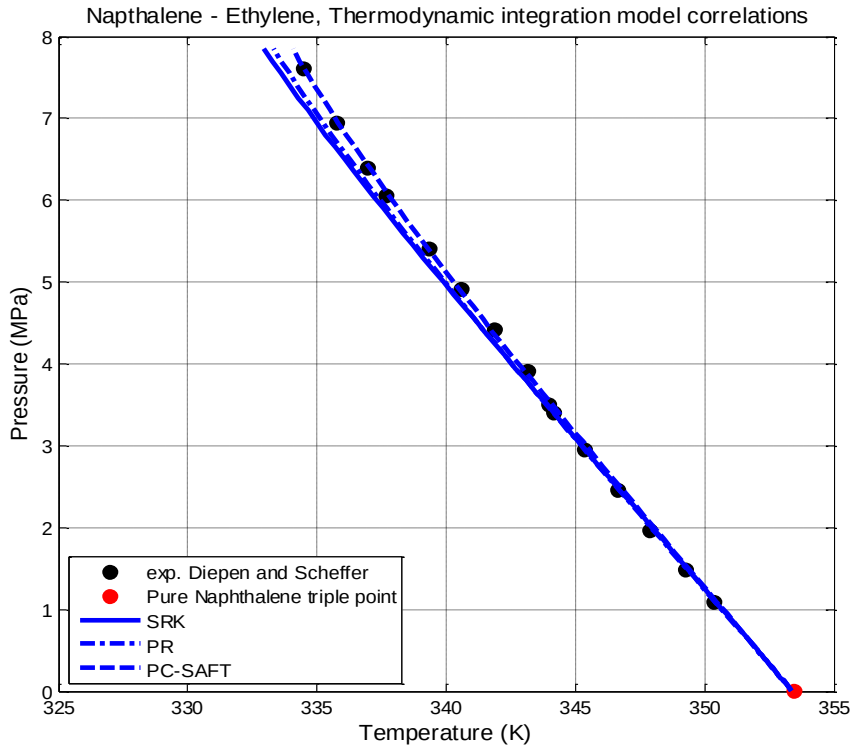

Figure 6-16: P-T projections of the SLG equilibrium curve of the Naphthalene - Ethylene system. Calculations with the Thermodynamic Integration model when k_{ij} parameters are used.

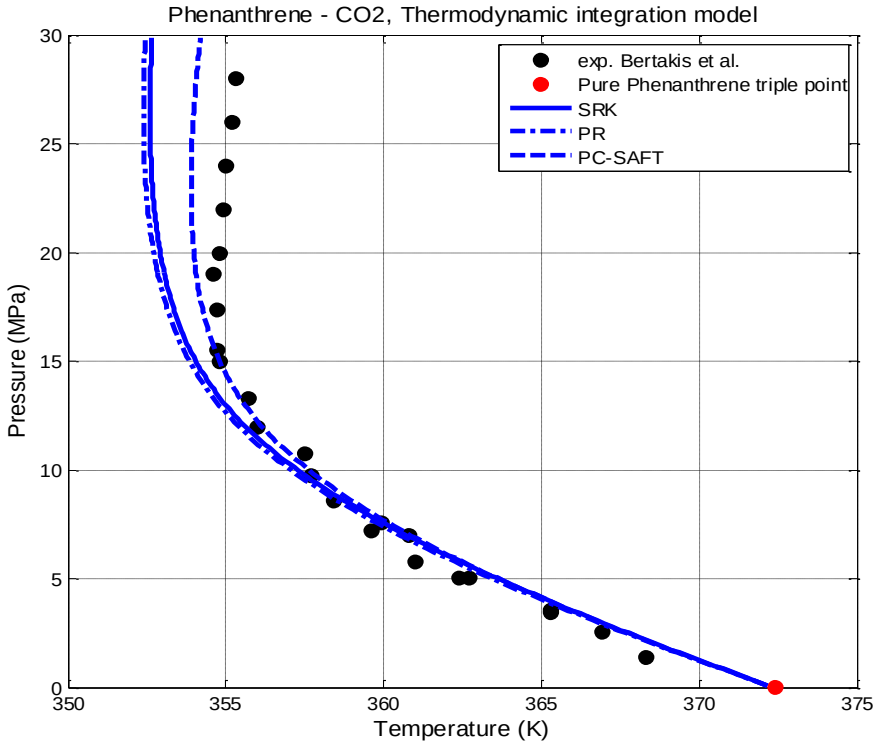

Figure 6-17: P-T projections of the SLG equilibrium curve of the Phenanthrene - CO_2 system. Calculations with the Thermodynamic Integration model are presented. The use of BIPs is complementary for the specific system.

6.4. Conclusions

In this work, solid models of different complexity have been coupled with different fluid EoS and the performance of each model has been assessed. The success of each model on predicting the pure CO_2 SVE and SLE lines has been evaluated and also, the effect on the SFE behavior of CO_2 when impurities are added has been tested.

The performance of the different models has been validated against SLG experimental data available in the literature. Two mixtures of CO_2 with N_2 and H_2 have been modeled and three other binary mixtures, where Naphthalene and Phenanthrene form the solid phase have been modeled to further assess the accuracy of the solid models. The most accurate predictive results in terms of solid model were achieved with the thermodynamic integration model for the $CO_2 – N_2$ system and when interaction parameters, fitted to binary VLE data at a low temperature have been used, the Jager and Span EoS coupled with PC-SAFT resulted in the most accurate description of the equilibrium curve. As far as the $CO_2 – H_2$ system is concerned, the correlation model resulted in the most accurate predictive results when the SRK and the PC-SAFT EoS were used and again the use of BIPs resulted in Jager and Span EoS being the most accurate model. For the mixtures of naphthalene and phenanthrene with CO_2 and naphthalene with ethylene, the thermodynamic integration model generally outperformed the correlation model, which in most cases was unable to reproduce the pure solid former triple point. This resulted in overall worse prediction or correlation of the SLG equilibrium line and higher deviations.

7. Conclusions and Further Work

Robust algorithmic schemes are necessary for the efficient calculation of solution branches for two and multiphase equilibrium problems that involve binary and complex multicomponent mixtures. Taking into account the small computation time that is needed for these calculations, robustness and reliability are more important than speed. Moreover, given the relative sensitivity of these algorithms to the initial estimates, suitable choice of them or extrapolation from previous calculated states is an important factor that determines convergence.

VLE of binary and multicomponent mixtures of CO_2 with other gases relevant to CCS applications can be sufficiently predicted or correlated with cubic and higher order equations of state. The most accurate predictive results were provided by PR and PC-SAFT equations of state with the average deviation between experimental data and calculations for the two EoS being very similar. The use of temperature independent BIPs resulted in quite accurate correlations for the binary mixtures and predictions for the multicomponent mixtures by both EoS.

The study of CO_2 mixtures was extended to two and multiphase SFE behavior. Solid models of different complexity were coupled with different fluid equations of state and the effect of impurities on the pure CO_2 solid – fluid saturation curves was investigated. Furthermore, the performance of each resulting model was validated against SLG experimental data available in the literature. Very accurate predictive results were achieved for the $CO_2 – N_2$ and $CO_2 – H_2$ systems with all the solid models developed in this work. The use of interaction parameters, fitted to binary VLE data at a low temperature for those two systems resulted into considerable improvement of the modeling results. For the mixtures of naphthalene and phenanthrene with CO_2 and naphthalene with ethylene, the use of BIPs was complementary in most cases and the thermodynamic integration was proven to be the most accurate solid model.

Further work that can be conducted as follow-up to this thesis is the extension of the bead spring method to the calculation of VLLE branches. The identification of VLLE boundaries is of importance to those who study global phase diagrams and also multiple liquid phases have been associated with carbon dioxide injection in low temperature reservoirs. Moreover, VLE experimental data of ternary and quaternary mixtures of CO_2 relevant to this work are still limited. Suggestions could include the experimental measurement of ternary mixtures like $CO_2 – SO_2 – N_2$, $CO_2 – O_2 – N_2$, $CO_2 – N_2 – H_2S$ and also mixtures that include H_2O, taking into account that it is the major impurity in these fluid streams. Finally, there is particular scarcity in two and three phase solid – fluid equilibrium experimental data of binary mixtures of CO_2 with the aforementioned components and no

ternary mixture data. Measurement of CO_2 - N_2 mixtures at two phase SFE conditions and CO_2 - O_2, CO_2 – Ar at SLG conditions could lead to a more elaborate validation of the solid modeling approaches and the fluid EoS.

Apart from the stand alone modeling of the phase equilibria of the mixtures that are relevant to CCS processes, the thermodynamic models developed in this work can be integrated in flow simulators that perform Computational Fluid Dynamics (CFD) calculations. A calculation of this type which is related to CCS applications is the CO_2 dispersion that occurs from pipeline rapture. As it has already been mentioned, a rapture results into a sudden decompression of the pipeline and subsequent cooling of the CO_2 stream. The whole process is modeled as isenthalpic decompression and because of the rapid cooling, the stream presents complex phase transitions from a dense phase to VL coexistence and solidification. Accurate representation of the two and multiphase equilibria and also robust algorithms and techniques that require minimal computation cost, are important for the successful description of the whole process and the integration of the models. An efficient approach that can significantly reduce the computational cost of calling flash and stability analysis algorithms at every point of a CFD mesh at multiple time steps is the generation of fine grids with pre-calculated one and two phase properties from the thermodynamic model and subsequent use of the tabulated data from the CFD simulator. This way, the iterative calculation of the phase boundaries and the thermodynamic properties is avoided and linear or higher order interpolation schemes can produce very accurate continuous description of the properties if the initial grid is generated correctly.

Appendix A: Derivation of the Bead Spring Equation

The idea behind Eq. (4.13) stems from the observation that the phase boundary that we wish to compute for a C component mixture is a one dimensional curve embedded in a C+2 multidimensional space spanned by temperature, pressure and the C molar compositions of the incipient phase. Michelsen[41] showed that is possible to traverse this curve, by introducing a specification equation and by changing the value of one of the C+2 variables (i.e. the specification). Setting a specification value for one of the independent variables defines a hyperplane, while the rest of the equations define the phase boundary. For this specification value, the phase equilibrium point is the intersection of this hyperplane and the phase boundary curve. This opens the possibility of replacing the specification equation by another one, which defines a different hypersurface.

Since the target is to construct a scheme that also calculates directly the cricondentherm and cricondenbar points, we attempt to construct a specification equation based on the partial derivatives of Q with respect to P or T. Equation $\frac{\partial Q}{\partial P} = c$ defines a set of hypersurfaces. For a given $c = c_0$, the intersection with the phase boundary curve will result in an equilibrium point $(T_0, P_0, \mathbf{w_0})$, where $\mathbf{w_0}$ is the molar composition of the incipient phase. If we replace Q with $Q - \frac{1}{2}\,\theta\,(P - P_0)^2 - \frac{1}{2}\,\theta\,(P - P_1)^2$ and use as specification equation the expression $\frac{\partial\left(Q - \frac{1}{2}\theta\,(P-P_0)^2 - \frac{1}{2}\theta\,(P-P_1)^2\right)}{\partial P} = 0$, for specific values of θ the solution will move in the vicinity of P_0 towards P_1. The same solution could be obtained if the initial equation was used with a different value for c (i.e. $\frac{\partial Q}{\partial P} = c'$). This form can be interpreted as the introduction of two springs that connect the point P with points P_0 and P_1.

The pressure derivative of the expression shown above results to the following equation (which corresponds to Eq. (4.13) in our scheme):

$$\frac{\partial Q}{\partial P} - \theta(P - P_0) - \theta\,(P - P_1) = 0 \Leftrightarrow \frac{\partial Q}{\partial P} + \theta \cdot (P_1 - 2P + P_0) = 0 \qquad \text{(A1)}$$

If P_0 is the pressure of the previously converged equilibrium point (P_{l-1}), P_1 is the pressure estimate P_{l+1}^{est}, and P_l the unknown pressure P, we get:

$$\frac{\partial Q}{\partial P} + \theta \cdot \left(P_{l+1}^{est} - 2P_l + P_{l-1}\right) = 0 \qquad \text{(A2)}$$

This equation defines a set of smooth hypersurfaces in the close vicinity of the phase boundary curve. The intersection of each hypersurface with the phase boundary curve is a phase equilibrium point. Starting from an equilibrium point and using Eq. (A2) as

specification equation, the curve can be traversed and also by setting the θ parameter equal to zero, the cricondentherm point can be determined directly.

The second term in Eq. (A2) defines a line. Depending on the choice of θ, the intersection (solution of Eq. A2) of this line with the $\left.\frac{\partial Q}{\partial P}\right|_{T,w} = c(T,P,w)$ surface, can be bounded in the range $[P_{l-1}, P_{l+1}^{est}]$. When the temperature is used instead of pressure, the intersection is bounded in the range $[T_{l-1}, T_{l+1}^{est}]$. This intersection indicates the new value for c, which corresponds to a hypersurface in the neighborhood of the previous converged point, the intersection of which with the phase boundary curve is the resulting new equilibrium point.

The minimum value of θ which results in an intersection point in the range $\left[P_{l-1}, P_{l+1}^{est}\right]$ corresponds to the solution of the equation:

$$-\theta \cdot \left(P_{l+1}^{est} - 2P_l + P_{l-1}\right) = \frac{\partial Q}{\partial P} \Leftrightarrow 2\theta \cdot \left(P_l - \frac{P_{l-1} + P_{l+1}^{est}}{2}\right) = \frac{\partial Q}{\partial P} \qquad \text{(A3)}$$

for $P_l = P_{l+1}^{est}$ i.e.:

$$\theta_{min} = \frac{\left.\frac{\partial Q}{\partial P}\right|_{\text{at } P_{l+1}^{est}}}{\delta P} \qquad \text{(A4)}$$

If $\frac{\partial Q}{\partial P}$ is smooth enough, then $\theta_{min,P_{l+1}^{est}} \approx \theta_{min,P_{l-1}}$. This way an estimate for θ can be determined from the previous calculated equilibrium point. In this study, efficiently large values for θ have been chosen, which ensure that this condition is fulfilled. Typical values for θ used in this work are provided in Table 4-1.

Appendix B: Equation set in the Bead Spring Method

In the proposed method, the K values of the C components of a mixture, the equilibrium temperature and pressure are determined by simultaneously solving a system of $C+2$ non-linear equations. The independent variables are chosen to be $\ln K_i$, $\ln T$ and $\ln P$. The non-linear set of equations for the two phase problem is:

$$f_i = \ln K_i + \ln \hat{\varphi}_i^{\,v} - \ln \hat{\varphi}_i^{\,l} = 0, \qquad i = 1, 2 \dots C \tag{B1}$$

$$f_{C+1} = \sum_{i=1}^{C} (y_i - x_i) = 0 \tag{B2}$$

$$f_{C+2} = \frac{\partial Q}{\partial P} + \theta \cdot \left(S_{l+1}^{est} - 2S_l + S_{l-1} \right) = 0, \qquad S = T \text{ or } P \tag{B3}$$

The compositions of the liquid and the vapor phase are calculated using:

$$x_i = \frac{z_i}{1 - \beta + \beta K_i}, \qquad y_i = \frac{K_i z_i}{1 - \beta + \beta K_i} \tag{B4}$$

where β is the vapor fraction. When β = 0, the feed phase is the liquid, whereas, when β = 1, the vapor is the feed phase. In this case, the above equations reduce to:

$$\begin{aligned} y_i &= K_i x_i, \qquad \beta = 0 \\ x_i &= \frac{y_i}{K_i}, \qquad \beta = 1 \end{aligned} \tag{B5}$$

As it has already been mentioned, the Newton's method is utilized for the solution of the non-linear equation set, thus the Jacobian of the system has to be calculated. The terms of the Jacobian matrix are:

$$\frac{\partial f_i}{\partial \ln K_j} = \delta_{ij} + \left. \frac{\partial \ln \hat{\varphi}_i^{\,v}}{\partial y_j} \right|_{P,T} (1 - \beta) \frac{x_j y_j}{z_j} + \left. \frac{\partial \ln \hat{\varphi}_i^{\,l}}{\partial x_j} \right|_{P,T} \beta \frac{x_j y_j}{z_j} \tag{B6}$$

$$\frac{\partial f_i}{\partial \ln T} = T \left(\left. \frac{\partial \ln \hat{\varphi}_i^{\,v}}{\partial T} \right|_{P,y} - \left. \frac{\partial \ln \hat{\varphi}_i^{\,l}}{\partial T} \right|_{P,x} \right) \tag{B7}$$

$$\frac{\partial f_i}{\partial \ln P} = P \left(\left. \frac{\partial \ln \hat{\varphi}_i^{\,v}}{\partial P} \right|_{T,y} - \left. \frac{\partial \ln \hat{\varphi}_i^{\,l}}{\partial P} \right|_{T,x} \right) \tag{B8}$$

$$\frac{\partial f_{c+1}}{\partial \ln K_j} = \frac{x_j y_j}{z_j} \tag{B9}$$

$$\frac{\partial f_{c+1}}{\partial \ln T} = \frac{\partial f_{c+1}}{\partial \ln P} = 0 \tag{B10}$$

If the calculation is initiated from the dew line:

$$\frac{\partial f_{c+2}}{\partial \ln K_j} = (-\beta)\frac{x_j y_j}{z_j}\left(\left.\frac{\partial \ln \hat{\varphi}_j{}^{l}}{\partial P}\right|_{T,x} - \left.\frac{\partial \ln \hat{\varphi}_j{}^{v}}{\partial P}\right|_{T,y}\right) \tag{B11}$$

$$\frac{\partial f_{c+2}}{\partial \ln T} = \sum_{i=1}^{C}\left[x_i\left(\frac{\partial^2 \ln \hat{\varphi}_i{}^{l}}{\partial P\,\partial \ln T} - \frac{\partial^2 \ln \hat{\varphi}_i{}^{v}}{\partial P\,\partial \ln T}\right)\right] \tag{B12}$$

$$\frac{\partial f_{c+2}}{\partial \ln P} = \sum_{i=1}^{C}\left[x_i\left(\frac{\partial^2 \ln \hat{\varphi}_i{}^{l}}{\partial P\,\partial \ln P} - \frac{\partial^2 \ln \hat{\varphi}_i{}^{v}}{\partial P\,\partial \ln P}\right)\right] \tag{B13}$$

Similarly, if the calculation is initiated from the bubble line:

$$\frac{\partial f_{c+2}}{\partial \ln K_j} = (1-\beta)\frac{x_j y_j}{z_j}\left(\left.\frac{\partial \ln \hat{\varphi}_j{}^{v}}{\partial P}\right|_{T,y} - \left.\frac{\partial \ln \hat{\varphi}_j{}^{l}}{\partial P}\right|_{T,x}\right) \tag{B14}$$

$$\frac{\partial f_{c+2}}{\partial \ln T} = \sum_{i=1}^{C}\left[y_i\left(\frac{\partial^2 \ln \hat{\varphi}_i{}^{v}}{\partial P\,\partial \ln T} - \frac{\partial^2 \ln \hat{\varphi}_i{}^{l}}{\partial P\,\partial \ln T}\right)\right] \tag{B15}$$

$$\frac{\partial f_{c+2}}{\partial \ln P} = \sum_{i=1}^{C}\left[y_i\left(\frac{\partial^2 \ln \hat{\varphi}_i{}^{v}}{\partial P\,\partial \ln P} - \frac{\partial^2 \ln \hat{\varphi}_i{}^{l}}{\partial P\,\partial \ln P}\right)\right] \tag{B16}$$

Depending on which variable (T or P) is the spring variable, one term has to be added either to $\frac{\partial f_{c+2}}{\partial \ln T}$ or to $\frac{\partial f_{c+2}}{\partial \ln P}$. If temperature is the spring variable then:

$$\frac{\partial f_{c+2}}{\partial \ln T} = \frac{\partial f_{c+2}}{\partial \ln T} - 2 \cdot \theta \cdot T \tag{B17}$$

while if it is the pressure:

$$\frac{\partial f_{c+2}}{\partial \ln P} = \frac{\partial f_{c+2}}{\partial \ln P} - 2 \cdot \theta \cdot P \tag{B18}$$

Derivatives of the f_{C+2} equation lead to second order derivatives of the fugacity coefficients with respect to pressure and mixed second derivatives with respect to pressure and temperature. These derivatives are calculated numerically.

$$\frac{\partial^2 \ln\hat{\varphi}_i}{\partial P\,\partial \ln P} = \frac{1}{\delta P}\left[P \cdot \left(\left.\frac{\partial \ln\hat{\varphi}_i}{\partial P}\right|_{P+\delta P} - \left.\frac{\partial \ln\hat{\varphi}_i}{\partial P}\right|_{P}\right)\right]$$

$$\frac{\partial^2 \ln\hat{\varphi}_i}{\partial P\,\partial \ln T} = \frac{1}{\delta P}\left[T \cdot \left(\left.\frac{\partial \ln\hat{\varphi}_i}{\partial T}\right|_{P+\delta P} - \left.\frac{\partial \ln\hat{\varphi}_i}{\partial T}\right|_{P}\right)\right] \qquad \text{(B19)}$$

We have found also advantageous to calculate the pressure derivatives of the fugacity coefficients in the $\frac{\partial f_{c+2}}{\partial \ln K_j}$ terms of the Jacobian in a perturbed pressure $P = P + \delta P$. This modification enhanced in some cases the convergence properties in the vicinity of the critical point.

Appendix C: Binary and Ternary isopleths of CO_2 mixtures

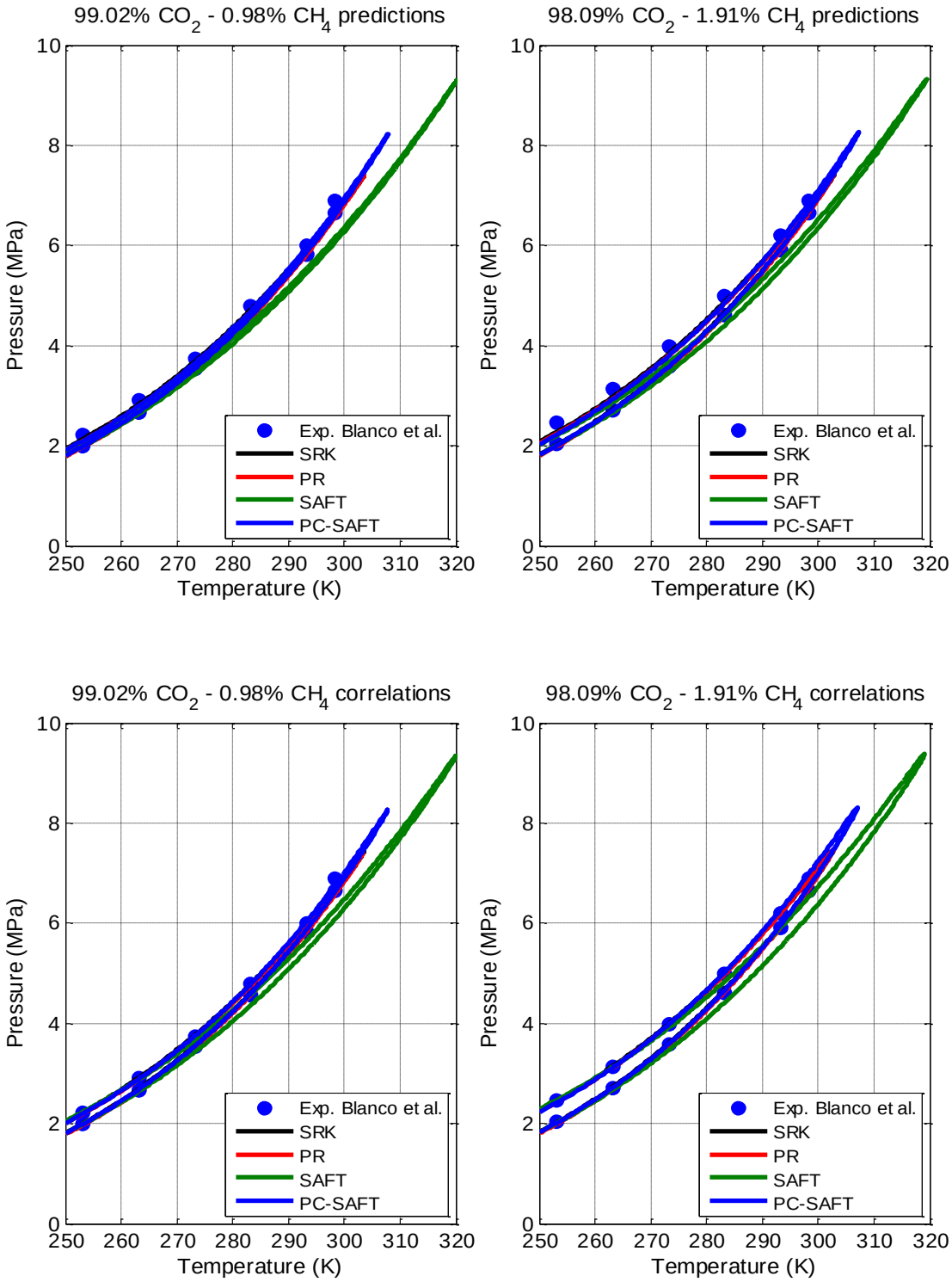

Figure C-1: Phase envelopes of 99.02% carbon dioxide – 0.98% methane, 98.09% carbon dioxide – 1.91% methane (mole) mixtures. Top panels show predictions ($k_{ij} = 0$), whereas bottom panels show correlations ($k_{ij} \neq 0$).

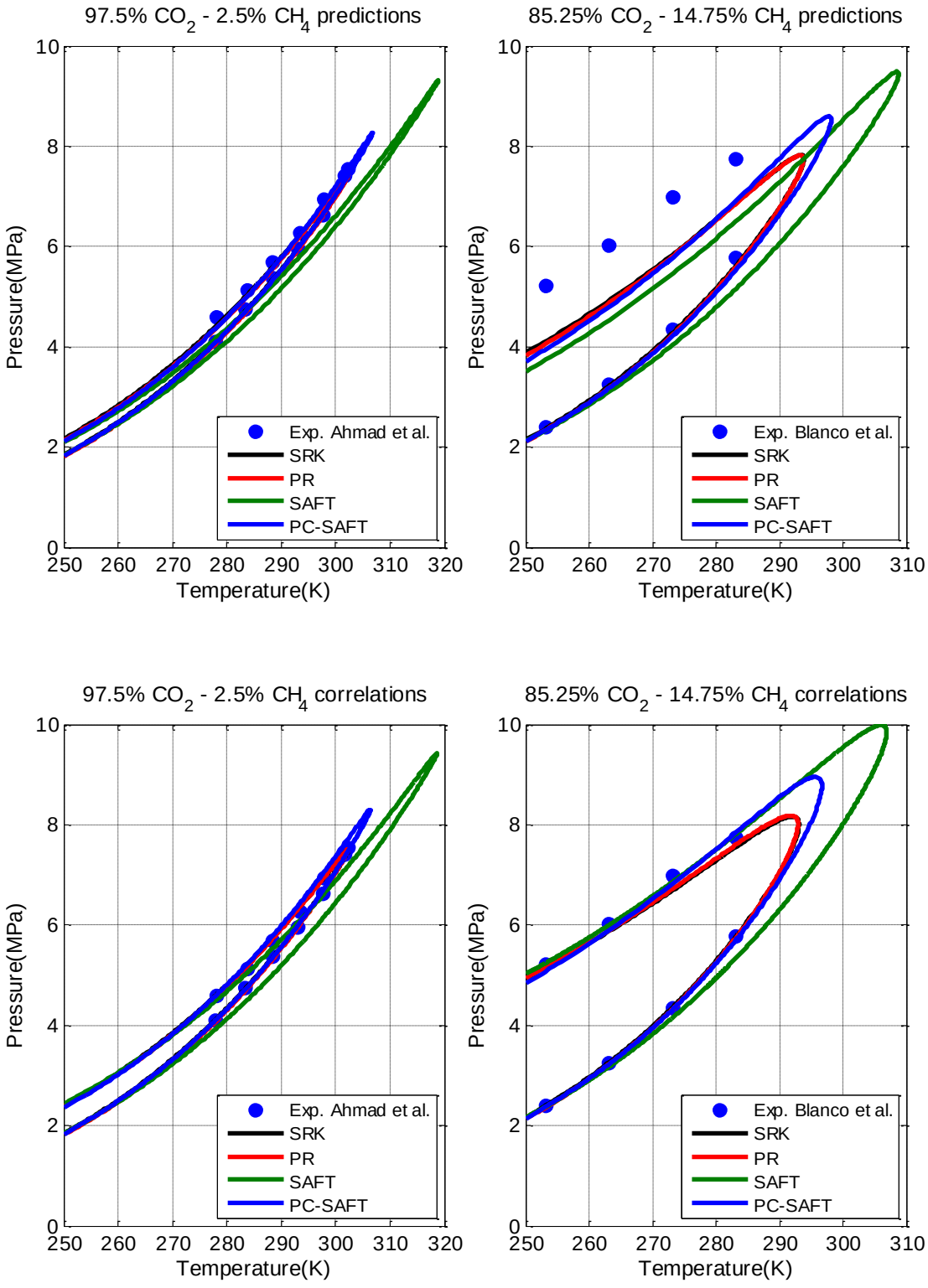

Figure C-2: Phase envelopes of 97.5% carbon dioxide – 2.5% methane, 85.25% carbon dioxide – 14.75% methane (mole) mixtures. Top panels show predictions ($k_{ij} = 0$), whereas bottom panels show correlations ($k_{ij} \neq 0$).

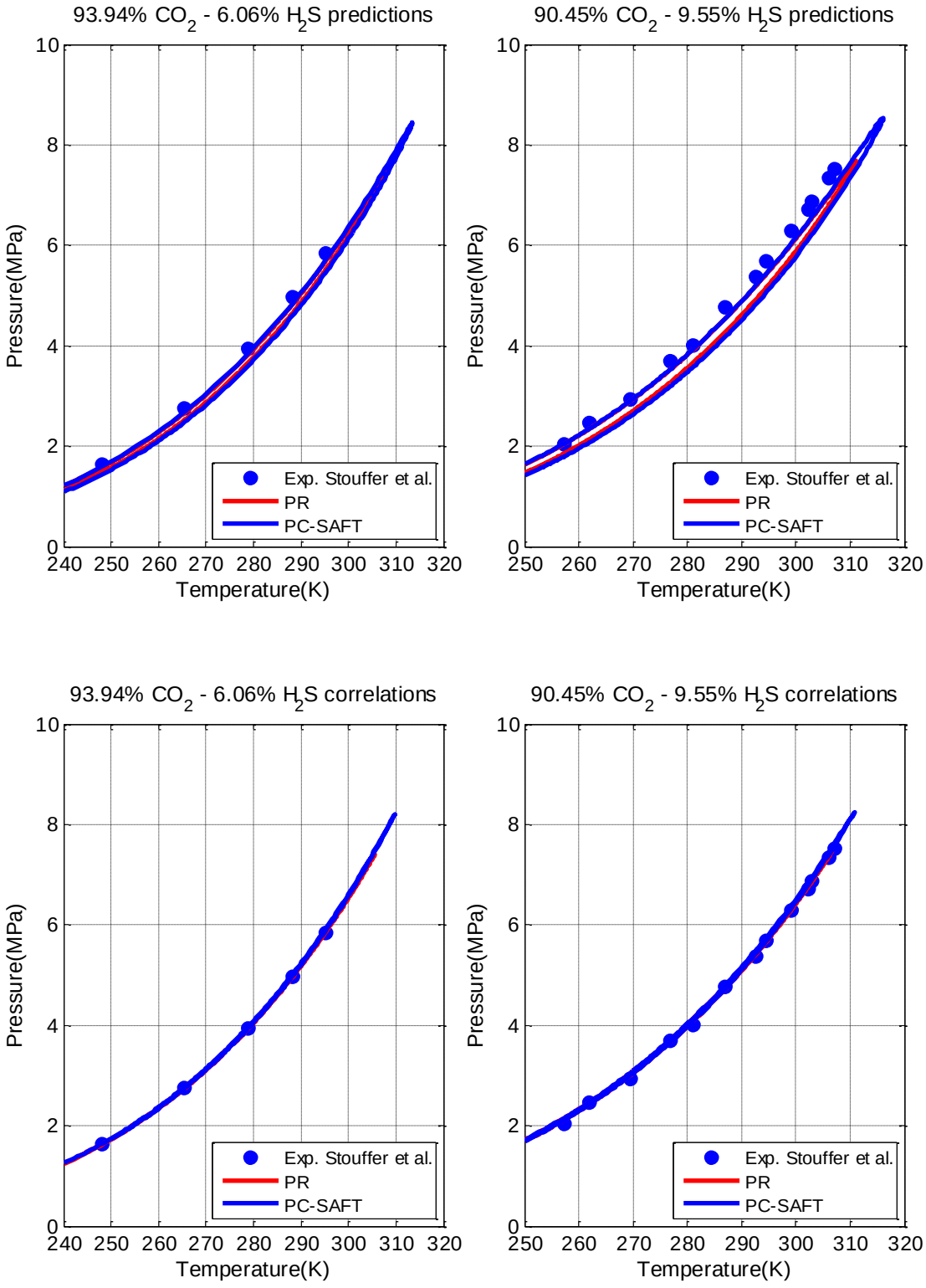

Figure C-3: Phase envelopes of 93.94% carbon dioxide – 6.06% hydrogen sulfide, 90.45% carbon dioxide – 9.55% hydrogen sulfide (mole) mixtures. Top panels show predictions ($k_{ij} = 0$), whereas bottom panels show correlations ($k_{ij} \neq 0$).

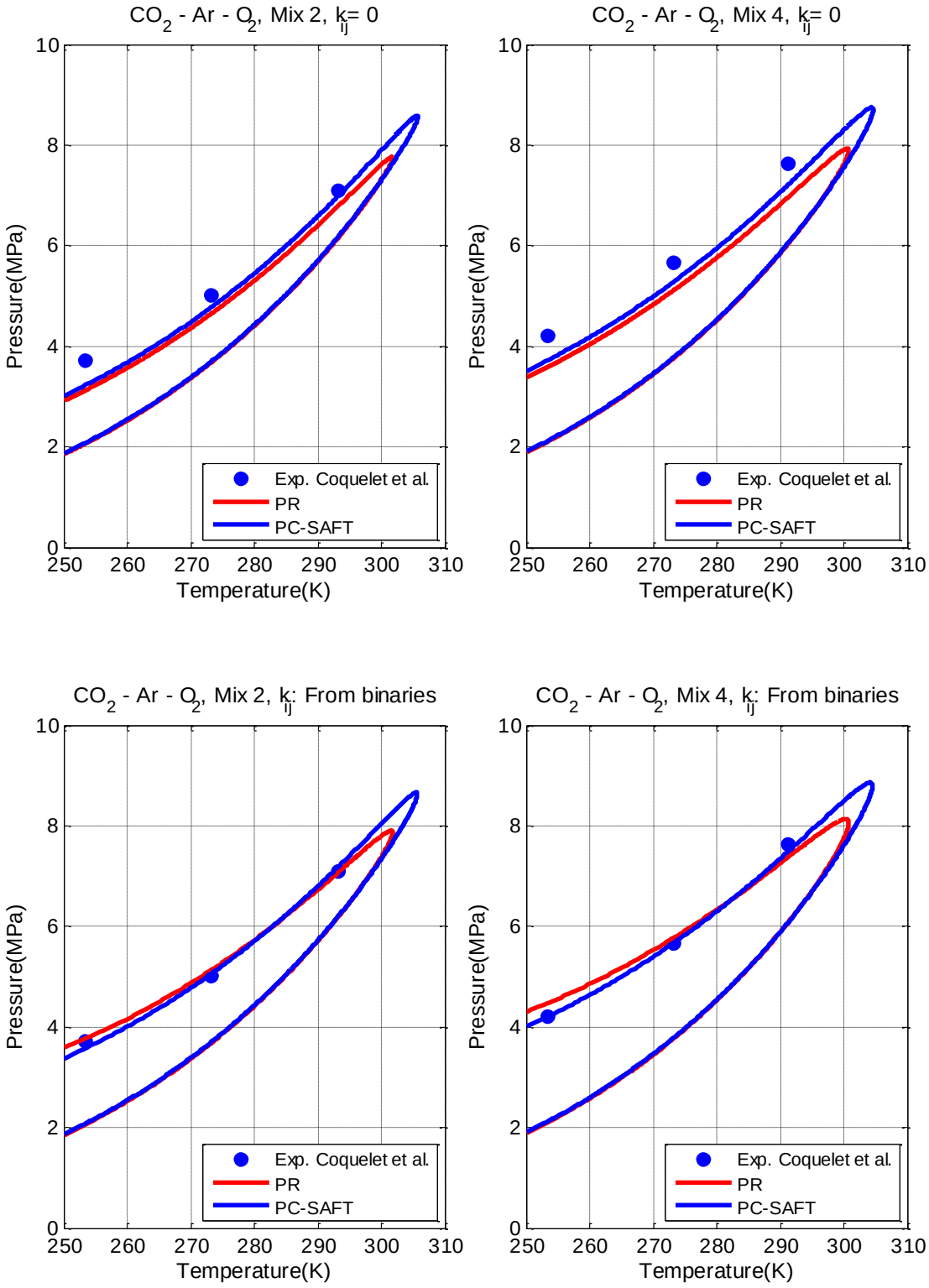

Figure C-4: Phase envelopes of carbon dioxide – argon - oxygen, mixtures 2 and 4 (see Table 5-11). Top panels show predictions ($k_{ij} = 0$), whereas bottom panels show calculations with k_{ij} fitted to experimental binary VLE data.

References

1. Metz B, Davidson O, de Coninck H, Loos M, Meyer L, IPCC. *2006: IPCC Special Report of Carbon Dioxide Capture and Storage. Prepared by Working Group III of the Intergovernmental Panel on Climate Change*. New York, 2005.
2. Alivizatos P, Buchanan M. *Basic research needs for carbon capture: beyond 2020*. www.sc.doe.gov/bes/reports/files/CCB2020_rpt.pdf2010.
3. Meeting the energy challenge: A white paper on energy. In: industry Dota, ed. www.berr.gov.uk/files/file39387.pdf2007.
4. MacDowell N, Florin N, Buchard A, et al. An overview of CO2 capture technologies. *Energy & Environmental Science*. 2010;3:1645-1669.
5. Boot-Handford ME, Abanades JC, Anthony EJ, et al. Carbon capture and storage update. *Energy & Environmental Science*. 2014;7:130-189.
6. Porter RTJ, Fairweather M, Pourkashanian M, Woolley RM. The range and level of impurities in CO2 streams from different carbon capture sources. *International Journal of Greenhouse Gas Control*. 2015;36:161-174.
7. Woolley RM, Fairweather M, Wareing CJ, et al. An integrated, multi-scale modelling approach for the simulation of multiphase dispersion from accidental CO2 pipeline releases in realistic terrain. *International Journal of Greenhouse Gas Control*. 2014;27:221-238.
8. Prausnitz JM, Lichtenthaler RN, de Azevedo EG. Molecular Thermodynamics of Fluid-Phase Equilibria (3rd edition). New Jersey: Prentice-Hall, 1999.
9. Soave G. Equilibrium constants from a modified Redlich-Kwong equation of state. *Chemical Engineering Science*. 1972;27:1197-1203.
10. Peng D-Y, Robinson DB. A New Two-Constant Equation of State. *Industrial & Engineering Chemistry Fundamentals*. 1976;15:59-64.
11. Kontogeorgis GM, Folas GK. Thermodynamic Models for Industrial Applications: John Wiley & Sons, Ltd, 2010.
12. Michelsen ML, Mollerup JM. Thermodynamic Models: Fundamentals & Computational Aspects (2nd edition). Denmark: Tie-Line Publications, 2007.
13. Chapman WG, Gubbins KE, Jackson G, Radosz M. SAFT: Equation-of-state solution model for associating fluids. *Fluid Phase Equilibria*. 1989;52:31-38.
14. Huang SH, Radosz M. Equation of state for small, large, polydisperse, and associating molecules. *Industrial & Engineering Chemistry Research*. 1990;29:2284-2294.
15. Huang SH, Radosz M. Equation of state for small, large, polydisperse, and associating molecules: extension to fluid mixtures. *Industrial & Engineering Chemistry Research*. 1991;30:1994-2005.
16. Gross J, Sadowski G. Perturbed-Chain SAFT: An Equation of State Based on a Perturbation Theory for Chain Molecules. *Industrial & Engineering Chemistry Research*. 2001;40:1244-1260.
17. Wertheim MS. Fluids with highly directional attractive forces. I. Statistical thermodynamics. *J Stat Phys*. 1984;35:19-34.
18. Wertheim MS. Fluids with highly directional attractive forces. II. Thermodynamic perturbation theory and integral equations. *J Stat Phys*. 1984;35:35-47.
19. Wertheim MS. Fluids with highly directional attractive forces. III. Multiple attraction sites. *J Stat Phys*. 1986;42:459-476.
20. Wertheim MS. Fluids with highly directional attractive forces. IV. Equilibrium polymerization. *J Stat Phys*. 1986;42:477-492.
21. Seiler M, Groß J, Bungert B, Sadowski G, Arlt W. Modeling of Solid/Fluid Phase Equilibria in Multicomponent Systems at High Pressure. *Chemical Engineering & Technology*. 2001;24:607-612.
22. Jäger A, Span R. Equation of State for Solid Carbon Dioxide Based on the Gibbs Free Energy. *Journal of Chemical & Engineering Data*. 2012;57:590-597.
23. Michelsen ML. The isothermal flash problem. Part I. Stability. *Fluid Phase Equilibria*. 1982;9:1-19.

24. Mitsos A, Barton PI. A dual extremum principle in thermodynamics. *AIChE Journal.* 2007;53:2131-2147.
25. Harding ST, Floudas CA. Phase stability with cubic equations of state: Global optimization approach. *AIChE Journal.* 2000;46:1422-1440.
26. McDonald CM, Floudas CA. Global Optimization and Analysis for the Gibbs Free Energy Function Using the UNIFAC, Wilson, and ASOG Equations. *Industrial & Engineering Chemistry Research.* 1995;34:1674-1687.
27. Androulakis IP, Maranas CD, Floudas CA. αBB: A global optimization method for general constrained nonconvex problems. *Journal of Global Optimization.* 1995;7:337-363.
28. McDonald CM, Floudas CA. Global optimization for the phase stability problem. *AIChE Journal.* 1995;41:1798-1814.
29. McDonald CM, Floudas CA. Global optimization for the phase and chemical equilibrium problem: Application to the NRTL equation. *Computers and Chemical Engineering.* 1995;19:1111-1139.
30. Falk JE, Soland RM. An algorithm for seperable nonconvex programming problems. *Management Science.* 1969;15:550-569.
31. Gautam R, Seider WD. Computation of phase and chemical equilibrium: Part I. Local and constrained minima in Gibbs free energy. *AIChE Journal.* 1979;25:991-999.
32. Gautam R, Seider WD. Computation of phase and chemical equilibrium: Part II. Phase-splitting. *AIChE Journal.* 1979;25:999-1006.
33. Gautam R, Seider WD. Computation of phase and chemical equilibrium: Part III. Electrolytic solutions. *AIChE Journal.* 1979;25:1006-1015.
34. Gupta AK, Raj Bishnoi P, Kalogerakis N. A method for the simultaneous phase equilibria and stability calculations for multiphase reacting and non-reacting systems. *Fluid Phase Equilibria.* 1991;63:65-89.
35. Sun AC, Seider WD. Homotopy-continuation method for stability analysis in the global minimization of the Gibbs free energy. *Fluid Phase Equilibria.* 1995;103:213-249.
36. Tan S, Radosz M. Gibbs Topological Analysis for Constructing Phase Diagrams of Binary and Ternary Mixtures. *Industrial & engineering chemistry research.* 2002;41:5848-5855.
37. Ryll O, Blagov S, Hasse H. Convex envelope method for the determination of fluid phase diagrams. *Fluid Phase Equilibria.* 2012;324:108-116.
38. Michelsen ML. The isothermal flash problem. Part II. Phase-split calculation. *Fluid Phase Equilibria.* 1982;9:21-40.
39. Michelsen ML. Simplified flash calculations for Cubic Equations of State. *Industrial & Engineering Chemistry Process Design and Development.* 1986;25:184-188.
40. Whitson CH, Michelsen ML. The negative flash. *Fluid Phase Equilibria.* 1989;53:51-71.
41. Michelsen ML. Calculation of phase envelopes and critical points for multicomponent mixtures. *Fluid Phase Equilibria.* 1980;4:1-10.
42. Nghiem LX, Li Y-K, Heidemann RA. Application of the tangent plane criterion to saturation pressure and temperature computations. *Fluid Phase Equilibria.* 1985;21:39-60.
43. Quiñones-Cisneros SE, Deiters UK. An efficient algorithm for the calculation of phase envelopes of fluid mixtures. *Fluid Phase Equilibria.* 2012;329:22-31.
44. Deiters UK, Kraska T. Chapter 5 - Stability and Equilibrium. In: Deiters UK, Kraska T. Supercritical Fluid Science and Technology. Great Britain: Elsevier, 2012:99-155.
45. Ortiz-Vega DO, Cristancho DE, Hall KR, Iglesias-Silva GA. Generalized phase boundary determination algorithm for multicomponent mixtures. *Ind. Eng. Chem. Res.* 2011;50:97-101.
46. Venkatarathnam G. Density Marching Method for Calculating Phase Envelopes. *Industrial & engineering chemistry research.* 2014;53:3723-3730.
47. Ziervogel RG, Poling BE. A simple method for constructing phase envelopes for multicomponent mixtures. *Fluid Phase Equilibria.* 1983;11:127-135.
48. Michelsen ML. Saturation point calculations. *Fluid Phase Equilibria.* 1985;23:181-192.

49. Nichita D. Phase Envelope Construction for Mixtures with Many Components. *Energy & fuels.* 2008;22:488-495.
50. Iglesias-Silva GA, Bonilla-Petriciolet A, Eubank PT, Holste JC, Hall KR. An algebraic method that includes Gibbs minimization for performing phase equilibrium calculations for any number of components or phases. *Fluid Phase Equilibria.* 2003;210:229-245.
51. Michelsen ML. A simple method for calculation of approximate phase boundaries. *Fluid Phase Equilibria.* 1994;98:1-11.
52. Michelsen ML. Advanced Course on Thermodynamic Models - Fundamentals & Computational aspects. 2014.
53. Konynenburg PHV, Scott RL. Critical Lines and Phase Equilibria in Binary Van Der Waals Mixtures. *Philosophical Transactions of the Royal Society of London. Series A.* 1980;298:495-540.
54. Kohn JP, Kurata F. Heterogeneous phase equilibria of the methane—hydrogen sulfide system. *AIChE Journal.* 1958;4:211-217.
55. Espinosa S, Raeissi S, Brignole EA, Peters CJ. Prediction of double retrograde vaporization: transitions in binary mixtures of near critical fluids with components of homologous series. *The Journal of Supercritical Fluids.* 2004;32:63-71.
56. Alfradique MF, Castier M. Effect of combining rules for cubic equations of state on the prediction of double retrograde vaporization. *Fluid Phase Equilibria.* 2005;230:1-8.
57. Raeissi S, Peters CJ. On the phenomenon of double retrograde vaporization: multi-dew point behavior in the binary system ethane + limonene. *Fluid Phase Equilibria.* 2001;191:33-40.
58. Raeissi S, Peters CJ. Thermodynamic Analysis of the Phenomenon of Double Retrograde Vaporization. *The Journal of Physical Chemistry B.* 2004;108:13771-13776.
59. Coquelet C, Valtz A, Arpentinier P. Thermodynamic study of binary and ternary systems containing CO2 + impurities in the context of CO2 transportation. *Fluid Phase Equilibria.* 2014;382:205-211.
60. Topliss RJ, Dimitrelis D, Prausnitz JM. Computational aspects of a non-cubic equation of state for phase-equilibrium calculations. Effect of density-dependent mixing rules. *Computers & Chemical Engineering.* 1988;12:483-489.
61. Chen RJJ, Chappelear PS, Kobayashi R. Dew-point loci for methane-butane binary system. *Journal of Chemical & Engineering Data.* 1974;19:53-58.
62. Taraf R, Behbahani R, Moshfeghian M. Direct Prediction of Cricondentherm and Cricondenbar Coordinates of Natural Gas Mixtures using Cubic Equation of State. *International Journal of Thermophysics.* 2008;29:1954-1967.
63. Poling BE, Prausnitz JM, O'Connell JP. The Properties of Gases and Liquids (5th edition). Singapore: McGraw-Hill, 2007.
64. Diamantonis NI, Economou IG. Evaluation of Statistical Associating Fluid Theory (SAFT) and Perturbed Chain-SAFT Equations of State for the Calculation of Thermodynamic Derivative Properties of Fluids Related to Carbon Capture and Sequestration. *Energy & Fuels.* 2011;25:3334-3343.
65. Diamantonis NI, Boulougouris GC, Tsangaris DM, et al. Thermodynamic and transport property models for carbon capture and sequestration (CCS) processes with emphasis on CO2 transport. *Chemical Engineering Research and Design.* 2013;91:1793-1806.
66. Diamantonis NI, Boulougouris GC, Mansoor E, Tsangaris DM, Economou IG. Evaluation of Cubic, SAFT, and PC-SAFT Equations of State for the Vapor–Liquid Equilibrium Modeling of CO2 Mixtures with Other Gases. *Industrial & Engineering Chemistry Research.* 2013;52:3933-3942.
67. Ahmad M, Gernert J, Wilbers E. Effect of impurities in captured CO2 on liquid–vapor equilibrium. *Fluid Phase Equilibria.* 2014;363:149-155.
68. Rivas C, Fernandez J, Artal M, Velasco I, Blanco S, Fernández J. Influence of Methane in CO2Transport and Storage for CCS Technology. *Environmental science & technology.* 2012;46:13016-13023.

69. Coquelet C, Valtz A, Dieu F, Richon D, Arpentinier P, Lockwood F. Isothermal P, x, y data for the argon + carbon dioxide system at six temperatures from 233.32 to 299.21 K and pressures up to 14 MPa. *Fluid Phase Equilibria.* 2008;273:38-43.
70. Caubet F. The liquifaction of gas mixtures. *Z. Kompr. Fluess. Gase Pressluft-Ind.* 1904;8:65.
71. Stouffer C, Kellerman S, Hall K, Holste J, Gammon B, Marsh K. Densities of Carbon Dioxide + Hydrogen Sulfide Mixtures from 220 K to 450 K at Pressures up to 25 MPa. *Journal of chemical & engineering data.* 2001;46:1309-1318.
72. Chapoy A, Nazeri M, Kapateh M, Burgass R, Coquelet C, Tohidi B. Effect of impurities on thermophysical properties and phase behaviour of a CO2-rich system in CCS. *International Journal of Greenhouse Gas Control.* 2013;19:92-100.
73. DIPPR 801, Evaluated Standards Thermophysical Property Values. American Institute of Chemical Engineers; 2013.
74. Ghosh A, Chapman WG, French RN. Gas solubility in hydrocarbons—a SAFT-based approach. *Fluid Phase Equilibria.* 2003;209:229-243.
75. Tihic A. *Group Contribution sPC-SAFT Equation of State*: Chemical and Biochemical Engineering, Technical University of Denmark; 2008.
76. Chickos JS, Acree WE. Enthalpies of Sublimation of Organic and Organometallic Compounds. 1910–2001. *Journal of Physical and Chemical Reference Data.* 2002;31:537-698.
77. Corazza ML, Cardozo Filho L, Vladmir Oliveira J, Dariva C. A robust strategy for SVL equilibrium calculations at high pressures. *Fluid Phase Equilibria.* 2004;221:113-126.
78. Bertakis E, Lemonis I, Katsoufis S, et al. Measurement and thermodynamic modeling of solid–liquid–gas equilibrium of some organic compounds in the presence of CO2. *The Journal of Supercritical Fluids.* 2007;41:238-245.
79. Spiliotis N, Magoulas K, Tassios D. Prediction of the solubility of aromatic hydrocarbons in supercritical CO2 with EoSGE models. *Fluid Phase Equilibria.* 1994;102:121-141.
80. Fandiño O, Trusler JPM, Vega-Maza D. Phase behavior of (CO2 + H2) and (CO2 + N2) at temperatures between (218.15 and 303.15) K at pressures up to 15 MPa. *International Journal of Greenhouse Gas Control.* 2015;36:78-92.
81. Cheong PL, Zhang D, Ohgaki K, Lu BCY. High pressure phase equilibria for binary systems involving a solid phase. *Fluid Phase Equilibria.* 1986;29:555-562.
82. Diefenbacher A, Türk M. Phase equilibria of organic solid solutes and supercritical fluids with respect to the RESS process. *The Journal of Supercritical Fluids.* 2002;22:175-184.
83. McHugh MA, Yogan TJ. Three-phase solid-liquid-gas equilibria for three carbon dioxide-hydrocarbon solid systems, two ethane-hydrocarbon solid systems, and two ethylene-hydrocarbon solid systems. *Journal of Chemical & Engineering Data.* 1984;29:112-115.
84. Lemert RM, Johnston KP. Solid-liquid-gas equilibria in multicomponent supercritical fluid systems. *Fluid Phase Equilibria.* 1989;45:265-286.
85. Fukné-Kokot K, König A, Knez Ž, Škerget M. Comparison of different methods for determination of the S–L–G equilibrium curve of a solid component in the presence of a compressed gas. *Fluid Phase Equilibria.* 2000;173:297-310.
86. Diepen GAM, Scheffer FEC. On Critical Phenomena of Saturated Solutions in Binary Systems. *Journal of the American Chemical Society.* 1948;70:4081-4085.